Radiation Effects

in

Metal-Oxide-Semiconductor Devices

by

Alfred Kin-Wa Chan

A Thesis
Submitted to the Faculty of Graduate Studies
in Partial Fulfillment of the Requirements
for the Degree of

Master of Science

Department of Electrical & Computer Engineering
University of Manitoba
Winnipeg, Manitoba

© May, 1993

National Library of Canada
Acquisitions and Bibliographic Services Branch
395 Wellington Street
Ottawa, Ontario
K1A 0N4

Bibliothèque nationale du Canada
Direction des acquisitions et des services bibliographiques
395, rue Wellington
Ottawa (Ontario)
K1A 0N4

Your file Votre référence

Our file Notre référence

The author has granted an irrevocable non-exclusive licence allowing the National Library of Canada to reproduce, loan, distribute or sell copies of his/her thesis by any means and in any form or format, making this thesis available to interested persons.

L'auteur a accordé une licence irrévocable et non exclusive permettant à la Bibliothèque nationale du Canada de reproduire, prêter, distribuer ou vendre des copies de sa thèse de quelque manière et sous quelque forme que ce soit pour mettre des exemplaires de cette thèse à la disposition des personnes intéressées.

The author retains ownership of the copyright in his/her thesis. Neither the thesis nor substantial extracts from it may be printed or otherwise reproduced without his/her permission.

L'auteur conserve la propriété du droit d'auteur qui protège sa thèse. Ni la thèse ni des extraits substantiels de celle-ci ne doivent être imprimés ou autrement reproduits sans son autorisation.

ISBN 0-315-81743-7

Canada

Name ___

Dissertation Abstracts International is arranged by broad, general subject categories. Please select the one subject which most nearly describes the content of your dissertation. Enter the corresponding four-digit code in the spaces provided.

APPLIED SCIENCE — 0544 — U·M·I

SUBJECT TERM — SUBJECT CODE

Subject Categories

THE HUMANITIES AND SOCIAL SCIENCES

COMMUNICATIONS AND THE ARTS
- Architecture 0729
- Art History 0377
- Cinema 0900
- Dance 0378
- Fine Arts 0357
- Information Science 0723
- Journalism 0391
- Library Science 0399
- Mass Communications 0708
- Music 0413
- Speech Communication 0459
- Theater 0465

EDUCATION
- General 0515
- Administration 0514
- Adult and Continuing 0516
- Agricultural 0517
- Art 0273
- Bilingual and Multicultural 0282
- Business 0688
- Community College 0275
- Curriculum and Instruction 0727
- Early Childhood 0518
- Elementary 0524
- Finance 0277
- Guidance and Counseling 0519
- Health 0680
- Higher 0745
- History of 0520
- Home Economics 0278
- Industrial 0521
- Language and Literature 0279
- Mathematics 0280
- Music 0522
- Philosophy of 0998
- Physical 0523
- Psychology 0525
- Reading 0535
- Religious 0527
- Sciences 0714
- Secondary 0533
- Social Sciences 0534
- Sociology of 0340
- Special 0529
- Teacher Training 0530
- Technology 0710
- Tests and Measurements 0288
- Vocational 0747

LANGUAGE, LITERATURE AND LINGUISTICS
- Language
  - General 0679
  - Ancient 0289
  - Linguistics 0290
  - Modern 0291
- Literature
  - General 0401
  - Classical 0294
  - Comparative 0295
  - Medieval 0297
  - Modern 0298
  - African 0316
  - American 0591
  - Asian 0305
  - Canadian (English) 0352
  - Canadian (French) 0355
  - English 0593
  - Germanic 0311
  - Latin American 0312
  - Middle Eastern 0315
  - Romance 0313
  - Slavic and East European 0314

PHILOSOPHY, RELIGION AND THEOLOGY
- Philosophy 0422
- Religion
  - General 0318
  - Biblical Studies 0321
  - Clergy 0319
  - History of 0320
  - Philosophy of 0322
- Theology 0469

SOCIAL SCIENCES
- American Studies 0323
- Anthropology
  - Archaeology 0324
  - Cultural 0326
  - Physical 0327
- Business Administration
  - General 0310
  - Accounting 0272
  - Banking 0770
  - Management 0454
  - Marketing 0338
- Canadian Studies 0385
- Economics
  - General 0501
  - Agricultural 0503
  - Commerce-Business 0505
  - Finance 0508
  - History 0509
  - Labor 0510
  - Theory 0511
- Folklore 0358
- Geography 0366
- Gerontology 0351
- History
  - General 0578
  - Ancient 0579
  - Medieval 0581
  - Modern 0582
  - Black 0328
  - African 0331
  - Asia, Australia and Oceania 0332
  - Canadian 0334
  - European 0335
  - Latin American 0336
  - Middle Eastern 0333
  - United States 0337
- History of Science 0585
- Law 0398
- Political Science
  - General 0615
  - International Law and Relations 0616
  - Public Administration 0617
- Recreation 0814
- Social Work 0452
- Sociology
  - General 0626
  - Criminology and Penology 0627
  - Demography 0938
  - Ethnic and Racial Studies 0631
  - Individual and Family Studies 0628
  - Industrial and Labor Relations 0629
  - Public and Social Welfare 0630
  - Social Structure and Development 0700
  - Theory and Methods 0344
- Transportation 0709
- Urban and Regional Planning 0999
- Women's Studies 0453

THE SCIENCES AND ENGINEERING

BIOLOGICAL SCIENCES
- Agriculture
  - General 0473
  - Agronomy 0285
  - Animal Culture and Nutrition 0475
  - Animal Pathology 0476
  - Food Science and Technology 0359
  - Forestry and Wildlife 0478
  - Plant Culture 0479
  - Plant Pathology 0480
  - Plant Physiology 0817
  - Range Management 0777
  - Wood Technology 0746
- Biology
  - General 0306
  - Anatomy 0287
  - Biostatistics 0308
  - Botany 0309
  - Cell 0379
  - Ecology 0329
  - Entomology 0353
  - Genetics 0369
  - Limnology 0793
  - Microbiology 0410
  - Molecular 0307
  - Neuroscience 0317
  - Oceanography 0416
  - Physiology 0433
  - Radiation 0821
  - Veterinary Science 0778
  - Zoology 0472
- Biophysics
  - General 0786
  - Medical 0760

EARTH SCIENCES
- Biogeochemistry 0425
- Geochemistry 0996
- Geodesy 0370
- Geology 0372
- Geophysics 0373
- Hydrology 0388
- Mineralogy 0411
- Paleobotany 0345
- Paleoecology 0426
- Paleontology 0418
- Paleozoology 0985
- Palynology 0427
- Physical Geography 0368
- Physical Oceanography 0415

HEALTH AND ENVIRONMENTAL SCIENCES
- Environmental Sciences 0768
- Health Sciences
  - General 0566
  - Audiology 0300
  - Chemotherapy 0992
  - Dentistry 0567
  - Education 0350
  - Hospital Management 0769
  - Human Development 0758
  - Immunology 0982
  - Medicine and Surgery 0564
  - Mental Health 0347
  - Nursing 0569
  - Nutrition 0570
  - Obstetrics and Gynecology 0380
  - Occupational Health and Therapy 0354
  - Ophthalmology 0381
  - Pathology 0571
  - Pharmacology 0419
  - Pharmacy 0572
  - Physical Therapy 0382
  - Public Health 0573
  - Radiology 0574
  - Recreation 0575
- Speech Pathology 0460
- Toxicology 0383
- Home Economics 0386

PHYSICAL SCIENCES

Pure Sciences
- Chemistry
  - General 0485
  - Agricultural 0749
  - Analytical 0486
  - Biochemistry 0487
  - Inorganic 0488
  - Nuclear 0738
  - Organic 0490
  - Pharmaceutical 0491
  - Physical 0494
  - Polymer 0495
  - Radiation 0754
- Mathematics 0405
- Physics
  - General 0605
  - Acoustics 0986
  - Astronomy and Astrophysics 0606
  - Atmospheric Science 0608
  - Atomic 0748
  - Electronics and Electricity 0607
  - Elementary Particles and High Energy 0798
  - Fluid and Plasma 0759
  - Molecular 0609
  - Nuclear 0610
  - Optics 0752
  - Radiation 0756
  - Solid State 0611
- Statistics 0463

Applied Sciences
- Applied Mechanics 0346
- Computer Science 0984
- Engineering
  - General 0537
  - Aerospace 0538
  - Agricultural 0539
  - Automotive 0540
  - Biomedical 0541
  - Chemical 0542
  - Civil 0543
  - Electronics and Electrical 0544
  - Heat and Thermodynamics 0348
  - Hydraulic 0545
  - Industrial 0546
  - Marine 0547
  - Materials Science 0794
  - Mechanical 0548
  - Metallurgy 0743
  - Mining 0551
  - Nuclear 0552
  - Packaging 0549
  - Petroleum 0765
  - Sanitary and Municipal 0554
  - System Science 0790
- Geotechnology 0428
- Operations Research 0796
- Plastics Technology 0795
- Textile Technology 0994

PSYCHOLOGY
- General 0621
- Behavioral 0384
- Clinical 0622
- Developmental 0620
- Experimental 0623
- Industrial 0624
- Personality 0625
- Physiological 0989
- Psychobiology 0349
- Psychometrics 0632
- Social 0451

Nom ______________________________

Dissertation Abstracts International est organisé en catégories de sujets. Veuillez s.v.p. choisir le sujet qui décrit le mieux votre thèse et inscrivez le code numérique approprié dans l'espace réservé ci-dessous.

______________________________ [ ][ ][ ][ ] U·M·I

SUJET — CODE DE SUJET

Catégories par sujets

HUMANITÉS ET SCIENCES SOCIALES

COMMUNICATIONS ET LES ARTS
Architecture 0729
Beaux-arts 0357
Bibliothéconomie 0399
Cinéma 0900
Communication verbale 0459
Communications 0708
Danse 0378
Histoire de l'art 0377
Journalisme 0391
Musique 0413
Sciences de l'information 0723
Théâtre 0465

ÉDUCATION
Généralités 515
Administration 0514
Art 0273
Collèges communautaires 0275
Commerce 0688
Économie domestique 0278
Éducation permanente 0516
Éducation préscolaire 0518
Éducation sanitaire 0680
Enseignement agricole 0517
Enseignement bilingue et multiculturel 0282
Enseignement industriel 0521
Enseignement primaire. 0524
Enseignement professionnel 0747
Enseignement religieux 0527
Enseignement secondaire 0533
Enseignement spécial 0529
Enseignement supérieur 0745
Évaluation 0288
Finances 0277
Formation des enseignants 0530
Histoire de l'éducation 0520
Langues et littérature 0279
Lecture 0535
Mathématiques 0280
Musique 0522
Orientation et consultation 0519
Philosophie de l'éducation 0998
Physique 0523
Programmes d'études et enseignement 0727
Psychologie 0525
Sciences 0714
Sciences sociales 0534
Sociologie de l'éducation 0340
Technologie 0710

LANGUE, LITTÉRATURE ET LINGUISTIQUE
Langues
- Généralités 0679
- Anciennes 0289
- Linguistique 0290
- Modernes 0291

Littérature
- Généralités 0401
- Anciennes 0294
- Comparée 0295
- Mediévale 0297
- Moderne 0298
- Africaine 0316
- Américaine 0591
- Anglaise 0593
- Asiatique 0305
- Canadienne (Anglaise) 0352
- Canadienne (Française) 0355
- Germanique 0311
- Latino-américaine 0312
- Moyen-orientale 0315
- Romane 0313
- Slave et est-européenne 0314

PHILOSOPHIE, RELIGION ET THÉOLOGIE
Philosophie 0422
Religion
- Généralités 0318
- Clergé 0319
- Études bibliques 0321
- Histoire des religions 0320
- Philosophie de la religion 0322

Théologie 0469

SCIENCES SOCIALES
Anthropologie
- Archéologie 0324
- Culturelle 0326
- Physique 0327

Droit 0398
Économie
- Généralités 0501
- Commerce-Affaires 0505
- Économie agricole 0503
- Économie du travail 0510
- Finances 0508
- Histoire 0509
- Théorie 0511

Études américaines 0323
Études canadiennes 0385
Études féministes 0453
Folklore 0358
Géographie 0366
Gérontologie 0351
Gestion des affaires
- Généralités 0310
- Administration 0454
- Banques 0770
- Comptabilité 0272
- Marketing 0338

Histoire
- Histoire générale 0578
- Ancienne 0579
- Médiévale 0581
- Moderne 0582
- Histoire des noirs 0328
- Africaine 0331
- Canadienne 0334
- États-Unis 0337
- Européenne 0335
- Moyen-orientale 0333
- Latino-américaine 0336
- Asie, Australie et Océanie 0332

Histoire des sciences 0585
Loisirs 0814
Planification urbaine et régionale 0999
Science politique
- Généralités 0615
- Administration publique 0617
- Droit et relations internationales 0616

Sociologie
- Généralités 0626
- Aide et bien-àtre social 0630
- Criminologie et établissements pénitentiaires 0627
- Démographie 0938
- Études de l' individu et de la famille 0628
- Études des relations interethniques et des relations raciales 0631
- Structure et développement social 0700
- Théorie et méthodes. 0344
- Travail et relations industrielles 0629

Transports 0709
Travail social 0452

SCIENCES ET INGÉNIERIE

SCIENCES BIOLOGIQUES
Agriculture
- Généralités 0473
- Agronomie. 0285
- Alimentation et technologie alimentaire 0359
- Culture 0479
- Élevage et alimentation 0475
- Exploitation des péturages 0777
- Pathologie animale 0476
- Pathologie végétale 0480
- Physiologie végétale 0817
- Sylviculture et faune 0478
- Technologie du bois 0746

Biologie
- Généralités 0306
- Anatomie 0287
- Biologie (Statistiques) 0308
- Biologie moléculaire 0307
- Botanique 0309
- Cellule 0379
- Écologie 0329
- Entomologie 0353
- Génétique 0369
- Limnologie 0793
- Microbiologie 0410
- Neurologie 0317
- Océanographie 0416
- Physiologie 0433
- Radiation 0821
- Science vétérinaire 0778
- Zoologie 0472

Biophysique
- Généralités 0786
- Medicale 0760

SCIENCES DE LA TERRE
Biogéochimie 0425
Géochimie 0996
Géodésie 0370
Géographie physique 0368
Géologie 0372
Géophysique 0373
Hydrologie 0388
Minéralogie 0411
Océanographie physique 0415
Paléobotanique 0345
Paléoécologie 0426
Paléontologie 0418
Paléozoologie 0985
Palynologie 0427

SCIENCES DE LA SANTÉ ET DE L'ENVIRONNEMENT
Économie domestique 0386
Sciences de l'environnement 0768
Sciences de la santé
- Généralités 0566
- Administration des hipitaux 0769
- Alimentation et nutrition 0570
- Audiologie 0300
- Chimiothérapie 0992
- Dentisterie 0567
- Développement humain 0758
- Enseignement 0350
- Immunologie 0982
- Loisirs 0575
- Médecine du travail et thérapie 0354
- Médecine et chirurgie 0564
- Obstétrique et gynécologie 0380
- Ophtalmologie 0381
- Orthophonie 0460
- Pathologie 0571
- Pharmacie 0572
- Pharmacologie 0419
- Physiothérapie 0382
- Radiologie 0574
- Santé mentale 0347
- Santé publique 0573
- Soins infirmiers 0569
- Toxicologie 0383

SCIENCES PHYSIQUES
Sciences Pures
Chimie
- Genéralités 0485
- Biochimie 487
- Chimie agricole 0749
- Chimie analytique 0486
- Chimie minérale 0488
- Chimie nucléaire 0738
- Chimie organique 0490
- Chimie pharmaceutique 0491
- Physique 0494
- PolymÇres 0495
- Radiation 0754

Mathématiques 0405
Physique
- Généralités 0605
- Acoustique 0986
- Astronomie et astrophysique 0606
- Electronique et électricité 0607
- Fluides et plasma 0759
- Météorologie 0608
- Optique 0752
- Particules (Physique nucléaire) 0798
- Physique atomique 0748
- Physique de l'état solide 0611
- Physique moléculaire 0609
- Physique nucléaire 0610
- Radiation 0756

Statistiques 0463

Sciences Appliqués Et Technologie
Informatique 0984
Ingénierie
- Généralités 0537
- Agricole 0539
- Automobile 0540
- Biomédicale 0541
- Chaleur et ther modynamique 0348
- Conditionnement (Emballage) 0549
- Génie aérospatial 0538
- Génie chimique 0542
- Génie civil 0543
- Génie électronique et électrique 0544
- Génie industriel 0546
- Génie mécanique 0548
- Génie nucléaire 0552
- Ingénierie des systämes 0790
- Mécanique navale 0547
- Métallurgie 0743
- Science des matériaux 0794
- Technique du pétrole 0765
- Technique minière 0551
- Techniques sanitaires et municipales 0554
- Technologie hydraulique 0545

Mécanique appliquée 0346
Géotechnologie 0428
Matières plastiques (Technologie) 0795
Recherche opérationnelle 0796
Textiles et tissus (Technologie) 0794

PSYCHOLOGIE
Généralités 0621
Personnalité 0625
Psychobiologie 0349
Psychologie clinique 0622
Psychologie du comportement 0384
Psychologie du développement 0620
Psychologie expérimentale 0623
Psychologie industrielle 0624
Psychologie physiologique 0989
Psychologie sociale 0451
Psychométrie 0632

RADIATION EFFECTS IN METAL-OXIDE-SEMICONDUCTOR DEVICES

BY

ALFRED KIN-WA CHAN

A Thesis submitted to the Faculty of Graduate Studies of the University of Manitoba in partial fulfillment of the requirements for the degree of

MASTER OF SCIENCE

© 1993

Permission has been granted to the LIBRARY OF THE UNIVERSITY OF MANITOBA to lend or sell copies of this thesis, to the NATIONAL LIBRARY OF CANADA to microfilm this thesis and to lend or sell copies of the film, and UNIVERSITY MICROFILMS to publish an abstract of this thesis.

The author reserves other publications rights, and neither the thesis nor extensive extracts from it may be printed or otherwise reproduced without the author's permission.

Abstract

The radiation damage in metal-oxide-semiconductor (MOS) devices induced by microwave electron cyclotron resonance N_2O plasmas has been studied. The radiation damage was determined by measuring the change of the interface trap density (D_{it}) and the oxide charge density (Q_o) in MOS devices. The radiation damage was measured as a function of SiO_2 film thickness in the range 200–1000 Å and device temperature in the range, 25–300 °C, during plasma radiation. Both thermally grown and plasma-enhanced chemical vapor deposited SiO_2 films were used for this study. The experimental results show that D_{it} increases to 10^{12}–10^{13} cm^{-2} eV^{-1} with increasing thermal SiO_2 thickness. Annealing in a forming gas at 400 °C removes most of the radiation-induced damage. As the device temperature is increased from 25 to 200 °C during plasma radiation, D_{it} decreases from 10^{13} to 10^{11} cm^{-2} eV^{-1}. A further increase in device temperature to 300 °C leads to an reverse trend, that is, to an increase in D_{it}. The temperature effects imply that the defect generation and annihilation processes occur simultaneously during plasma radiation. The reported results in this investigation can be explained in terms of the bond strain gradient and the recombination-enhanced defect reactions models.

Acknowledgments

The author would like to thank Dr. K. C. Kao for his advice and supervision of this thesis. The author is also indebted to his colleagues at the Material and Devices Research Laboratory, in particular, T. T. Chau, for his technical assistance and valuable suggestions to make this research work successful. A special thanks is given to K. Westra for his timely assistance. The financial support from the Natural Sciences and Engineering Research Council of Canada is also acknowledged.

Table of Contents

	Page
Abstract	i
Acknowledgments	ii
List of Figures	v
List of Tables	viii
1. Introduction	1
References for Chapter 1	4
2. Review of the Radiation Effects in MOS Devices	6
2.1 Defect Generation Mechanisms	7
2.1.1 Hole Transport in SiO_2	10
2.1.2 Origins of the Radiation-Induced Defects in MOS Devices	12
2.2 Annealing of Radiation-Induced Defects	15
2.2.1 Relaxation of Strained Bonds	17
2.2.2 Hydrogenation of Defects	19
References for Chapter 2	22
3. Experimental Procedures and Characterization Techniques	25
3.1 Silicon Substrate Cleaning Processes	25
3.2 SiO_2 Film Fabrication Processes	27
3.2.1 Thermal Oxidation	27
3.2.2 Plasma-Enhanced Chemical Vapor Deposition	28
3.3 Metallization Process	31
3.4 Plasma Radiation Process	33
3.5 Annealing Process	37
3.6 Characterization Techniques	39
3.6.1 Optical Emission Spectrometry Technique	40
3.6.2 Capacitance-Voltage Method	40
References for Chapter 3	44

4. Experimental Results and Discussion 46
4.1 Plasma Radiation and Annealing Effects in MOS Devices 46
4.1.1 Plasma Radiation Effects 47
4.1.2 Annealing Effects 47
4.2 Oxide Thickness Dependence 49
4.2.1 Pre-Irradiation 49
4.2.2 Plasma Radiation Effects 52
A. Interface Trap Density 52
B. Oxide Charge Density 61
4.2.3 Annealing Effects 68
4.3 Device Temperature Dependence 69
4.3.1 Pre-Irradiation 70
4.3.2 Plasma Radiation Effects 73
A. Interface Trap Density 73
B. Oxide Charge Density 80
4.3.3 Annealing Effects 86
4.4 Comparison Between Thermal and PECVD Oxides 89
4.4.1 Plasma Radiation Effects 90
A. Interface Trap Density 90
B. Oxide Charge Density 93
4.4.2 Annealing Effects 96
References for Chapter 4 98

5. Conclusions 101

Appendix A Capacitance-Voltage Method 104
(I) Calculation of Interface Trap Density 104
(II) Calculation of Oxide Charge Density 107
References for Appendix A 109

List of Figures

Figure | Page

2.1 A schematic representation of basic radiation effects in MOS structures. 8

2.2 Schematic diagrams illustrating two of the possible hole transport mechanisms within the SiO_2 bandgap. (a) hopping transport; (b) trap-mediated hole conduction process. 11

2.3 Hole trapping and removal processes in an MOS device during irradiation. 14

2.4 Illustrating the creation of oxide charge, neutral traps, and interface traps due to ionizing radiation in MOS devices. 16

2.5 Schematic diagrams of the Si-SiO_2 structure before and after annealing. (a) before annealing; (b) after annealing. 18

3.1 ECR plasma reactor system. 30

3.2 Schematic diagram of the plasma chamber and the processing chamber. 32

3.3 Midgap D_{it} as a function of radiation time for the MOS devices. 34

3.4 The cross-sections of test structures. (a) electrode sample; (b) anneal sample; (c) mask sample; (d) bare sample. 38

3.5 Schematic diagrams of the experimental set-up for C-V measurements. (a) high frequency C-V measurement; (b) quasi-static C-V measurement. 41

3.6 The overall experimental procedures for all the radiation experiments. 43

4.1 High frequency and quasi-static C-V curves for a bare sample measured after plasma radiation and then after PMA treatment. 48

4.2 Midgap D_{it} as a function of oxide thickness for the anneal sample sets prior to radiation. Curve 1: before any treatment; curve 2: after initial PMA treatment. 50

4.3 Q_o as a function of oxide thickness for the anneal sample sets prior to radiation. Curve 1: before any treatment; curve 2: after initial PMA treatment. 50
4.4 Midgap D_{it} as a function of oxide thickness for the electrode sample sets. Curve 1: after irradiation; curve 2: after final PMA treatment. 53
4.5 Midgap D_{it} as a function of oxide thickness for the mask sample sets. Curve 1: after irradiation; curve 2: after final PMA treatment. 53
4.6 Midgap D_{it} as a function of oxide thickness for the bare sample sets. Curve 1: after irradiation; curve 2: after final PMA treatment. 54
4.7 Midgap D_{it} as a function of oxide thickness for the anneal sample sets. Curve 1: after irradiation; curve 2: after final PMA treatment. 54
4.8 Bond Strain Gradient model 57
4.9 The optical emission spectrum of the N_2O plasma 60
4.10 Q_o as a function of oxide thickness for the electrode sample sets. Curve 1: after irradiation; curve 2: after final PMA treatment. 62
4.11 Q_o as a function of oxide thickness for the mask sample sets. Curve 1: after irradiation; curve 2: after final PMA treatment. 62
4.12 Q_o as a function of oxide thickness for the bare sample sets. Curve 1: after irradiation; curve 2: after final PMA treatment. 63
4.13 Q_o as a function of oxide thickness for the anneal sample sets. Curve 1: after irradiation; curve 2: after final PMA treatment. 63
4.14 Model of an MOS device during plasma radiation. 65
4.15 Midgap D_{it} as a function of device temperature for the anneal sample sets with oxide thickness of (a) 228 Å; (b) 941 Å. Curve 1: before any treatment; curve 2: after initial PMA treatment. 71

4.16 Q_o as a function of device temperature for the anneal sample sets with oxide thickness of (a) 228 Å; (b) 941 Å. Curve 1: before any treatment; curve 2: after initial PMA treatment. 72
4.17 Midgap D_{it} as a function of device temperature for the electrode sample sets with oxide thickness of (a) 228 Å; (b) 941 Å. Curve 1: after irradiation; curve 2: after final PMA treatment. 74
4.18 Midgap D_{it} as a function of device temperature for the mask sample sets with oxide thickness of (a) 228 Å; (b) 941 Å. Curve 1: after irradiation; curve 2: after final PMA treatment. 75
4.19 Midgap D_{it} as a function of device temperature for the anneal samples sets with oxide thickness of (a) 228 Å; (b) 941 Å. Curve 1: after irradiation; curve 2: after final PMA treatment. 76
4.20 Midgap D_{it} as a function of device temperature for the bare sample sets with oxide thickness of (a) 228 Å; (b) 941 Å. Curve 1: after irradiation; curve 2: after final PMA treatment. 77
4.21 Q_o as a function of device temperature for the electrode sample sets with oxide thickness of (a) 228 Å; (b) 941 Å. Curve 1: after irradiation; curve 2: after final PMA treatment. 81
4.22 Q_o as a function of device temperature for the mask sample sets with oxide thickness of (a) 228 Å; (b) 941 Å. Curve 1: after irradiation; curve 2: after final PMA treatment. 82
4.23 Q_o as a function of device temperature for the anneal sample sets with oxide thickness of (a) 228 Å; (b) 941 Å. Curve 1: after irradiation; curve 2: after final PMA treatment. 83
4.24 Q_o as a function of device temperature for the bare sample sets with oxide thickness of (a) 228 Å; (b) 941 Å. Curve 1: after irradiation; curve 2: after final PMA treatment. 84

List of Tables

Table Page

3.1 The combinations of various parameters for the plasma radiation experiments. 36

4.1 The D_{it} values measured after plasma radiation for the control, mask, bare, and anneal sample sets. 58

4.2 The D_{it} values of the MOS devices with electrode, mask, anneal, and bare structures after various processing steps. 91

4.3 The Q_o values of the MOS devices with electrode, mask, anneal, and bare structures after various processing steps. 94

Chapter 1

Introduction

Plasma processing has been well known to create detrimental effects in metal-oxide-semiconductor (MOS) devices [1-5]. This is because a plasma contains ionizing radiation such as ultraviolet (UV) light, X-rays, ions, electrons, neutral species, and other radicals. The exposure of MOS devices to such a plasma environment generates electrically active defects in the insulating oxide films. These defects can be classified into three categories: (a) the positive oxide charge; (b) the interface traps; and (c) the neutral traps. The radiation-induced defects in the oxide films are deleterious to device performance and induce instability problems. For example, degradation in reverse current and sudden change in breakdown voltage for MOS transistors are the typical radiation effects. In order to maintain the integrity of the MOS devices, it is necessary to reduce these defects formed either inside the SiO_2 bulk or at the Si-SiO_2 interface. Obviously, radiation damage is a critical issue that must be overcome before the integration of various plasma processes in integrated circuit (IC) fabrication becomes viable.

Nevertheless, plasma processing presents tremendous potential for submicron technology. Especially in recent advances in dry etching and plasma-enhanced chemical vapor deposition (PECVD) processes, they offer a new dimension to the IC fabrication technology. Since the conventional methods such as wet etching and thermal oxidation are incapable of producing high quality submicron structures, the demand for alternative

techniques such as plasma processing is ever increasing. This is because plasma etching is anisotropic and therefore micropatterns can be reproduced accurately for submicron features [6-8]. Also, the PECVD technique can be used to fabricate multilayer circuits and insulating gate oxides at low temperatures [9-11].

Many investigators have proposed various prototypes of plasma reactors [12-14] for low-temperature plasma processing. One of the most prominent designs is the microwave Electron-Cyclotron-Resonance (ECR) reactor which can be used for both etching and film deposition. The microwave ECR source can generate a high-density homogeneous plasma at low gas pressures [15], and hence it has become a very popular choice for microelectronics industry in recent years [14-16]. Since the interest in microwave ECR plasma processing has been widespreading; therefore the purpose of the present study is to investigate the radiation effects of such plasmas in MOS devices. We chose N_2O gas plasmas as the radiation source in this investigation because N_2O gas is often used in the PECVD process for fabricating SiO_2 films [10, 11, 17-19]. However, the deposited films exhibit high interface trap densities (10^{12}–10^{13} cm^{-2} eV^{-1}), indicating that the deposited films suffer severe plasma radiation damage during film deposition.

Optical emission spectrum (OES) of the N_2O plasma reveals that the UV light is the dominant light emitted from the plasma. Since the UV light is transparent to the aluminum gate electrode [20], it would therefore penetrate the oxide film underneath, thus creating radiation damage in MOS devices. Plasmas formed by other gases including etchant gases have a large component of UV light. Thus, the radiation damage by plasmas of other gases is expected to be similar to that by N_2O plasmas, though the

degree of damage may be different. Annealing of MOS devices after radiation in a forming gas has been well recognized as a method to anneal out the radiation-induced defects. We have also studied the annealing effects on the radiation damage in MOS devices. The future success of integrating plasma technologies into the mainstream device fabrication relies strongly on resolving the radiation damage issue. It is hoped that the present study may throw light on this issue.

In this thesis, chapter 2 gives a brief review of the radiation damage in MOS devices and the related theoretical models for elucidating this phenomenon. Chapter 3 describes the experimental techniques and procedures. Chapter 4 presents the experimental results and the theoretical models used to explain the radiation effects. Finally, conclusions are given in chapter 5.

References for Chapter 1:

[1] R. A. Gdula, "The Effects of Processing on Radiation Damage in SiO_2," *IEEE Trans. Electron Devices* **ED-26**(4), 644 (1979).

[2] L. M. Ephrath and D. J. DiMaria, "Review of RIE Induced Radiation Damage in Silicon Dioxide," *Solid State Technol.* **24**(4), 182 (1981).

[3] T. Sugano, *Applications of Plasma Processes to VLSI Technology*, John Wiley & Sons, New York, (1985).

[4] C. M. Dozier, "Ionizing Radiation in Microelectronics Processing," *Solid State Technol.* **29**(10), 105 (1986).

[5] T. P. Ma, Process-Induced Radiation Effects in *Ionizing Radiation Effects in MOS Devices and Circuits*, T. P. Ma and P. V. Dressendorfer, Eds., John Wiley & Sons, New York, 1989, Ch. 7.

[6] D. L. Flamm, D. E. Ibbotson, J. A. Mucha, and V. M. Donnelly, "XeF_2 and F-Atom Reactions with Si: Their Significance for Plasma Etching," *Solid State Technol.* **26**(4), 117 (1983).

[7] D. J. Economou, E. S. Aydil, and G. Barna, "In Situ Monitoring of Etching Uniformity in Plasma Reactors," *Solid State Technol.* **34**(4), 107 (1991).

[8] J. M. Cook and K. G. Donohoe, "Etching Issues at 0.35 μm and Below," *Solid State Technol.* **34**(4), 119 (1991).

[9] A. C. Adams, "Plasma Deposition of Inorganic Films," *Solid State Technol.* **26**(4), 135 (1983).

[10] J. Batey and E. Tierney, "Low Temperature Deposition of High-Quality Silicon Dioxide by Plasma-Enhanced Chemical Vapor Deposition," *J. Appl. Phys.* **60**, 3136 (1986).

[11] T. V. Herak and D. J. Thomson, "Effects of Substrate Temperature on the Electrical and Physical Properties of Silicon Dioxide Films Deposited from Electron Cyclotron Resonant Microwave Plasmas," *J. Appl. Phys.* **67**, 6347 (1990).

[12] R. A. Rudder, G. G. Fountain, and R. T. Markunas, "Remote Plasma-Enhanced Chemical-Vapor Deposition of Epitaxial Ge Films," *J. Appl. Phys.* **60**, 3519 (1986).

[13] S. R. Mejia, R. D. McLeod, K. C. Kao, and H. C. Card, "Electron-Cyclotron-Resonant Microwave Plasma System for Thin-Film Deposition," *Rev. Sci. Instrum.* **57**(3), 493 (1986).

[14] D. L. Flamm, "Trends in Plasma Sources and Etching," *Solid State Technol.* **34**(3), 47 (1991).

[15] S. Iizuka and N. Sato, "Plasma Structures in an Electron Cyclotron Resonance Plasma Processing Device," *J. Appl. Phys.* **70**, 4165 (1991).

[16] H. P. W. Hey, B. G. Sluijk, and D. G. Hemmes, "Ion Bombardment: A Determining Factor in Plasma CVD," *Solid State Technol.* **33**(4), 139 (1990).

[17] J. Batey, E. Tierney, J. Stasiak, and T. N. Nguyen, "Plasma-Enhanced CVD of High Quality Insulating Films," *Appl. Surface Sci.* **39**, 1 (1989).

[18] R. A. B. Devine, "Defect Reactivation and Structural Relaxation in Deposited Amorphous SiO_2," *J. Appl. Phys.* **70**, 3542 (1991).

[19] T. T. Chau, S. R. Mejia, and K. C. Kao, "New Approach to Low Temperature Deposition of High-Quality Thin Films by Electron Cyclotron Resonance Microwave Plasmas," *J. Vac. Sci. Technol. B.* **10**(5), 2170 (1992).

[20] K. Yokogawa, Y. Yajima, T. Mizutani, S. Nishimatsu, and K. Suzuki, "Positive Charges and E' Centers Formed by Vacuum Ultraviolet Radiation in SiO_2 Grown on Si," *J. J. Appl. Phys.* **29**, 2265 (1990).

Chapter 2

Review of the Radiation Effects in MOS Devices

Although processing plasmas are known to create radiation damage in MOS devices, some investigators have used various gas plasmas for annealing and surface cleaning purposes. Ma and Chin [1-4] had studied the radio-frequency (RF) plasma annealing effects in MOS devices. They claimed that the plasma radiation-induced carriers would undergo a nonradiative recombination at the defect sites under an applied RF field. This recombination process anneals out the radiation damage. Kassabov et al. [5-9] had also investigated the annealing effects of various gas plasmas. They used Ar, He, and H_2 gases as the plasma annealing ambients and found that the radiation-induced defect charges could be annealed out. Plasma radiation not only can anneal out defects, but also can create defects, depending on the radiation intensity and dose. However, in this chapter, we review only the radiation damage.

This chapter first describes the defect generation mechanisms, which are well documented in the literature [10-14]. Many investigators [10-14] have come to a conclusion about the possible processes for the generation of the trapped charges and the associated trap sites which will be reviewed in more details. We then discuss the probable origins of the radiation-induced defects commonly observed in MOS devices, and the necessary safeguards required to avoid or to eliminate the generation of defects

during ionizing radiation. One of the techniques known for its capability of reducing the amount of defects is the thermal annealing. Two of the prominent arguments regarding annealing mechanisms are described in a later section to explain the possible reactions for annealing out the radiation damage.

2.1 Defect Generation Mechanisms

When an MOS device is subjected to ionizing radiation such that the radiation process itself possesses enough energy to excite electrons into unbound states, electron-hole pairs are created in the materials of interest. In the case of MOS device, they are primarily silicon and silicon dioxide. The radiation can be composed of particles in various forms; for example, atomic ions, electrons, photons, or protons are the typical species involved. As long as the particles have energies greater than the bandgap of the material (9 eV for silicon dioxide), they can penetrate the material (SiO_2 film) and eventually create damage there. The radiation damage in the SiO_2 film typically consists of three components: (1) the accumulation of positive charges in the oxide; (2) an increase in the number of Si-SiO_2 interface traps; and (3) an increase in the number of neutral bulk traps. There are four distinct stages [12, 15] used to describe the radiation effects in MOS devices which result in the aforementioned defects. Figure 2.1 summarizes the sequence of events which occur in an MOS device upon irradiation.

In stage 1 shown in Fig. 2.1, we can see that initially the ionizing radiation interacts with the SiO_2 film to produce the electron-hole pairs. The amount of energy required to generate each charged pair is about 17

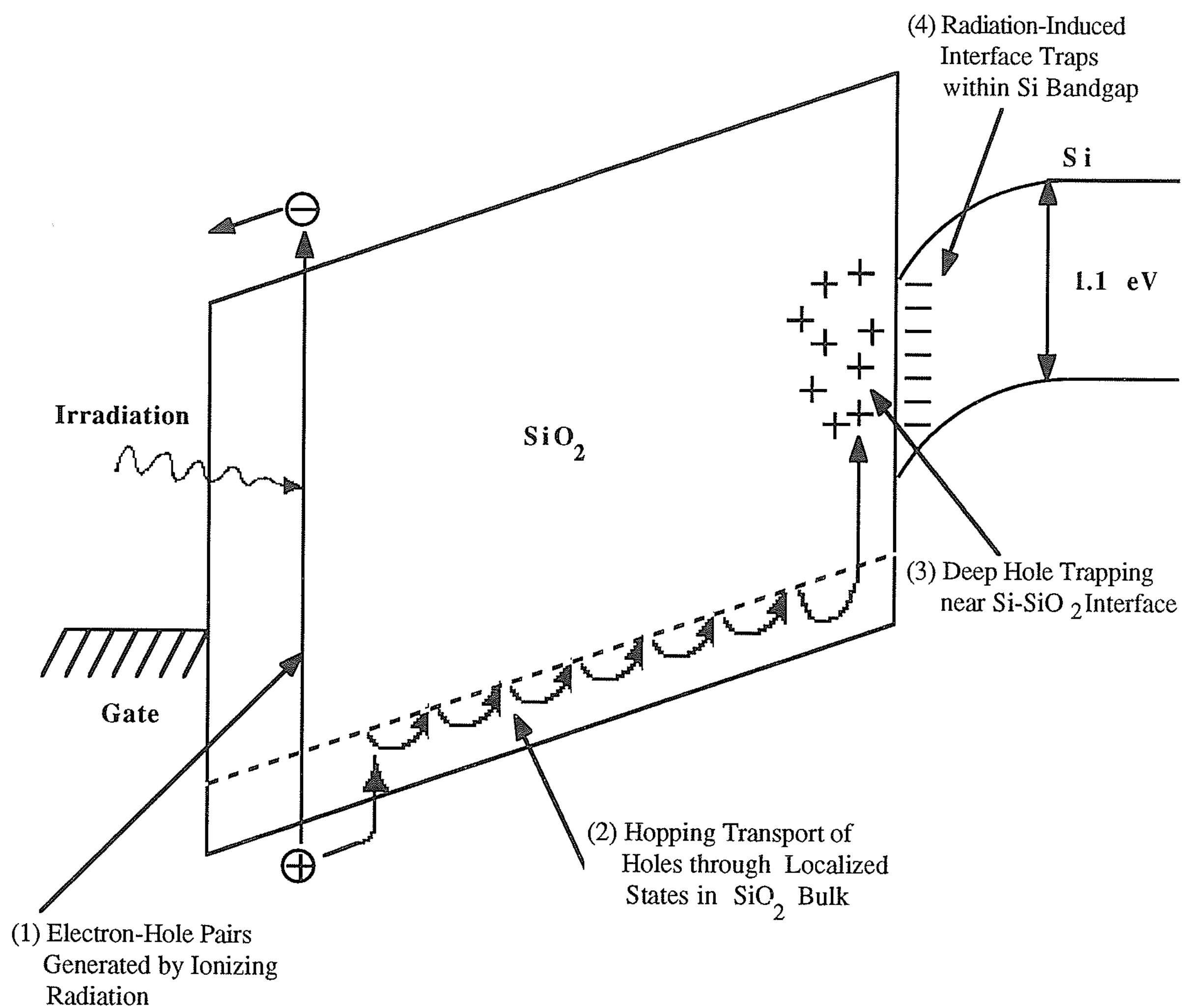

Fig. 2.1 A schematic representation of basic radiation effects in MOS structures. (After Oldham, McLean, Boesch Jr., and McGarrity [12])

to 18 eV in average [12, 15]. Once these charged pairs are created, one portion will undergo an initial recombination process. The other portion is subjected to further transport process through the oxide layer depending on the electric field at the time. Electrons are much more mobile than holes in SiO_2 [15-18]. They are usually swept out of the oxide in a time of 1 picosecond. On the other hand, it usually takes only a few picoseconds at most for the recombination process to be completed. This is the same amount of time required for the mobile electrons to be driven out of the oxide. This means that a major portion of the radiation-induced holes is left behind near their points of origin. This portion does not take part in the recombination process at all. Hence, the immobile holes remaining inside the SiO_2 are then transported toward the Si-SiO_2 interface via a complicated stochastic trap-hopping mechanism as indicated in stage 2. This hole transport model is based on the continuous-time random walk (CTRW) formalism developed by Montroll and Weiss [19]. The theoretical background regarding this formalism will be explained in the next sub-section.

As the holes approach the interface region, a fraction of them are captured by the intrinsic deep trapping sites. This hole trapping phenomenon is the third stage of the overall radiation response in the MOS device. It is responsible for the formation of the positive oxide charge and the bulk traps inside the SiO_2 film. The presence of these trapped holes induces the electron capture action where the electrons are usually provided from the silicon substrate. In addition, this phenomenon also plays a vital role in the build up of the interface states in stage 4. These simultaneous conditions subsequently form the interface states through the reactions happening at the Si-SiO_2 interface. These four distinct stages

represent the basic radiation effects in the MOS device. The origins of these defects are discussed in a later sub-section.

2.1.1 Hole Transport in SiO_2

The hole transport mechanism originated from the generalized CTRW model was used by Lax and others [20, 21] to describe the dispersive carrier transport in disordered solids. However, Ausman, Hughes, and McLean [22, 23] later adopted this model as a physical basis to describe the hole movement in SiO_2. The major feature of this transport model comes from the fact that it contains a broad distribution of individual microscopic events because of the variations in carrier mobility. Consequently, this results in a wide distribution of transit times of the individual holes throughout the material (SiO_2). On the basis of this broad distribution of event times, two distinct situations have been identified during the transport process. They are depicted schematically in Fig. 2.2.

The first mechanism concerns the holes transit across the SiO_2 film in a very short time. It is accomplished through a succession of rapid hopping events as shown in Fig. 2.2 (a). The success of each hopping event between adjoining traps is often enhanced by a phonon-assisted tunnelling transition, which depends on the thermal fluctuations inside the lattice network at the time. Due to the amorphous nature of the SiO_2 film, the random distribution of intersite hopping distances and bond angles causes the overlap of intersite charge transfer. As a result of these anomalous variations, the inherent hopping transfer processes lead to deviations in hopping times.

The second mechanism concerns the motion of the slower, immobile

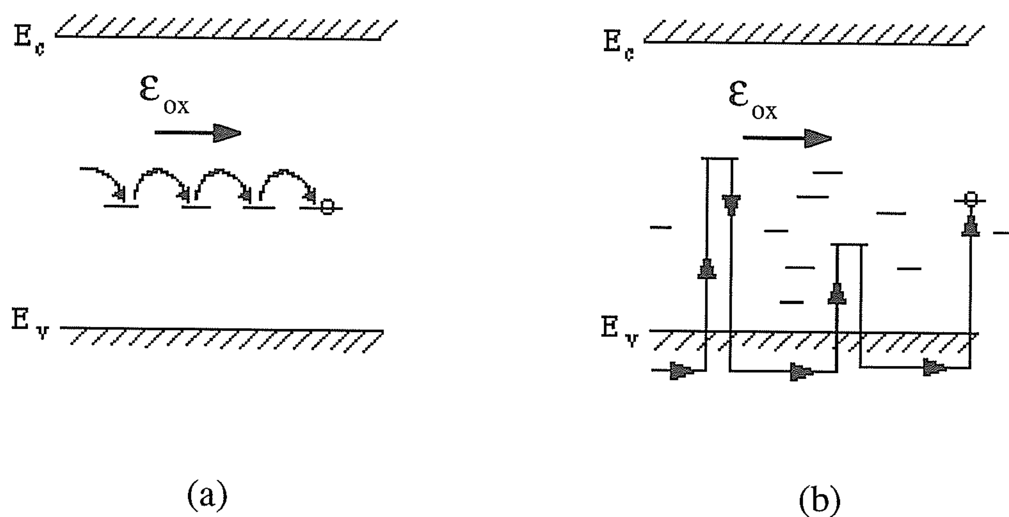

Fig. 2.2 Schematics diagrams illustrating two of the possible hole transport mechanisms within the SiO_2 bandgap: (a) hopping transport via direct hole tunneling between adjoining traps, (b) trap-mediated hole conduction process in valence band. (After McLean, Boesch Jr., and Oldham [15])

holes in which the movement is mediated by trapping through a sequence of multiple traps. Usually, the holes move via normal band conduction between the trapping events. The localized trap states are randomly distributed in energy E between the E_C (conduction band edge energy level) and the E_V (valence band edge energy level) as indicated in Fig. 2.2 (b). The variation in the trap energy level leads to the fluctuations in the thermal release rates from the traps. This results in stochastic transport as shown in Fig. 2.2 (b). These two mechanisms contribute to the dispersive nature of hole transport in SiO_2. They are the cornerstones for the formation of the radiation-induced defects in the SiO_2 bulk or at the Si-SiO_2 interface. These hole transport models describe how the various defects are created. The origins of the different defects are described in the next section.

2.1.2 Origins of the Radiation-Induced Defects in MOS Devices

The radiation damage in the MOS devices consists of three types of defects; they are the positive oxide charge, the interface traps, and the neutral bulk traps. The paths that lead to the formation of these individual defects may seem to be irrelevant at first glance; however detailed analysis proves them otherwise. Since electron-hole pairs are generated in SiO_2 upon irradiation, these carriers, along with those injected from the contacts through internal photoemission, will transport throughout the SiO_2 film according to the electric field at the time. We know that the mobile electrons are driven out of the oxide in a very short time. The holes remaining in the oxide are subjected to a further transport process as

described in the previous section. However, some holes which fall into traps inside the oxide during the transport process will be trapped there; others are captured by neutral bulk traps created during the ionizing radiation process, leading to the accumulation of trapped holes. This hole trapping event results in the formation of a net positive charge as illustrated in Fig. 2.3 [15]. Holes which have avoided trapping at this stage proceed to their normal transport process as they approach the Si-SiO_2 interface. Holes may also encounter electrons injected from the silicon substrate. In this case holes are subjected to a recombination process. The transporting holes may capture electrons from the Si substrate and create interface traps once they arrive at the interface. This clearly illustrates that the radiation-induced holes can be turned into positive oxide charge or interface traps depending on the eventual fate of those transporting holes.

The penetrating radiation also breaks up the bonding network of the SiO_2 film and leads to subsequent structural rearrangement. While some of the broken bonds may be able to restore their original status upon the initial electron-hole recombination process, others may remain broken and give rise to electrically active defects. These defects are the main source for the eventual build-up of various charges and associated traps depending on their location. For example, they can either serve as neutral trap sites for subsequent trapping of carriers (holes) in the SiO_2 bulk as described above or act as interface traps themselves at the interface. Moreover, the rupture of strained Si–O bonds located near the Si-SiO_2 interface can also result in the formation of interface traps because the non-bridging oxygen defects are easily diffused toward the interface [15, 24]. This leaves the dangling Si bonds behind, which subsequently form the interface traps. Besides the radiation-induced defects, there are the intrinsic ones located

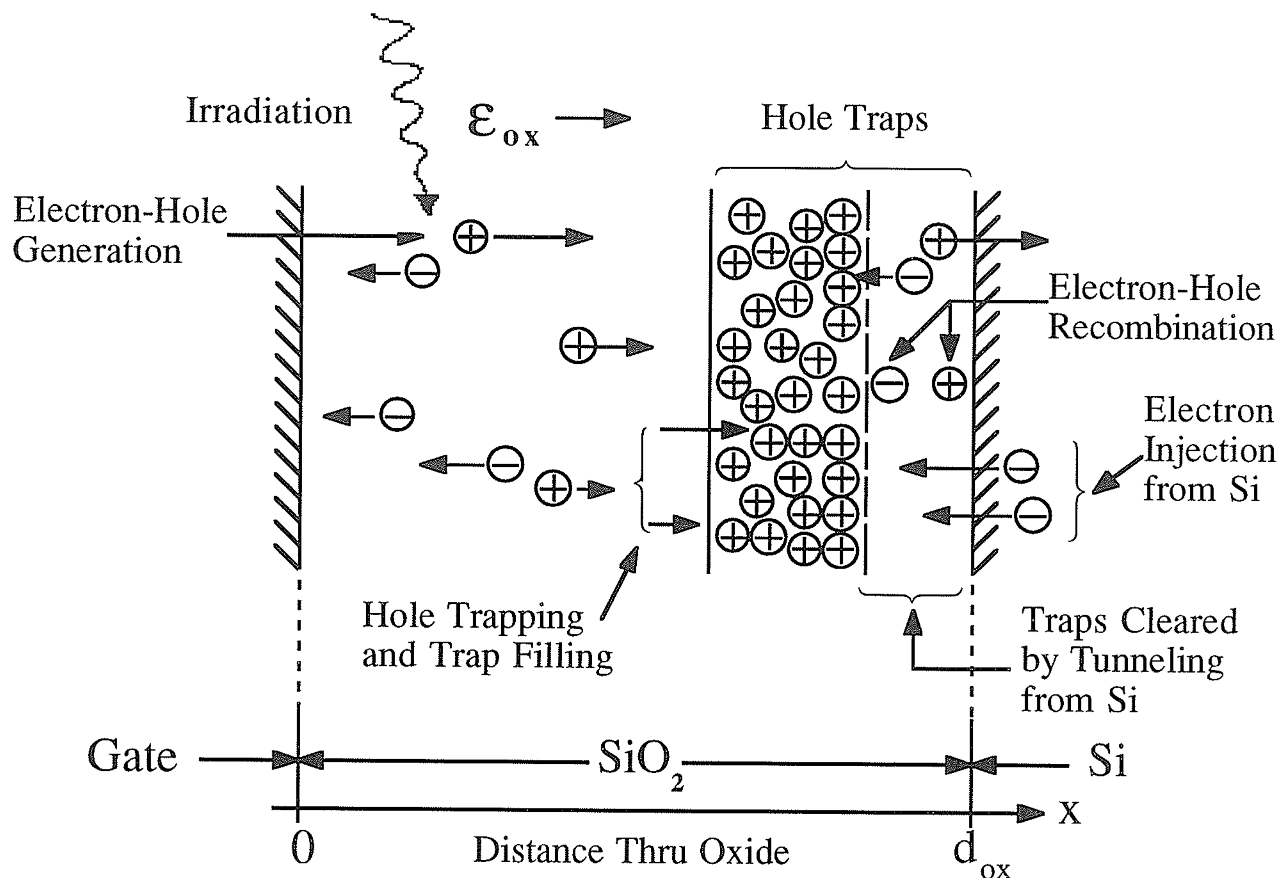

Fig. 2.3 Hole trapping and removal processes in an MOS device during irradiation. (After McLean, Boesch Jr., and Oldham [15])

inside the SiO_2 bulk or at the Si-SiO_2 interface. It has been reported [10, 16] that the relatively weak Si–H and Si–OH bonds are always present in SiO_2 and they are one of the main sources of impurities, because impurities such as hydrogen or hydroxyl groups could be released upon bond breaking activities. These impurities are very mobile within the SiO_2 film, and they can easily migrate to the Si-SiO_2 interface. Once they reach the interface, they can also break the Si–H bonds residing there. Hence, the dangling Si bonds are formed with either the H_2 or the H_2O as the by-products. The formation processes of the radiation-induced defects are summarized in Fig. 2.4.

2.2 Annealing of Radiation-Induced Defects

Thermal annealing is a commonly used technique to reduce the amount of defects and associated traps formed during the radiation of MOS devices. The exact mechanism is not clearly established but it is generally agreed that thermal energy is the key catalyst to promote and sustain the various reactions during annealing. Although the exact anneal reactions have not been identified and understood completely, there are two conclusive arguments which have been well documented in the literature. The first concerns the bond relaxation mechanism during annealing while the second relates to the hydrogenation of defects enhanced by annealing. These two mechanisms form the basis for the explanation of how radiation-induced charges and trap sites are compensated and passivated during the annealing process. These two mechanisms are used to explain the reduction of the radiation-induced positive oxide charge and interface trap density.

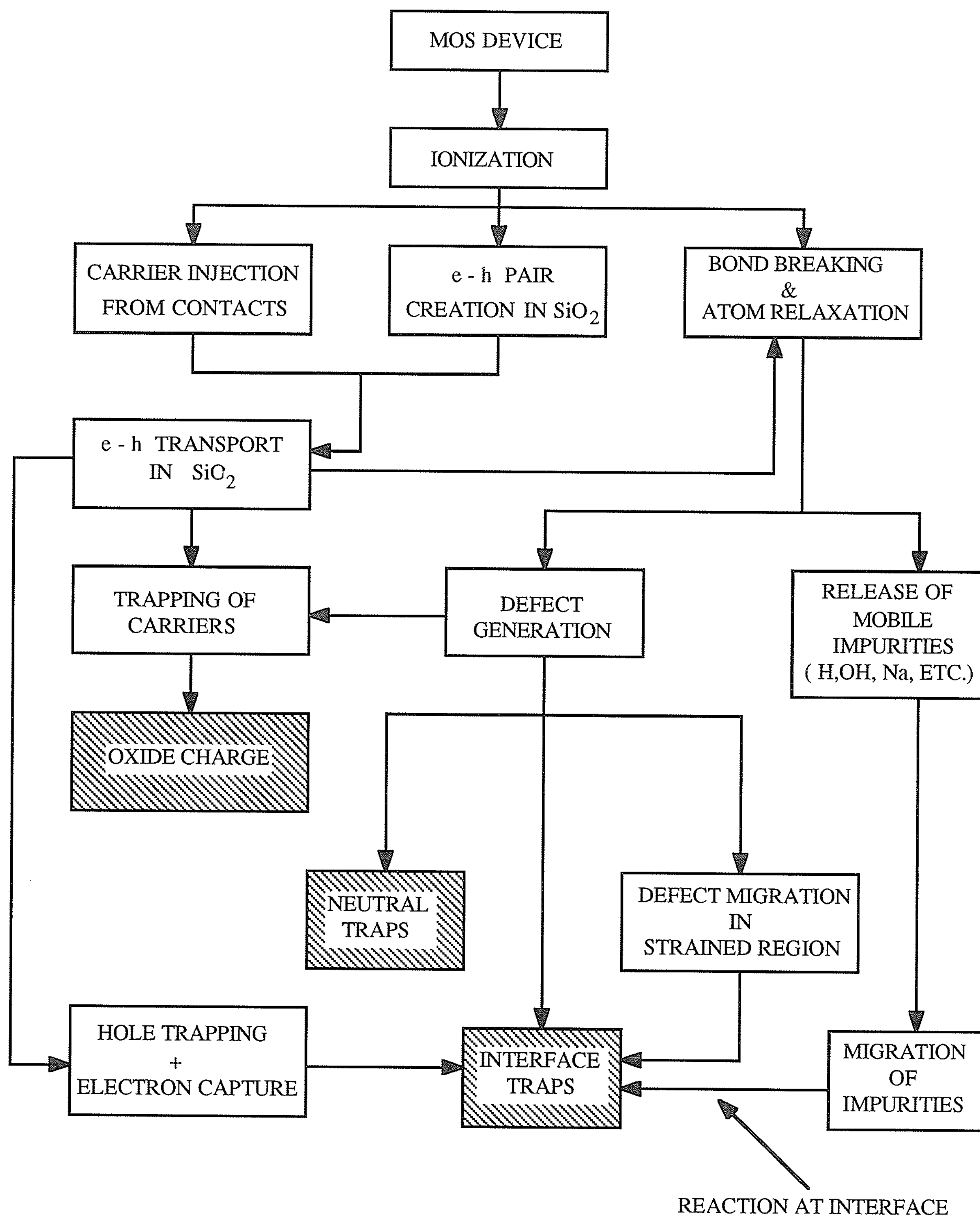

Fig. 2.4 Illustrating the creation of oxide charge, neutral traps, and interface traps due to ionizing radiation in MOS devices. (After Ma [13])

2.2.1 Relaxation of Strained Bonds

The thermal annealing model is based on the hypothesis that annealing tends to relieve the stress induced on the Si–O strained bonds at the Si-SiO_2 interface by a high temperature oxidation process [24-27]. These strained bonds located at the Si-SiO_2 interface are caused either by the lattice mismatch between the Si substrate and the SiO_2 film (intrinsic stress), or by the differences in the thermal expansion coefficients between the two materials (extrinsic stress). As a result, the annealing action can reduce the defects and related traps located at this strained region near the Si-SiO_2 interface through a thermal reorientation process [24]. This implies that it heals the strained bonds. Figures 2.5 (a) and (b) show schematically the bonding arrangement of the SiO_2 lattice network and its interface with the Si substrate before and after the annealing process, respectively. It can be seen that the dislocations of the Si–O bonds at the Si-SiO_2 interface region during the oxidation process make the Si–O bonds to stretch tightly to match the silicon lattice. Since the stress on these strain bonds is being applied either intrinsically or extrinsically, the distortions of the Si–O bonds appear throughout the interfacial region indiscriminately so as to match the silicon lattice. However, the strained Si-O bonds are relieved and rearranged after annealing as shown in Fig. 2.5 (b), because the heat treatment relaxes the stress on the SiO_2 lattice network and the Si-SiO_2 interfacial region through the thermal vibration of atoms. This thermal annealing process thus eliminates the bond distortions.

Ionizing radiation can penetrate the SiO_2 film and creates defects not only within the bulk, but also at the Si-SiO_2 interface. The purpose of annealing is to repair the bond rupture caused by the radiation. Thus, the

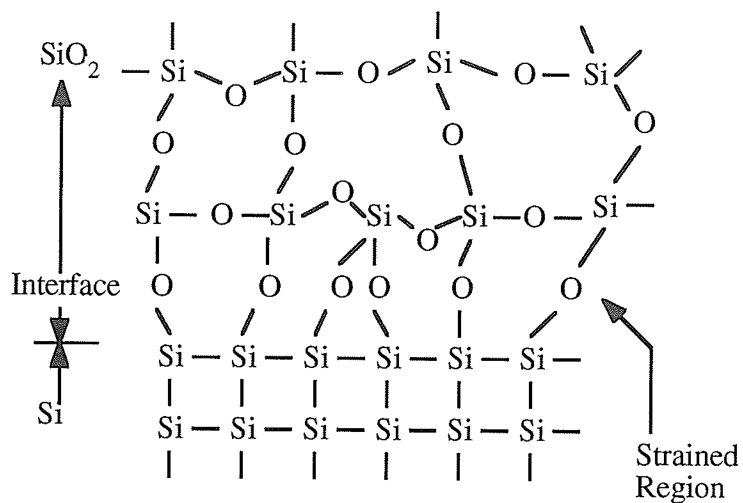

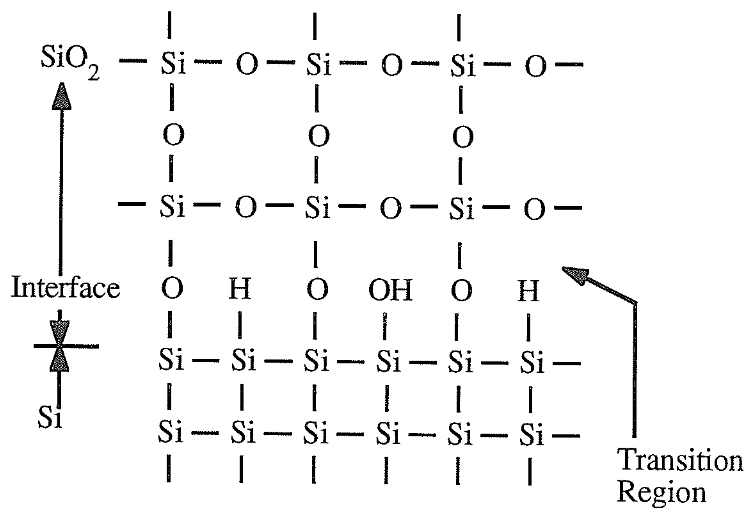

Fig. 2.5 Schematic diagrams of the Si-SiO_2 structure before and after annealing: (a) the dislocations and the stress incurred in the Si–O bonds before annealing; (b) the bond relaxation and reformation on the strained Si–O bonds after annealing. (After Schulz [28])

vacancies left between the broken Si–O bonds may be filled by other atoms that have been dislocated earlier. Also, the strained bonds between adjacent trap sites are annihilated again via lattice vibrations. The silicon dangling bonds are also known as the interface traps in which they all have an unpaired electron [24]. During annealing, neighboring dangling bonds may be paired thermally through the reorientation process [24, 28]. The same can be said for the oxide traps in which the non-bridging oxygen atoms responsible for trapping may be united through the lattice vibration process. This is because the vacancies created by bond rupture during ionizing radiation are filled by the atoms in the vicinity [24, 28]. The above arguments support the idea that thermal energy plays a vital role in accomplishing the annealing effects.

The radiation-induced defects residing near the Si-SiO_2 interface region are also passivated due to the diffusion of impurities, because impurities such as H and OH often found in SiO_2, may recombine with the trivalent silicon defects to form the electrically inactive Si-H and Si-OH bonds as shown in Fig. 2.5 (b) [10]. This chemical reaction forms the second argument regarding annealing mechanisms.

2.2.2 Hydrogenation of Defects

This second annealing mechanism relates the diffusion of hydrogen species to the Si-SiO_2 interface as a catalyst to activate the chemical reactions occurring there. The hydrogen sources may either come from the ambient introduced intentionally during the annealing process, or the moisture absorption by the SiO_2 surface in such a way that the hydroxyl (OH) group may act as an annealing agent [28]. The atomic hydrogen

released from the metal-SiO_2 interface is well recognized during post-metallization annealing (PMA) [29]. These mobile hydrogen species tend to diffuse to the Si-SiO_2 interface and react with the defects in the SiO_2 bulk or at the Si-SiO_2 interface.

Radiation-induced defects such as the positive oxide charge and the interface traps originate from the broken Si–O bonds due to the ionizing radiation. These defective bonds exist in the form of non-bridging oxygen hole centers ≡Si–O • (oxide hole traps), or as silicon dangling bonds ≡Si • (interface traps), in which "≡" denotes three back bonds with oxygens in the SiO_2 network and "•" denotes an unpaired electron. However, the arrival of the mobile hydrogen species enables the defects to be annihilated and restores the bonding network through the following processes:

$$\equiv\text{Si}\bullet + \text{H} \rightarrow \equiv\text{Si}:\text{H} \qquad (2.1)$$

$$\equiv\text{Si}^{+} + \text{OH}^{-} \rightarrow \equiv\text{Si}:\text{OH} \qquad (2.2)$$

$$\equiv\text{Si–O}\bullet + \text{H} \rightarrow \equiv\text{Si}:\text{OH} \qquad (2.3)$$

Processes (2.1) and (2.2) show that the dangling Si Bonds react with the hydrogen atom and the hydroxyl group to form the Si–H and the Si–OH bonds, respectively. Process (2.3) shows the reaction between the non-bridging oxygen hole center and the hydrogen atom, which produces the Si–OH bond. These reactions implies that hydrogen species are the key ingredients to passivate the defects so that the resulting products become electrically inactive in the MOS devices.

The hydrogenation effects described above confirms the importance of thermal energy in the annealing process. Basically, thermal energy serves

three main purposes: (1) it promotes the generation of active hydrogen species, most likely atomic hydrogen; (2) it enhances the diffusion of those hydrogen species; and (3) it drives the defect reaction processes. As a result, with the proper control of the annealing conditions such as the ambient and temperature, the electrically active defects can be passivated and deactivated during the annealing process.

References for Chapter 2:

[1] T. P. Ma and M. R. Chin, "RF Annealing in MOS Structures: An Experimental Simulation," *J. Appl. Phys.* **51**, 5458 (1980).

[2] M. R. Chin and T. P. Ma, "Voltage and Frequency Dependence of Simulated RF Plasma Annealing in MOS Structures," *Appl. Phys. Lett.* **40**, 490 (1982).

[3] T. P. Ma, Ionization Radiation Effects in SiO_2 and RF Plasma Annealing in *Semiconductor Silicon 1981*, R. Huff, R. Kriegler, and Y. Takeishi, Eds., Electrochem Soc., Pennington, N. J. 1981, p. 427-441.

[4] M. R. Chin, "RF Plasma Annealing on MOS Structures," Ph. D. Dissertation, Yale University, December 1981.

[5] J. Kassabov, E. Atanassova, D. Dimittrov, and E. Goranova, "Electrical Properties of Si-SiO_2 Structures Treated in Helium Plasma," *Microelectron. J.* **18**, 5 (1987).

[6] J. Kassabov, E. Atanassova, D. Dimittrov, and E. Goranova, "UV Radiation Effects of Argon Plasma on Si-SiO_2 Structures," *Microelectron. J.* **18**, 21 (1987).

[7] J. Kassabov, E. Atanassova, and D. Dimittrov, "Argon Plasma Treatment Effects on Si-SiO_2 Structures," *Solid-St. Electron.* **31**, 147 (1988).

[8] J. Kassabov, E. Atanassova, E. Goranova, D. Dimittrov and J. Vasileva, "Plasma Processing Effects on O_2–HCl Grown Si-SiO_2 Structures," *Solid-St. Electron.* **32**, 535 (1989).

[9] J. Kassabov, UV and Plasma Effects in the Si/SiO_2 System in *Insulating Films on Semiconductor 1991*, W. Eccleston and M. Uren, Eds., Adam Hilger, New York, 1991, p. 33-42.

[10] C. T. Sah, "Origin of Interface States and Oxide Charges Generated by Ionizing Radiation," *IEEE Trans. Nucl. Sci.* **NS-23**(6), 1563 (1976).

[11] L. M. Ephrath and D. J. DiMaria, "Review of RIE Induced Radiation Damage in Silicon Dioxide," *Solid State Technol.* **24**(4), 182 (1983).

[12] T. R. Oldham, F. B. McLean, H. E. Boesch Jr., and J. M. McGarrity, "An Overview of Radiation-Induced Interface Traps in MOS Structures," *Semicond. Sci. Technol.* **4**, 986 (1989).

[13] T. P. Ma, Historical Perspective in *Ionizing Radiation Effects in MOS Devices and Circuits*, T. P. Ma and P. V. Dressendorfer, Eds., John Wiley & Sons, New York, 1989, Ch. 1.

[14] D. B. Brown and N. S. Saks, "Time Dependence of Radiation Induced Interface Trap Formation in Metal-Oxide-Semiconductor Devices as a Function of Oxide Thickness and Applied Field," *J. Appl. Phys.* **70**, 3734 (1991).

[15] F. B. McLean, H. E. Boesch Jr., and T. R. Oldham, Electron-Hole Generation, Transport, and Trapping in SiO_2 in *Ionizing Radiation Effects in MOS Devices and Circuits*, T. P. Ma and P. V. Dressendorfer, Eds., John Wiley & Sons, New York, 1989, Ch. 3.

[16] A. G. Revesz, "Defect Structure and Irradiation Behavior of Noncrystalline SiO_2," *IEEE Trans. Nucl. Sci.* **NS-18**(6), 113 (1971).

[17] R. C. Hughes, "High Field Electronic Properties of SiO_2," *Solid-St. Electron.* **21**, 251 (1978).

[18] S. Othmer and J. R. Srour, "Electron Transport in SiO_2 Films at Low Temperature," in *The Physics of MOS Insulators*, G. Lucovsky, S. T. Pantelides, and F. L. Galeener, Eds., Pergamon Press, Elmsford, New York, 1980, p.49.

[19] E. W. Montroll and G. H. Weiss, "Random Walks on Lattices II," *J. Math. Phys.* **6**, 167 (1965).

[20] H. Scher and M. Lax, "Stochastic Transport in a Disordered Solid I. Theory," *Phys. Rev. B* **7**(10), 4491 (1973).

[21] H. Scher and E. W. Montroll, "Anomalous Transit-Time Dispersion in Amorphous Solids," *Phys. Rev. B* **12**(6), 2455 (1975).

[22] R. C. Hughes, "Time-Resolved Hole Transport," *Phys. Rev. B* **15**(4), 2012 (1977).

[23] F. B. McLean and G. A. Ausman, "Simple Approximate Solutions to Continuous-Time Random-Walk Transport," *Phys. Rev. B* **15**(2), 1052 (1977).

[24] C. T. Sah, "Models and Experiments on Degradation of Oxidized Silicon," *Solid-St. Electron.* **33**, 147 (1990).

[25] A. I. Akinwande and J. D. Plummer, "Quantitative Modeling of Si/SiO_2 Interface Fixed Charge I. Experimental Results," *J. Electrochem. Soc.* **134**, 2565 (1987).

[26] A. I. Akinwande and J. D. Plummer, "Quantitative Modeling of Si/SiO_2 Interface Fixed Charge II. Physical Modeling," *J. Electrochem. Soc.* **134**, 2573 (1987).

[27] T. P. Ma, Process-Induced Radiation Effects in *Ionizing Radiation Effects in MOS Devices and Circuits*, T. P. Ma and P. V. Dressendorfer, Eds., John Wiley & Sons, New York, 1989, Ch. 7.

[28] M. Schulz, "Interface States at the SiO_2-Si Interface," *Surface Sci.* **132**, 422 (1983).

[29] M. L. Reed, "Models of Si-SiO_2 Interface Reactions," *Semicond. Sci. Technol.* **4**, 980 (1989).

Chapter 3

Experimental Procedures and Characterization Techniques

This chapter begins with describing the experimental steps required for fabrication of MOS devices. This includes the silicon substrate cleaning processes and the subsequent oxide fabrication steps, and the metallization process. After that, the plasma radiation procedures and subsequent annealing treatments will be discussed in some detail.

We have measured the optical emission spectra (OES) of the N_2O plasmas and used the capacitance-voltage (C-V) method to measure the change of the interface trap density (D_{it}) and oxide charge density (Q_o) and hence to evaluate the variations of defect concentration before and after plasma radiation. These characterization techniques are also briefly described in the following sections.

3.1 Silicon Substrate Cleaning Processes

The silicon substrates were n-type, (100)-oriented, 2-8 Ω-cm. We used the RCA standard clean method [1] to clean the silicon substrates prior to the fabrication of SiO_2 films. The cleaning chemistry of the RCA standard clean was originally developed by Kern and Puotinen [2] regarding the cleaning solutions for silicon semiconductor technology. Recently, Kern

modified the cleaning methods based on his research in this area, and his modified method was used for this investigation.

The RCA standard clean is a two-step oxidizing treatment with hydrogen peroxide solutions. The two-step treatment consists of an alkaline mixture at high pH followed by an acidic mixture at low pH, and this is the basic framework for the RCA standard clean. The first step in the cleaning procedures starts with immersing the silicon substrates in a mixture of deionized water, and MOS electronic grade H_2O_2 and NH_4OH solutions. The volume ratio of H_2O:H_2O_2:NH_4OH is 5:1:1 The silicon substrates are then subjected to a second immersion in a mixture of deionized water, and MOS electronic grade H_2O_2 and HCl solutions. The volume ratio of H_2O:H_2O_2:HCl for the second solution is 6:1:1. These two steps are known as the standard clean 1 or SC-1 and the standard clean 2 or SC-2. The immersion time is 10 min at 75–80 °C in each of the solutions.

Following each treatment, the substrates are rinsed in flowing deionized water with resistance of 17.6 MΩ-cm to remove out any solid particulate that might reside on the silicon substrate surface. Subsequently, the substrates are subjected to a HF etching treatment by immersing them in a 100:1 H_2O:HF solution for 30 sec. This treatment not only removes the hydrous oxide film formed immediately after each SC-1 and SC-2 step, but also makes the substrate surfaces hydrophobic so that the moisture content on the surfaces can be minimized [1, 3].

3.2 SiO_2 Film Fabrication Processes

After the cleaning procedures, the silicon substrates were ready for oxide fabrication. Two different techniques were employed for the fabrication of the SiO_2 films; they were: (1) the thermal oxidation and (2) the plasma-enhanced chemical vapor deposition (PECVD). Since the oxides fabricated from these two methods were structurally different, it is interesting to see whether the growth mechanism might play a role in the sensitivity of the MOS devices to the ionizing radiation. In the following, we will describe these two methods separately.

3.2.1 Thermal Oxidation

Thermal oxidation is a growth technique based on mainly the diffusion of the oxidizing species into the silicon substrate surface. The SiO_2 films are generally grown on the silicon surface. With the rupture of the Si-Si bonds on the silicon surface through thermal activation, the oxidants react with the Si following the reaction:

$$Si + O_2 \xrightarrow{\text{thermal energy}} SiO_2 \qquad (3.1)$$

The thermal SiO_2 films used in this experiment were grown in dry oxygen at 1100 °C. Before the silicon substrates were loaded into the diffusion furnace for thermal oxidation, a droplet (~ 2 ml) of HCl was placed onto the quartz boat that held the substrates. The boat was immediately placed inside the quartz tube in the furnace. Dry oxygen was

then used to flush the quartz tube for about 30 min. This was the pre-clean procedure for the quartz tube before the thermal oxidation of silicon substrates actually to take place. The addition of HCl to the oxidation ambient is known to prevent the occurrence of oxidation-induced stacking faults [4] and to reduce the transition metal contamination [5, 6] in the on-growing SiO_2 film. This is because the Cl atoms introduced intentionally would react with the Na atoms in the chamber, thus lowering the possibility of sodium contamination.

After the completion of the pre-clean step, the silicon substrates were placed onto the quartz boat. The oxidation process took place at 1100 °C and dry oxygen was fed continuously to quartz tube inside the furnace at the same time. The oxidation process was terminated when the desired oxide thickness had been grown. For this investigation, the SiO_2 films were grown with thicknesses varying from 200 to 1000 Å. Following oxidation, the oxidized samples were quickly (~ 5 sec) removed from the hot zone area to a cool area and cooled there for 30 min. They were then taken out of the furnace for next processing.

3.2.2 Plasma-Enhanced Chemical Vapor Deposition

The PECVD technique used for this investigation involves magnetic confinement of the energetic particles (electrons and ions) generated by the microwave gas plasmas. The advantage is that the energy required for producing a given plasma can be reduced to a minimum at the electron-cyclotron-resonance (ECR) condition [7]. The interactions among the energetic particles from the microwave gas plasmas of the gas mixture of SiH_4 and an oxidant such as N_2O or O_2, follow the chemical reactions:

$$N_2O \xrightarrow{\text{dissociation}} N_2 + O \quad (3.2)$$

$$SiH_4 + 2O \rightarrow SiO_2 + 2H_2 \quad (3.3)$$

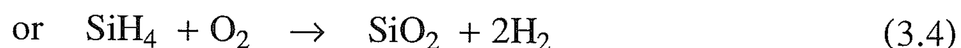

or $$SiH_4 + O_2 \rightarrow SiO_2 + 2H_2 \quad (3.4)$$

These reactions indicate that SiO_2 film would be deposited onto the silicon substrate surface. In this case, the SiO_2 is grown layer by layer on the substrate surface. In thermal oxidation, the silicon substrate plays a direct role during the oxidation process, because the silicon reacts directly with the oxidizing agents to grow SiO_2 film onto the silicon surface.

The PECVD films were deposited using the ECR microwave plasma processing reactor developed in the Materials and Devices Research Laboratory at the University of Manitoba. This plasma reactor is shown in Fig. 3.1. The details of this reactor have been published elsewhere [7, 8]. The typical deposition parameters for the PECVD process are: a gas mixture of 10 % SiH_4 and N_2O with a flow ratio of 10:1 N_2O:SiH_4 sccm. The magnetic field for the ECR condition was 875 G with the microwave absorption power being 6 W at a frequency of 2.45 GHz. Typical substrate temperature was held at 300 °C and the deposition time was used to control the deposited film thickness. The usual deposition procedure began with loading the silicon substrates into the processing chamber and they were placed on the floor of the chamber. The silicon substrates were positioned

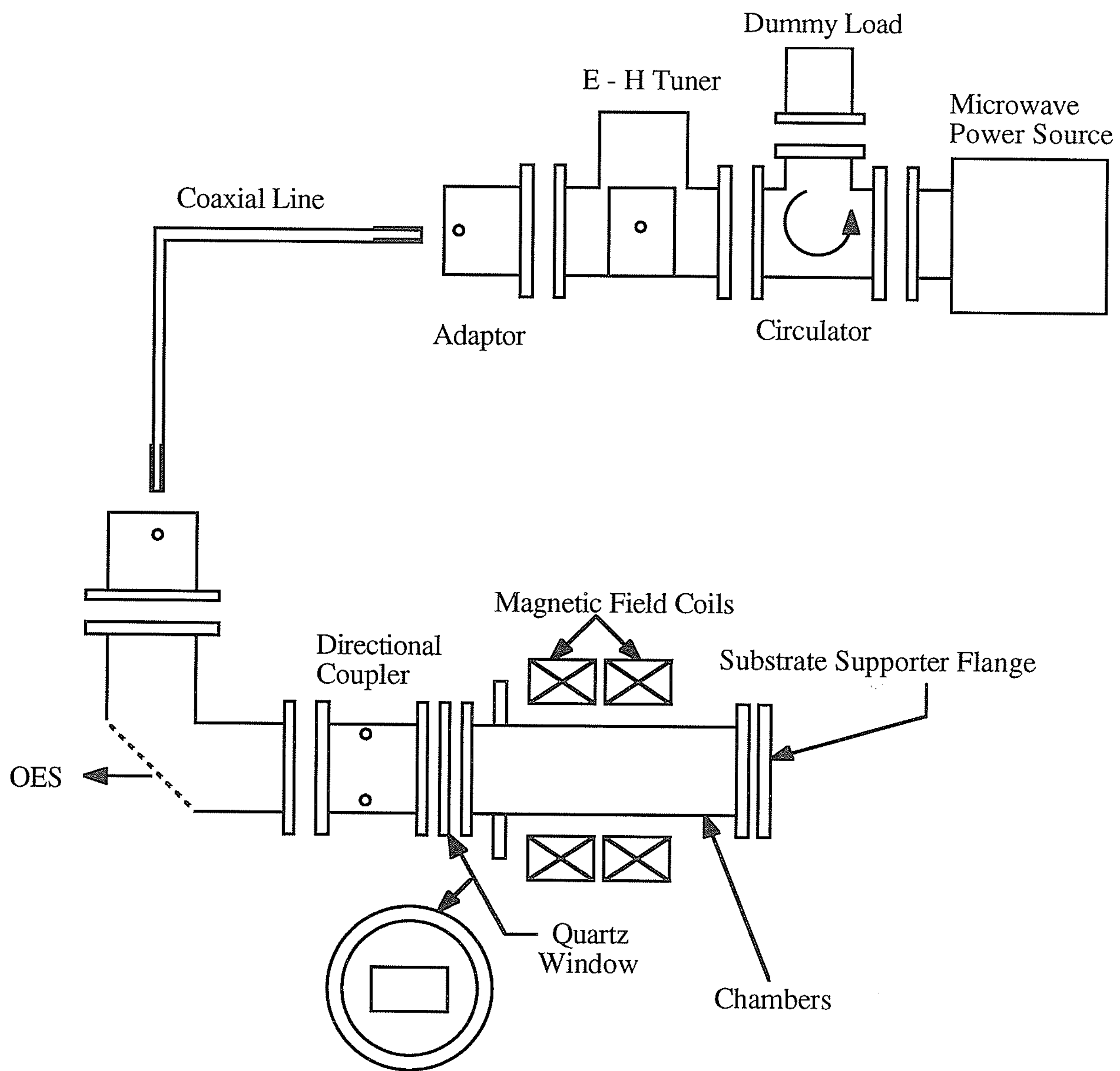

Fig. 3.1 ECR plasma reactor system (After Chau, Mejia, and Kao [7])

positioned in front of the "species selector and energy controller" (SSEC) [7] as shown in Fig. 3.2. The chamber pressure was about 1 mTorr. After the completion of the deposition process, the samples were unloaded for further processing.

3.3 Metallization Process

Thermal oxidation would also produce a SiO_2 film on the back of the silicon substrate. This SiO_2 film must be removed before an aluminum (Al) electrode is deposited on the silicon surface. This unwanted SiO_2 film is removed by an HF etching step using 100:1 H_2O:HF solution as etchant. In the PECVD technique, the SiO_2 film is deposited on the front side of the silicon substrate. Thus, such an etching step is not required.

After the necessary etching step had been completed, the samples were immediately loaded into a vacuum chamber for metallization. There are two metallization steps required for the fabrication of MOS devices and they are the gate electrode and the back contact. The Al films were thermally evaporated on the back of the silicon substrates first under a vacuum of 10^{-6} Torr. The second metallization step was conducted on the SiO_2 surface to form an MOS device. Again this was performed at 10^{-6} Torr onto the SiO_2 through a shadow mask to form 5×10^{-3} cm^2 area gate electrodes in circular shape. Both the back contacts and gate electrodes had thicknesses of about 1000 Å. This metallization process is the final step for the fabrication of MOS devices.

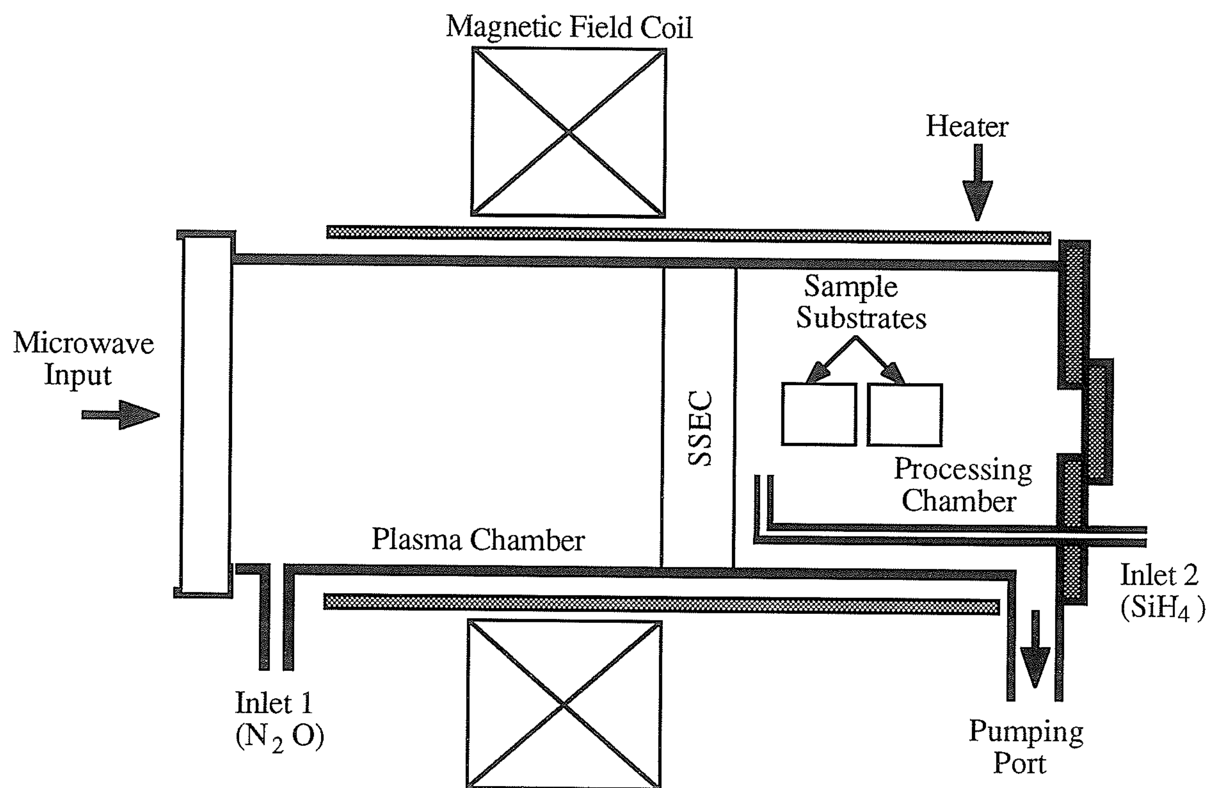

Fig. 3.2 Schematic diagram of the plasma chamber and the processing chamber. (After Chau, Mejia, and Kao [7])

3.4 Plasma Radiation Process

The plasma radiation was conducted in the same plasma reactor system as shown in Fig. 3.1. However, this time only N_2O gas was used to create the gas plasma as a radiation source. N_2O gas is often used in the PECVD process to deposit SiO_2 films [7-12]. Generally, the deposited SiO_2 films have some radiation damage such as a high density of interface traps (10^{12}–10^{13} cm^{-2} eV^{-1}). To understand the cause of such damage, we therefore study the effect of the N_2O plasma alone on the thermal and PECVD SiO_2 films. This also enables us to determine if the ultraviolet (UV) radiation from the processing plasmas is the main radiation source responsible for radiation damage, because UV light is the dominant light emitted from the N_2O plasma.

In order to find the defect generation mechanism, we used the same deposition parameters for plasma radiation. Thus, the N_2O plasma was produced at a microwave frequency of 2.45 GHz with the magnetic field at 875 G under the ECR condition. The chamber pressure was maintained at 10–11 mTorr so that the flow rate of the N_2O gas could be set at 10 sccm. The absorbed power was about 6 W. The duration of plasma radiation process determines the rate of defect generation as shown in Fig. 3.3. The oxide films of the MOS devices are 465 Å thick for thermal SiO_2 with the device temperature at 25 °C during plasma radiation. The D_{it} value increases from 8.3×10^{12} to 1.5×10^{13} cm^{-2} eV^{-1} for radiation times from 1 to 5 min, respectively. However, further increase in radiation time does not cause significant change in D_{it}. The value of D_{it} saturates at about 2×10^{13} cm^{-2} eV^{-1}. We chose the radiation time of 30 min throughout the plasma radiation processes, in order to ensure that the rate of defect

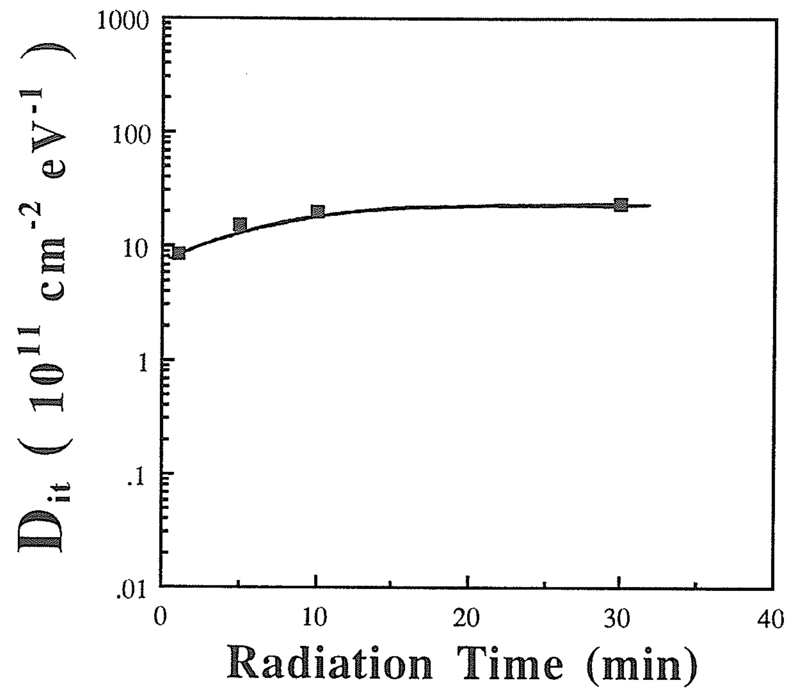

Fig. 3.3 Midgap D_{it} as a function of radiation time for the MOS devices with thermal SiO_2 films of 465Å in thickness.

generation does not play an important role in determining the radiation damage.

As for the device temperature during irradiation, we used four different temperatures: room temperature (~ 25 °C), 100 °, 200 °, and 300 °C. At room temperature, we used the devices with thermal SiO_2 film thicknesses of 228, 323, 465, 571, 741, and 941Å. All the SiO_2 film thicknesses were measured using the capacitance method [13]. For device temperatures higher than 100 °C and beyond, we used only two SiO_2 film thicknesses and they were 228 Å and 941 Å. Also at device temperature of 300 °C, we studied the MOS devices with the PECVD SiO_2 films at a thickness of 941 Å. Table 3.1 summarizes the combinations of the various parameters for the plasma radiation experiments.

Four different test structures were used for each radiation experiment. After the SiO_2 film fabrication process, the Si-SiO_2 structure was evaporated with Al contact and it was subsequently cut into four pieces. Two pieces were subjected to the Al gate electrode deposition process, while the other two pieces remained bare without gate electrode. Each piece contains 15–20 MOS devices after metallization and is about 1 cm^2. The two pieces with the Al gate electrodes are called the "electrode" and "anneal" samples, while the other two without Al gate electrode are called the "mask"and "bare" samples.

The anneal sample was annealed prior to plasma radiation in order to investigate whether this processing step has a radiation-hardening effect. The electrode sample was just irradiated for comparison purposes. For the mask sample, Al gate electrodes were deposited through a shadow mask in which the shadow mask was not removed from the test structure. The whole structure was then loaded into the plasma processing chamber for

Table 3.1 The combinations of various parameters for the plasma radiation experiments.

Device Temperature (°C)	Thermal SiO_2 Film Thickness (Å)					
	228	323	465	571	741	941
25	√	√	√	√	√	√
100	√	–	–	–	–	√
200	√	–	–	–	–	√
300	√	–	–	–	–	√ *

* This experimental condition used also for the radiation experiment for the MOS devices with PECVD SiO_2 films.

radiation experiment. The main purpose of using the mask is to shield the oxide areas from the plasma radiation so that UV radiation is the only radiation source that can penetrate the Al gate electrode to the SiO_2 film underneath. The bare sample was irradiated so that by comparing with those having Al gate electrodes, the electrode shielding effects can be examined based on the differences in the amount of radiation damage generated. Figures 3.4 (a)–(d) show the schematic diagrams of these four different samples.

The plasma radiation experiments began with loading the MOS devices into the plasma processing chamber as shown in Fig. 3.2. The devices were positioned underneath the magnetic field coil. Since the SSEC was removed, the microwave plasma was in direct contact with the devices. The radiation process proceeded according to the operating parameters described above for all devices for this investigation. During plasma radiation, no bias was applied to the MOS devices, thus the devices being subjected only to the oxide fields at that time. Once the radiation process was completed, the devices were taken out of the chamber for characterization.

3.5 Annealing Process

The annealing treatment after the metallization process was conducted in a forming gas (10% H_2 in N_2) ambient at 400 °C for 30 min in a diffusion furnace. It was generally referred to as the post-metallization-anneal (PMA). This treatment was used as a method to reduce interface traps and to partially lower the oxide charge density [5, 13]. The PMA treatment began with passing the forming gas through the furnace chamber

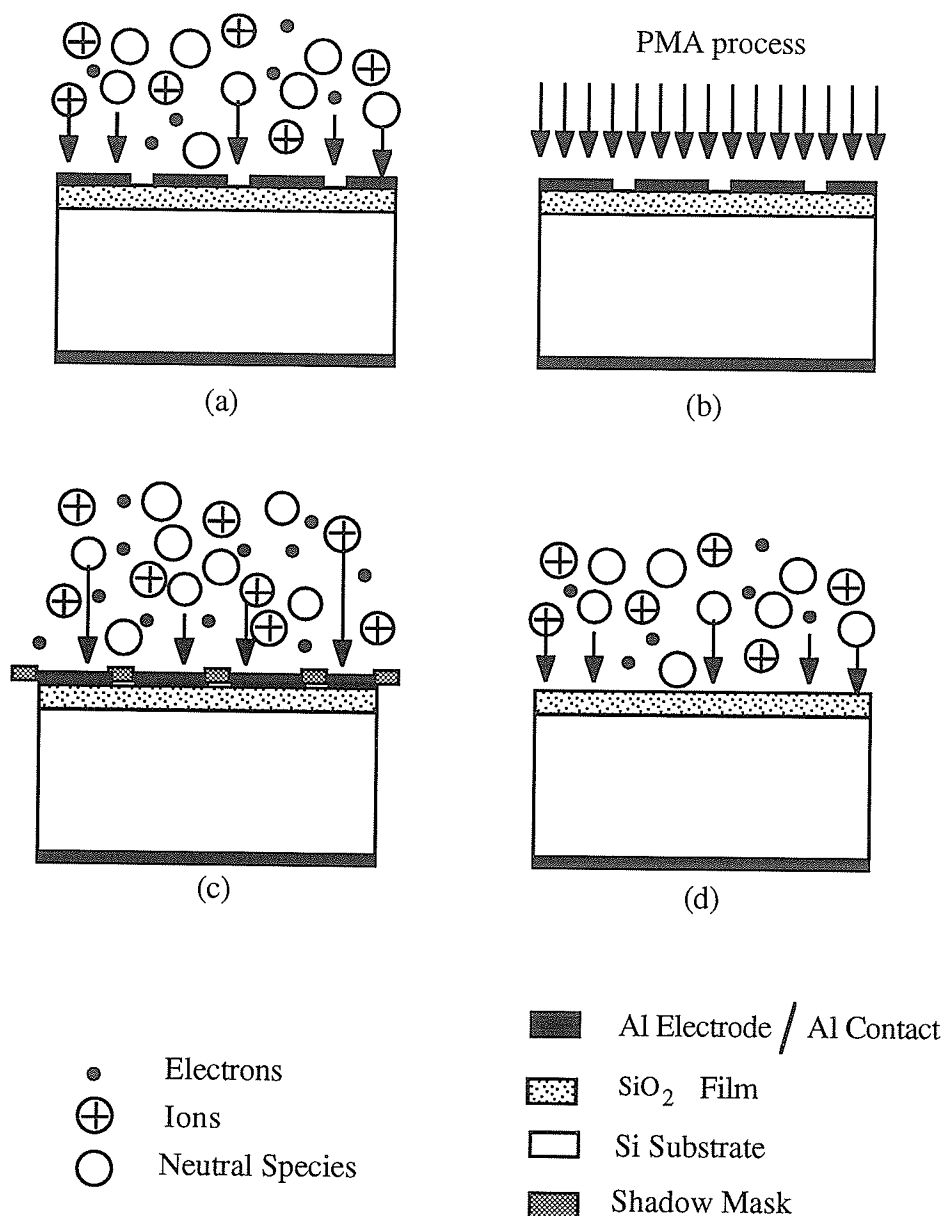

Fig. 3.4 The cross-sections of the four test structures. (a) electrode sample, Al-SiO_2-Si (MOS) structure during plasma radiation; (b) anneal sample, Al-SiO_2-Si (MOS) structure annealed in forming gas (PMA) prior to plasma radiation; (c) mask sample, Al-SiO_2-Si (MOS) structure covered by a shadow mask during plasma radiation; (d) bare sample, Si-SiO_2 structure during plasma radiation.

and allowing it to flow for about 15 min in order to minimize the amount of dust particles inside the chamber. The MOS devices were loaded onto a quartz boat and properly positioned so that the devices were at 400 °C inside the quartz tube chamber. As the annealing process came to an end, the quartz boat was quickly (~ 5 sec) pulled out of the high temperature region to the low temperature region for cooling. Cool down time was 60 min. The same annealing process was used for all devices whenever needed for annealing treatment. After plasma radiation, the electrode, mask, bare, and anneal samples underwent the same PMA process to study the annealing effects on the radiation-induced damage and other defects.

3.6 Characterization Techniques

We used the optical emission spectra (OES) to identify the kind of species in the microwave N_2O plasma, and used the capacitance-voltage (C-V) method to measure the concentration of defects in the MOS devices before and after plasma radiation and ensuing annealing treatment. The defects to be determined are mainly the interface traps and the oxide charges. The radiation-induced neutral traps cannot be detected by the usual steady-state measurements such as the C-V method. The neutral traps generally do not affect the device performance unless the charge carriers are introduced to the oxide and become trapped.

3.6.1 Optical Emission Spectrometry Technique

As shown in Fig. 3.1 earlier, the axial optical emission from the plasma was sampled through a quartz window. A set of quartz lenses and mirrors were used to focus the emitting light on a 25 μm slit of a Jarrell-Ash Monospec 27 spectrometer. It was equipped with a 1200 groove/mm grating and 1024 diode array EGG-PARC multichannel analyzer. The OES is usually taken at the chamber operating pressure, which is in the range of 10^{-1}–10^{-3} Torr. The OES provides information about species in the plasma.

3.6.2 Capacitance-Voltage Method

The high frequency (1 MHz) and the quasi-static C-V characteristics were measured at room temperature with a Booton 72AD capacitance meter, a Keithley 610C electrometer, a HP 7035B X-Y recorder, and a HP 4140B pA-meter/DC voltage source. Figure 3.5 illustrates the experimental set-up for the C-V measurements. The MOS devices were usually placed inside a probe box in which a probe tip was adjusted to make contact with the Al gate electrodes of the devices. The C-V curves were plotted using the X-Y recorder by applying a voltage bias ramped from + 4 V to – 4 V on these devices with the ramp rate of 50 m V s^{-1}. The interface trap density and the oxide charge density could be evaluated according to the changes in the "flat-band shifts" and the "stretch out" of the C-V curves. The methods for extracting the values of D_{it} and Q_o are given in Appendix A.

In this investigation, we checked the yield of each sample before C-V measurements were recorded by measuring the breakdown current. The

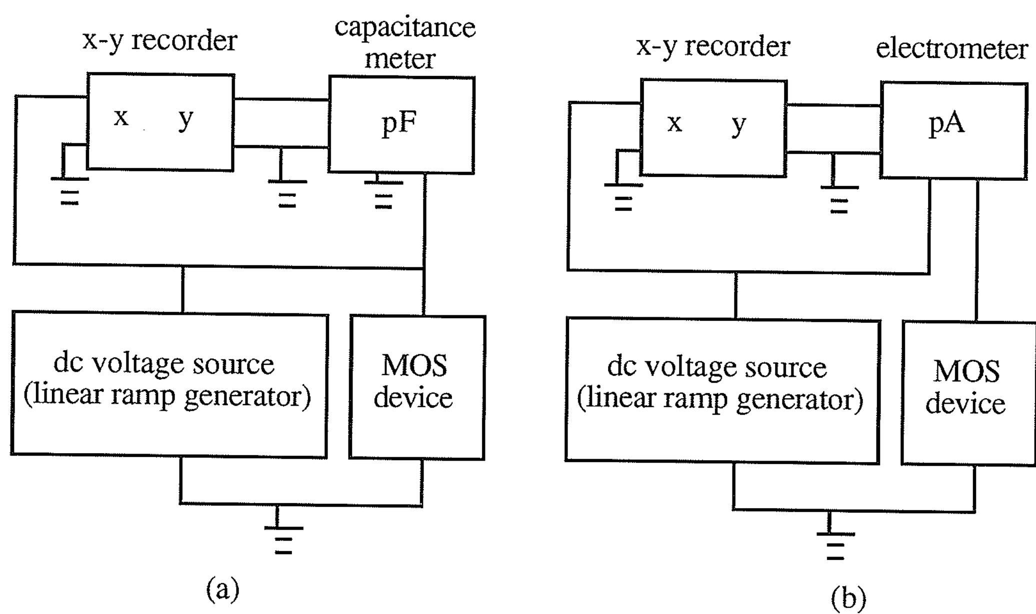

Fig. 3.5 Schematic diagrams of the experimental set-up for C-V measurements. (a) high frequency C-V measurement; (b) quasi-static C-V measurement.

yield of the MOS devices is about 50 % in general for all samples. We had measured two C-V measurements for each sample before and after each processing step. Figure 3.6 summarizes the overall experimental procedures for all the plasma radiation experiments.

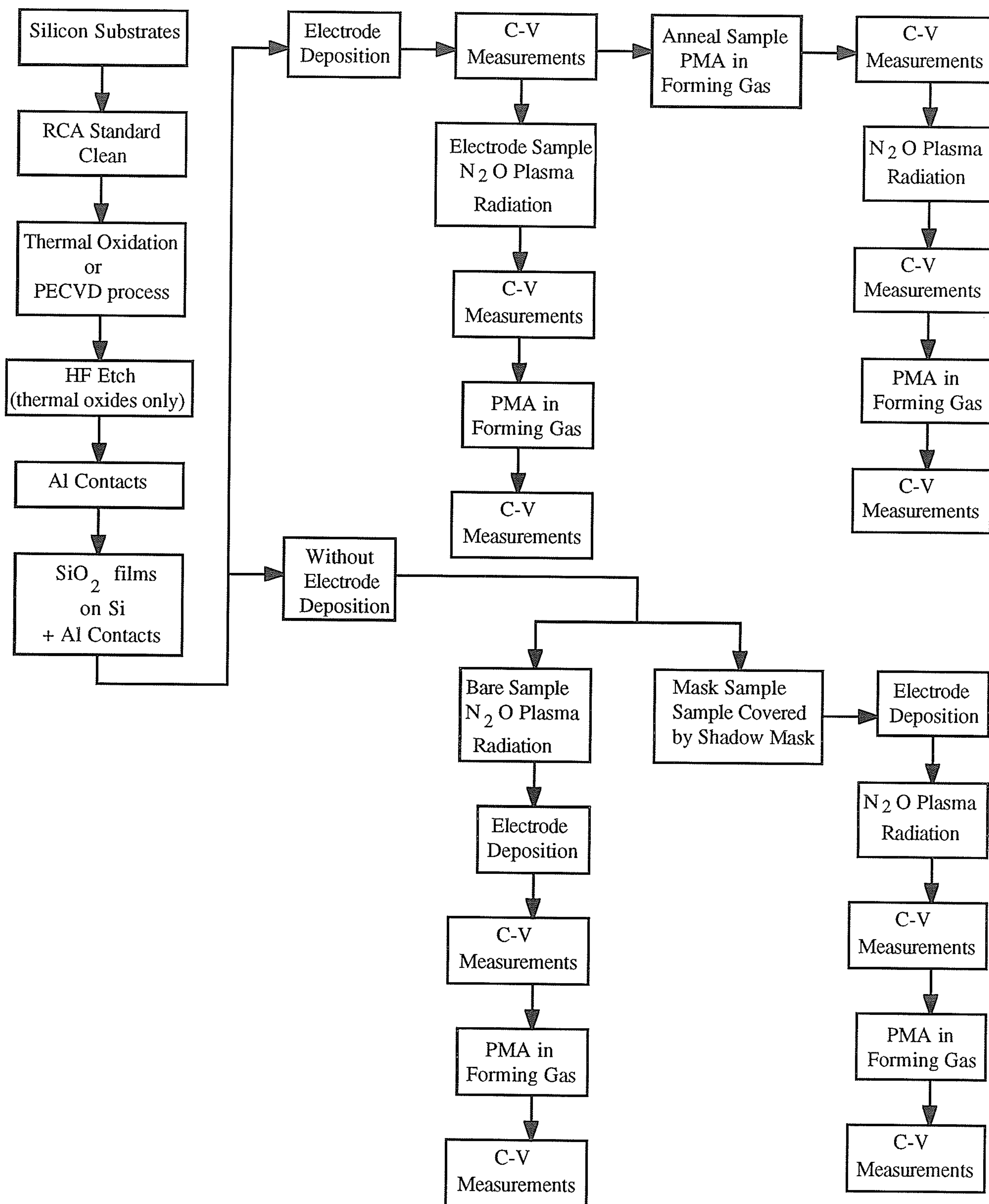

Fig. 3.6 The overall experimental procedures for all the radiation experiments.

References for Chapter 3:

[1] W. Kern, "The Evolution of Silicon Wafer Cleaning Technology," *J. Electrochem. Soc.* **137**, 1887 (1990).

[2] W. Kern and D. A. Puotinen, "Cleaning Solutions Based on Hydrogen Peroxide for use in Silicon Semiconductor Technology," *RCA Rev.* **31**, 187 (1970).

[3] S. A. Bell and D. W. Hess, "Radiation Damage to Thermal Silicon Dioxide Films in Radio Frequency and Microwave Downstream Photoresist Stripping Systems," *J. Electrochem. Soc.* **139**, 2904 (1992).

[4] S. P. Murarka, H. J. Levinstein, R. B. Marcus, and R. S. Wagner, "Oxidation of Silicon without the Formation of Stacking Faults," *J. Appl. Phys.* **48**, 4001 (1977).

[5] R. R. Razouk and B. E. Deal, "Dependence of Interface State Density on Silicon Thermal Oxidation Process Variables," *J. Electrochem. Soc.* **126**, 1573 (1979).

[6] J. Ruzyllo, "Preoxidation Surface Treatment in Thermal Oxidation of Silicon," in *The Physics and Chemistry of* SiO_2 *and the Si-*SiO_2 *Interface*, C. Helms and B. E. Deal Eds., Plenum Press, New York, 1988, pp 391-400.

[7] T. T. Chau, S. R. Mejia, and K. C. Kao, "New Approach to Low Temperature Deposition of High-Quality Thin Films by Electron Cyclotron Resonance Microwave Plasmas," *J. Vac. Sci. Technol. B* **10**(5), 2170 (1992).

[8] T. T. Chau, S. R. Mejia, and K. C. Kao, Canadian Patent Pending 2029518, 1990.

[9] J. Batey and E. Tierney, "Low Temperature Deposition of High-Quality Silicon Dioxide by Plasma-Enhanced Chemical Vapor Deposition," *J. Appl. Phys.* **60**, 3136 (1986).

[10] J. Batey, E. Tierney, J. Stasiak, and T. N. Nguyen, "Plasma-Enhanced CVD of High Quality Insulating Films," *Appl. Surface Sci.* **39**, 1 (1989).

[11] T. V. Herak and D. J. Thomson, "Effects of Substrate Temperature on the Electrical and Physical Properties of Silicon Dioxide Films Deposited from Electron Cyclotron Resonant Microwave Plasmas," *J. Appl. Phys.* **67**, 6347 (1990).

[12] R. A. B. Devine, "Defect Reactivation and Structural Relaxation in Deposited Amorphous SiO_2," *J. Appl. Phys.* **70**, 3542 (1991).

[13] E. H. Nicollian and J. R. Brews, *MOS (Metal Oxide Semiconductor) Physics and Technology*, John Wiley & Sons New York (1982).

Chapter 4

Experimental Results and Discussion

This chapter documents the experimental results about the radiation effects in MOS devices. The interface trap density (D_{it}) and the oxide charge density (Q_o) of the devices were measured under various experimental conditions. The typical effects of N_2O plasma radiation on the MOS devices will be discussed first and then followed with the effects of the SiO_2 film thickness, the device temperature, and the type of oxide film fabrication method during irradiation. The effects of post-metallization-anneal (PMA) treatment after radiation will also be studied. All results can be explained in terms of the bond strain gradient and the recombination-enhanced defects reactions models.

4.1 Plasma Radiation and Annealing Effects in MOS Devices

This section describes the typical radiation effects in MOS devices. The change of the measured C-V characteristics is used as the indication of the effects of plasma radiation and the subsequent annealing.

4.1.1 Plasma Radiation Effects

The value of D_{it} of the MOS devices increases after the N_2O plasma radiation. At the same time, either positive or negative charges can be observed in these devices. This depends on the pre-radiation treatment and the structure of the MOS devices during irradiation. Figure 4.1 shows the high frequency (HF) and the quasi-static (QS) C-V curves of a bare sample. This sample has a SiO_2 film thickness of 941 Å. It was irradiated at a device temperature of 25 °C. The HF C-V curve is stretched out while the QS C-V curve becomes flattened after plasma radiation. This indicates a significant increase in D_{it} due to the accumulation of interface traps at the Si-SiO_2 interface. The D_{it} is about 2×10^{13} cm^{-2} eV^{-1}. It can also be seen that the HF C-V curve is shifted to the positive voltage axis implying that negative charges are created because of electron trapping by the oxide traps. The amount of Q_o is at -2×10^{11} q cm^{-2}.

4.1.2 Annealing Effects

After the MOS devices have been subjected to radiation, most of the radiation-induced defects can be removed by annealing the devices in a forming gas at 400 °C as shown in Fig. 4.1. The distortions in both the HF and the QS C-V curves have been eliminated after a PMA treatment, indicating that the D_{it} has been reduced from 2×10^{13} cm^{-2} eV^{-1} to about 1×10^{10} cm^{-2} eV^{-1}. Also, the HF C-V curve shows a shift to the left compared to the one after plasma radiation, indicating a reduction of the negative Q_o. The Q_o has been reduced from -2×10^{11} q cm^{-2} to -5×10^{10} q cm^{-2} after annealing.

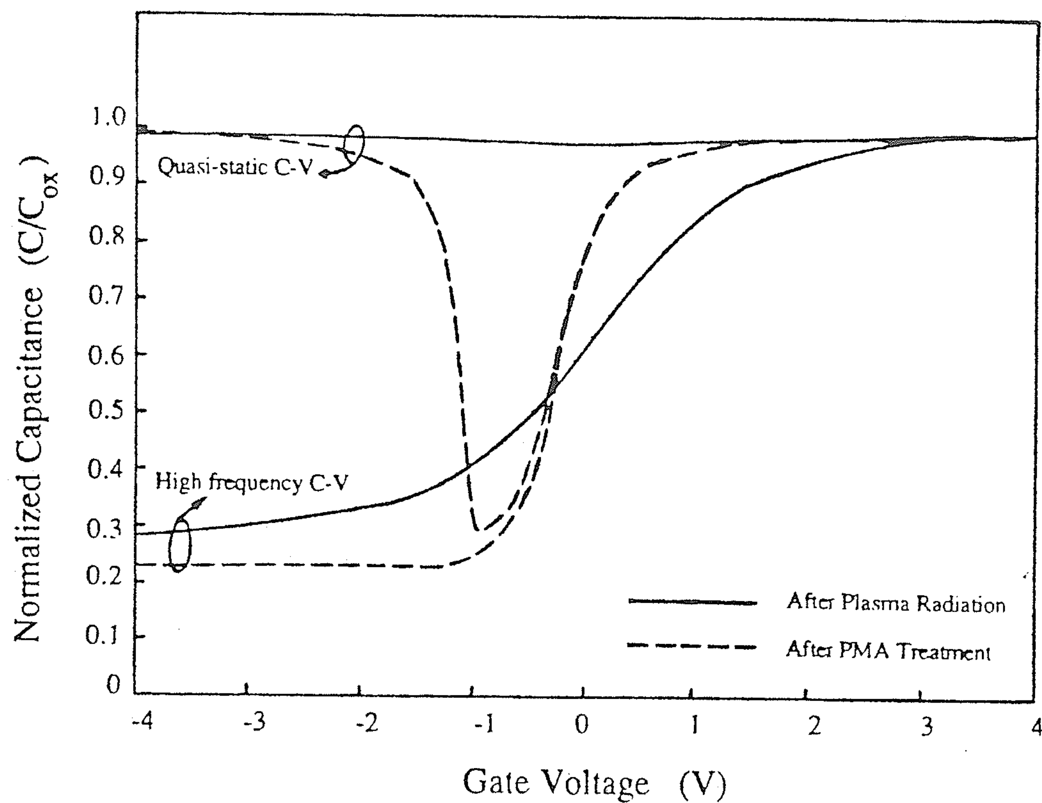

Fig. 4.1 High frequency and quasi-static C-V curves for a bare sample measured after plasma radiation and then after PMA treatment. The SiO_2 film thickness of the device: 941 Å. The device temperature during radiation: 25 °C.

4.2 Oxide Thickness Dependence

It is known that the concentration of radiation-induced defects depends on the oxide thickness (t_{ox}) of the MOS devices. The radiation-induced interface trap density at the Si-SiO_2 interface follows a power law t_{ox}^n dependence [1-3]. The values of the exponent n ranging from 0.5 to 2 have already been reported [1-3]. The oxide thickness also plays a role in the trapping kinetics of carriers in the underlying films [4-6]. This can eventually result in the of the type of oxide charge (positive or negative) being created.

We used six different thermal SiO_2 thicknesses, namely, 228, 323, 465, 571, 741, and 941 Å for this investigation. The results are described and discussed below.

4.2.1 Pre-Irradiation

Figures 4.2 and 4.3 show the D_{it} and the Q_o as functions of oxide thickness for the anneal samples. In these figures, curves 1 and 2 represent the values of D_{it} and Q_o before any treatment and after an initial PMA treatment, respectively. These values of D_{it} and Q_o are used as references for subsequent comparison with those after irradiation and after final PMA treatment.

In Fig. 4.2, the D_{it} value in curve 1 increases with decreasing oxide thickness. This oxide thickness dependence of the D_{it} has been reported by Hung et al. [7] and Fuknda et al. [8], who have suggested that it is due to the processing conditions. However, the initial D_{it} values for devices of various

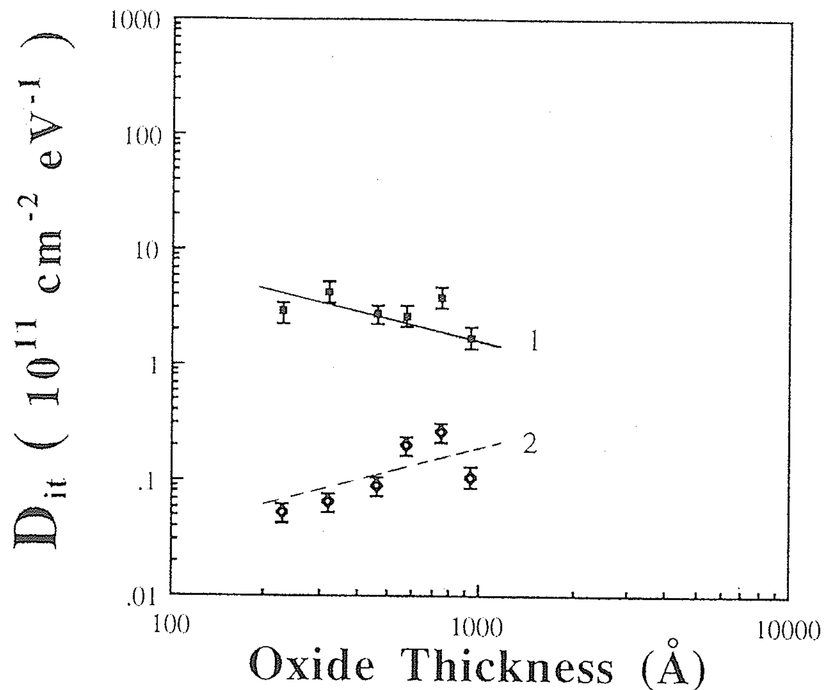

Fig. 4.2 Midgap D_{it} as a function of oxide thickness for the anneal sample sets prior to radiation. Curve 1: before any treatment; curve 2: after initial PMA treatment.

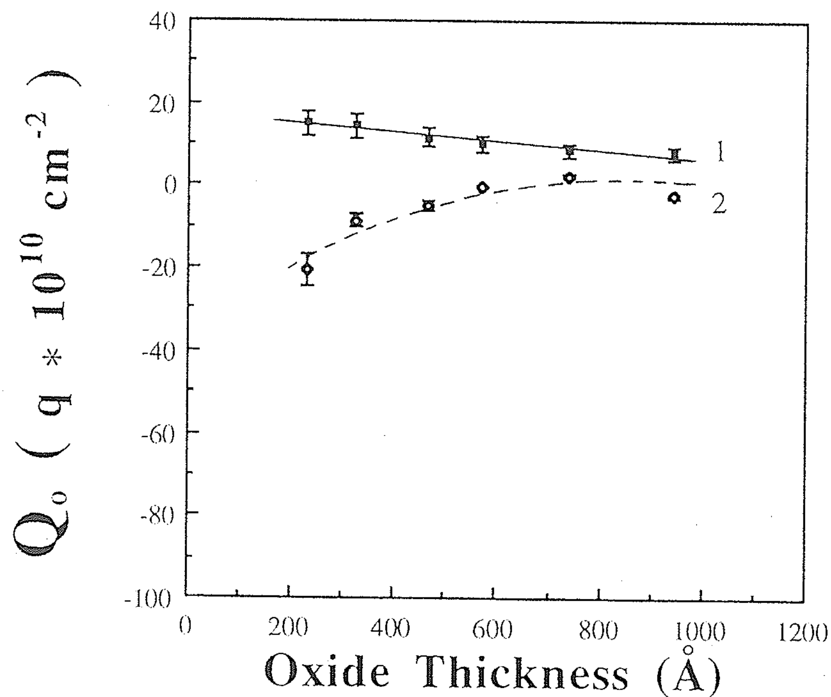

Fig. 4.3 Q_o as a function of oxide thickness for the anneal sample sets prior to radiation. Curve 1: before any treatment; curve 2: after initial PMA treatment.

oxide thicknesses prior to radiation all lie in the range of 10^{11} cm^{-2} eV^{-1}. The error contribution from the D_{it} value will also be of this order. However, the D_{it} value after plasma radiation is about 10^{12}–10^{13} cm^{-2} eV^{-1}. Therefore, the discrepancy in the initial D_{it} level can be considered negligible as compared to the D_{it} value due to radiation damage.

Curve 2 indicates the lowest possible D_{it} values that can be reached for the standard MOS devices without plasma radiation. The D_{it} value varies from 5 x 10^9 to 2 x 10^{10} cm^{-2} eV^{-1} as the oxide thickness increases from 228 Å to 941 Å. Similar values have also been reported by Nicollian and Brews [9]. It will be shown later that the D_{it} values for the devices with radiation damage will be greatly reduced after the PMA treatment.

In Fig. 4.3, curve 1 shows that the Q_o value generally increases inversely with the oxide thickness. It increases from 6–15 x 10^{10} q cm^{-2} as oxide thickness decreases from 941 to 228 Å. This dependence can be attributed to the concentration of the excess oxygen species at the interface before the termination of the oxidation process. According to the Deal-Grove oxidation kinetics [10], the thinner the oxides, the higher is the oxygen concentration at the interface. The large oxygen concentration generally leads to a higher oxide charge density [7].

In Fig. 4.3, curve 2 shows that the Q_o value increases (in magnitude) with decreasing oxide thickness. These negative charges are introduced by the initial PMA treatment. Under thermal annealing, electrons are induced from the substrate into the oxide bulk [11]. Thus, not only are the positive charges neutralized by the negative charges; but also an excessive amount of negative charges is accumulated. This is demonstrated by the downwards shift of curve 2 from curve 1, showing a net amount of negative charges.

4.2.2 Plasma Radiation Effects

A. Interface Trap Density

The relationship between the D_{it} and the oxide thickness t_{ox} is shown in Figs. 4.4-4.7 for the four aforementioned sample sets. In all of these figures, curve 1 represents the D_{it} values after plasma radiation. On the other hand, curve 2 represents the D_{it} values after final PMA treatment and it will be discussed later.

Curves 1 of Fig. 4.4-4.7 show that D_{it} increases with increasing oxide thickness. This thickness dependence is consistent for the four sample sets. We have calculated the slopes of curve 1 for each sample set and they are 0.55, 0.52, 0.42, and 0.39 for the electrode, mask, bare, and anneal sample sets, respectively. These values indicate that the increase in D_{it} after plasma radiation follows the power law t_{ox}^{n} dependence with n varying from 0.3 to 0.6.

Many investigators [2, 3, 12] have utilized the Co^{60} and the gamma-ray as radiation sources in their irradiation studies. These are high-energy radiation sources with energies extending to the 1 MeV range. They have reported D_{it} also follows the power law t_{ox}^{n} but with n of the range 0.5–2. Conversely, the ECR microwave plasmas used in our investigation provide only low-energy radiation with energies less than 50 eV. Since low-energy radiation produces fewer electron-hole pairs, thus fewer defects are created as expected. We believe that the discrepancy in the values of exponent n obtained here can be attributed to difference of radiation energy from the different types of radiation sources used.

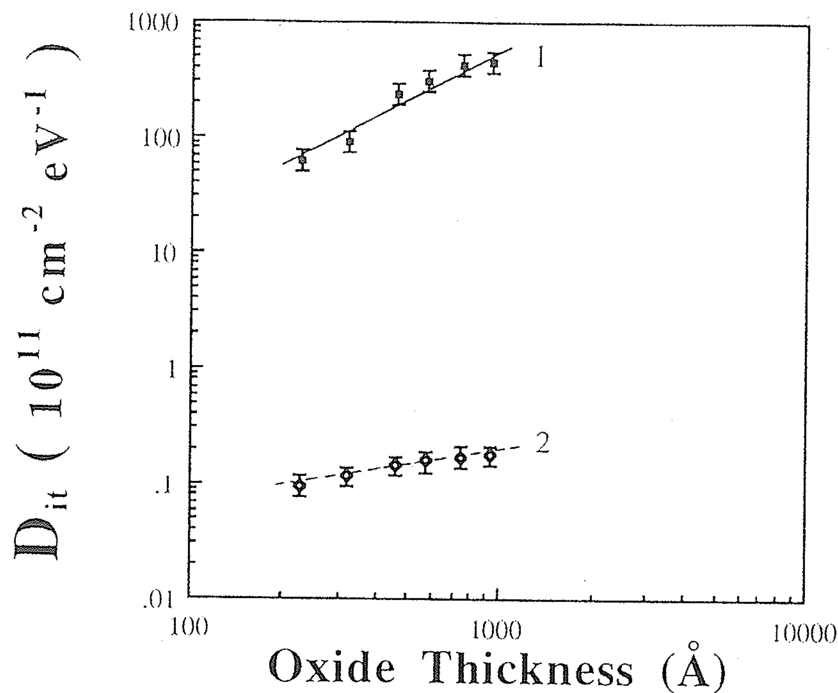

Fig. 4.4 Midgap D_{it} as a function of oxide thickness for the electrode sample sets. Curve 1: after irradiation; curve 2: after final PMA treatment.

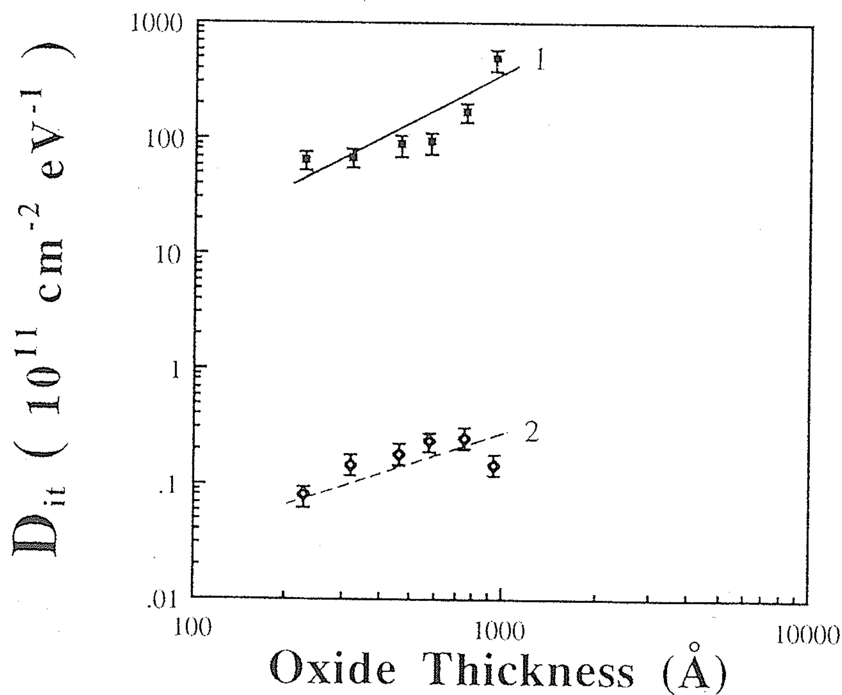

Fig. 4.5 Midgap D_{it} as a function of oxide thickness for the mask sample sets. Curve 1: after irradiation; curve 2: after final PMA treatment.

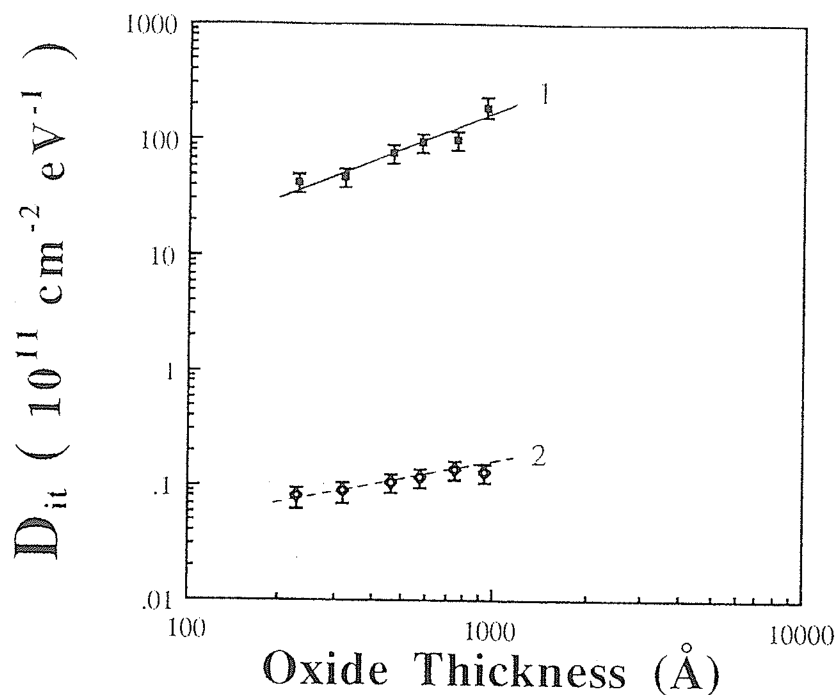

Fig. 4.6 Midgap D_{it} as a function of oxide thickness for the bare sample sets. Curve 1: after irradiation; curve 2: after final PMA treatment.

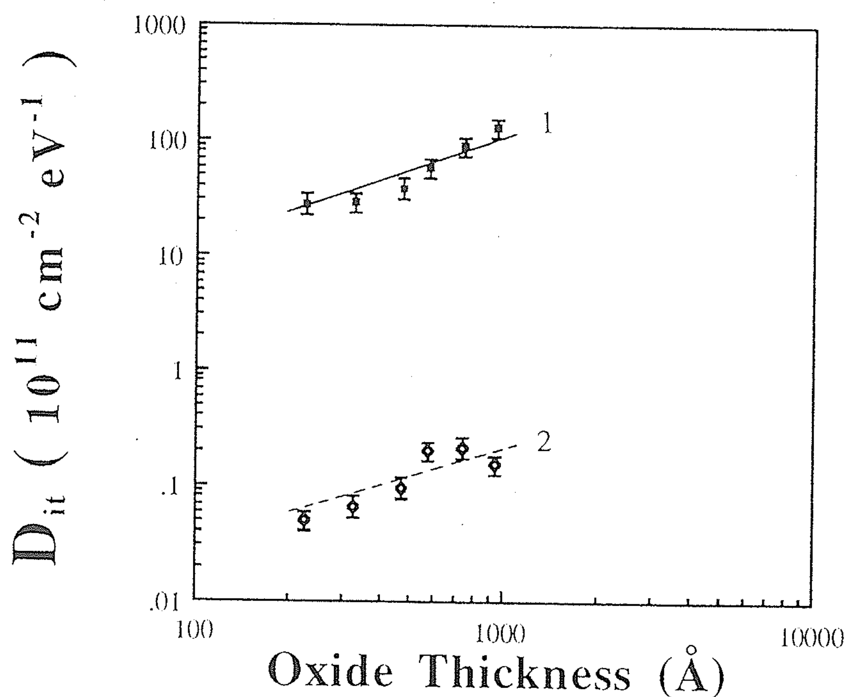

Fig. 4.7 Midgap D_{it} as a function of oxide thickness for the anneal sample sets. Curve 1: after irradiation; curve 2: after final PMA treatment.

Nevertheless, compared to the pre-irradiation D_{it} value at 10^{11} cm^{-2} eV^{-1} (curve 1 in Fig. 4.2), the plasma radiation has severely damaged the Si-SiO_2 interface, thus leading to such a sharp increase in D_{it}. This result is consistent with the oxide films deposited by the PECVD process because the MOS devices fabricated by PECVD oxides have a high density of interface traps. It is likely that the MOS devices fabricated by PECVD oxides have already been subjected to N_2O plasma radiation during SiO_2 deposition.

On the basis of the bond strain gradient (BSG) model developed by Grunthaner et al. [13], in the bulk of the thermal SiO_2, the bonding network consists of silicon bonds mostly in six-tetrahedra rings. The Si–O–Si bridge is usually bonded at an angle of 144° [14, 15]. This is the ideal structure. However, due to the amorphous nature of thermal oxides, anomalous bonding structures are expected to occur. Grunthaner et al. [14] have reported that the thermal oxide structure has 4-member rings and 8-member rings with bond angles at 120° and 180°, respectively. These are the strained bonds in the oxide network. The strained bonds can also be found at the Si-SiO_2 interface region. Because of the lattice mismatch between Si and SiO_2, a considerable amount of stress and distortion is placed at the interface. It has been established that most 4-member (120°) rings are present in this region [13, 14]. This interfacial layer consists of compositional change of SiO_x, from the silicon lattice (x=0) to the tetrahedrally bonded SiO_2 amorphous glass (x=2) [16]. Some of the Si–O bond centers are stretched tightly to match the lattice network due to the deficiency of oxygen in some bond sites. The amount of strain is therefore directly related to the proximity to the Si-SiO_2 interface. This is known as the strain gradient. This transition layer is estimated to be between 15-30 Å

[13, 14], and is largely dependent on the processing chemistry during fabrication.

When the ionizing radiation penetrates the MOS devices, rupture of the strained Si-O bonds will occur in the oxide. Consequently, the broken strained Si-O bond, denoted as $[(SiO)_3 \equiv Si\text{-}O \bullet \ \bullet Si \equiv (OSi)_3]$, may trap the incoming carriers to restore the vacant site. This is accomplished through the trapping of an electron by the silicon dangling bond, $(\bullet Si \equiv (OSi)_3)$, or the capture of a hole by the oxygen dangling bond, $((SiO)_3 \equiv Si\text{-}O \bullet)$. Therefore, this activity is said to be amphoteric in nature [16]. According to the BSG model [13, 14], the oxygen dangling bond tends to propagate in the direction of increasing strain; whereas the silicon dangling bond stays at its original position, as illustrated in Fig. 4.8. Once the oxygen dangling bond arrives at the interface region, it may encounter with other Si centers and be trapped there, forming an interface trap.

Based on the BSG model, we believe that the thick oxides absorb more radiation than the thin ones. This increases the probability for more electron-hole pair generation for thicker oxides, and leads to more strain bonds to be broken in the oxide bulk. Moreover, the thick oxides have a relatively larger strain gradient found from the Si-SiO_2 interface to the oxide bulk [5, 13, 14, 17]. This larger strain gradient can efficiently transport more defects to the interface region. Therefore, more oxygen dangling bond defects will migrate to the Si-SiO_2 interface to form interface traps.

Of the four sample sets, the electrode and mask sample sets have consistently higher D_{it} than the bare and anneal sample sets after plasma radiation. Table 4.1 shows the D_{it} values of the four sample sets against the oxide thickness. The initial PMA for the anneal samples reduces the

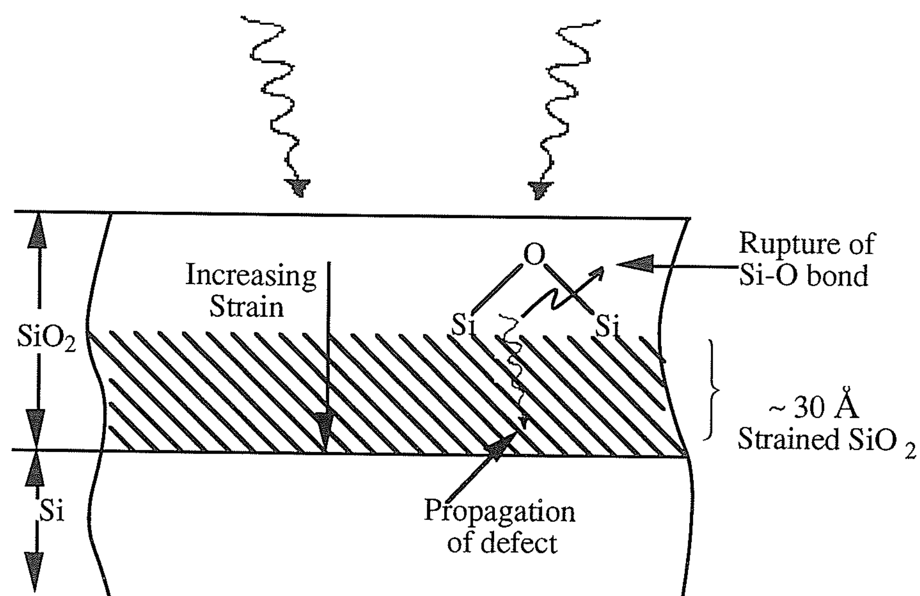

Fig. 4.8 Bond Strain Gradient model: showing the rupture of Si-O bond and the subsequent propagation of the defects toward the $Si\text{-}SiO_2$ interface. (After F. Grunthaner, P. Grunthaner, and Maserjian [13])

Table 4.1 The D_{it} values measured after plasma radiation for the control, mask, bare, and anneal sample sets in which each set contains six different oxide thicknesses.

	D_{it} (10^{11} cm^{-2} eV^{-1})			
Oxide Thickness (Å)	**Electrode Sample**	**Mask Sample**	**Bare Sample**	**Anneal Sample**
228	61.59	65.45	42.48	25.00
228	63.15	66.60	56.94	27.98
323	90.15	68.94	46.32	28.50
323	90.33	70.20	47.81	29.04
465	238.00	87.80	69.57	36.60
465	251.20	89.20	82.37	38.80
571	227.90	92.40	94.37	55.40
571	398.20	94.30	96.50	57.84
741	423.50	165.40	98.19	84.44
741	433.20	170.10	104.20	89.54
941	456.70	455.40	194.60	115.90
941	474.70	489.00	234.00	150.90

number of strained bonds in the oxides. Since the oxide network is subjected to bond rearrangement and lattice relaxation processes under thermal annealing, the amount of strained bonds is lowered. This reduces the number of bonds susceptible to breakage upon ionizing radiation. Fewer defects will migrate to the Si-SiO_2 interface for the generation of interface traps. Therefore, the anneal sample set has the lowest D_{it} after irradiation. The bare sample set has a slightly higher degree of D_{it} than the anneal sample set. Without the electrodes acting as a top shield, we would expect that more energetic particles would penetrate and impede the oxides.

The electrode and the mask sample sets have higher values of D_{it} than the anneal sample set. Though the electrode sample set generally has a slightly higher D_{it} than the mask sample. This may be due to the difference in area of exposure to the ionizing radiation. The mask samples were masked by shadow masks leaving only the electrode areas of the samples to have direct contact with the energetic particles. Thus, fewer particles will be able to penetrate the underlying oxides. Consequently, fewer strained bonds will be broken. Nevertheless, the results of D_{it} from both of these two sample sets demonstrate that as long as there is area exposed to the ionizing radiation, radiation damage will be created. Even though the Al gate electrode is known to protect against the particle bombardment such as the electron or ions, we believe that the UV radiation is the main cause in generating most of the defects, because UV radiation is transparent to the Al gate electrode [18]. Also, the optical emission spectrum of the N_2O plasma shown in Fig. 4.9 indicates that the plasma emits a high intensity of UV radiation. The penetration of such radiation is most likely the major mechanism responsible for the radiation damage.

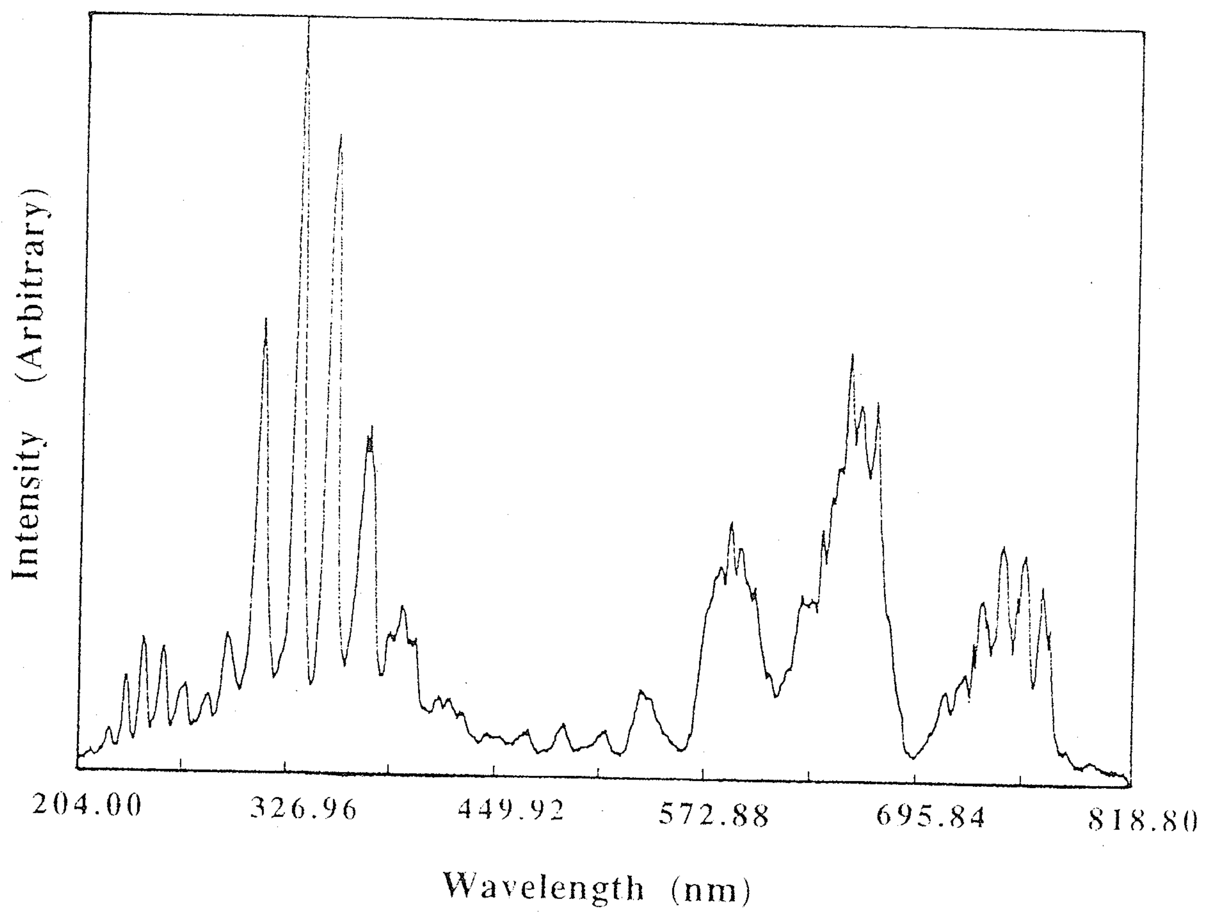

Fig. 4.9 The optical emission spectrum of the N_2O plasma.

B. Oxide Charge Density

Figures 4.10-4.13 show the values of Q_o as functions of oxide thickness for the four sample sets. Curve 1 in each figure represents the Q_o values after plasma radiation. Of the four sample sets, there are two different trends displayed by curve 1. One trend concerns the electrode and mask sample sets in which there is a change of charge polarity from negative to positive. This implies that the number of radiation-induced positive charges increases with increasing oxide thickness. The other trend shows that negative charge generation decreases with increasing oxide thickness. This means that electron trapping becomes the dominant process during irradiation regardless of the oxide thickness of the samples. This trend can be observed in both the bare and anneal sample sets.

For the electrode and mask sample sets, the oxide charge polarity is changed from negative to positive as oxide thickness increases. This means that the amount of the negative charges generated decreases as oxide thickness increases as shown in Figs. 4.10 and 4.11, implying that electron trapping is more prominent in thinner oxides. Negative charges can also be found in the bare and anneal sample sets; especially for the samples with thin oxides as shown in Figs. 4.12 and 4.13. This oxide thickness phenomenon can be explained on the basis of the BSG model. Most of the silicon dangling bonds remain behind in the oxide bulk upon the rupture of the strained Si–O bonds. Thinner oxides have a smaller strain gradient thus making the silicon dangling bonds even less likely to move toward the Si-SiO_2 interface. This in turn means that the thinner oxides contain more oxide bulk traps, thus trapping of electrons more likely to occur.

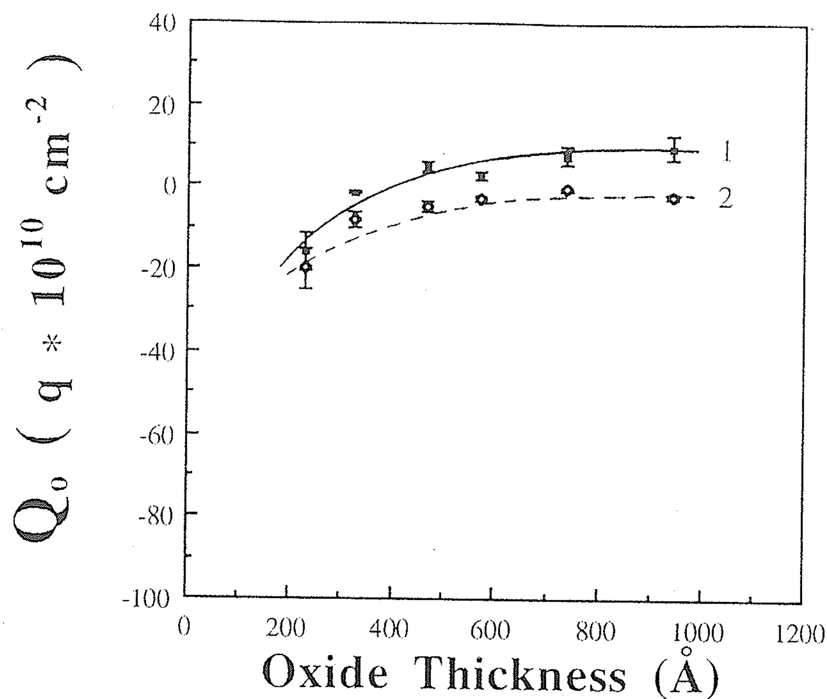

Fig. 4.10 Q_o as a function of oxide thickness for the electrode sample sets. Curve 1: after irradiation; curve 2: after final PMA treatment.

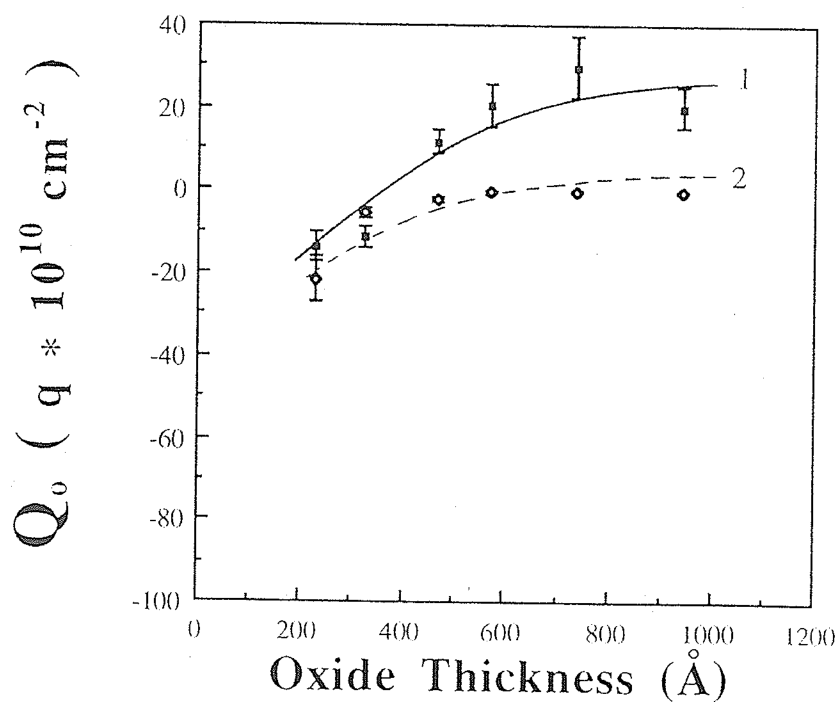

Fig. 4.11 Q_o as a function of oxide thickness for the mask sample sets. Curve 1: after irradiation; curve 2: after final PMA treatment.

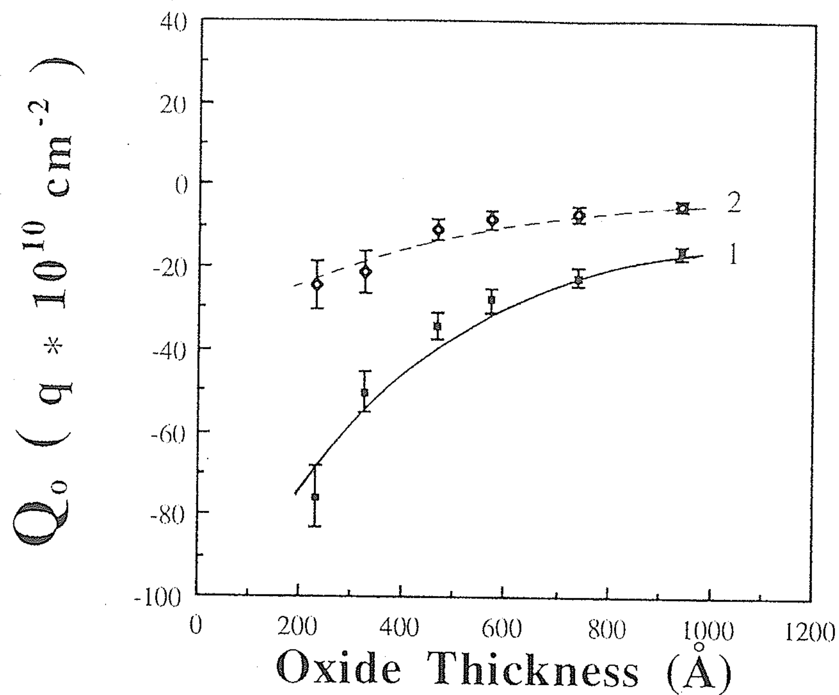

Fig. 4.12 Q_o as a function of oxide thickness for the bare sample sets. Curve 1: after irradiation; curve 2: after final PMA treatment.

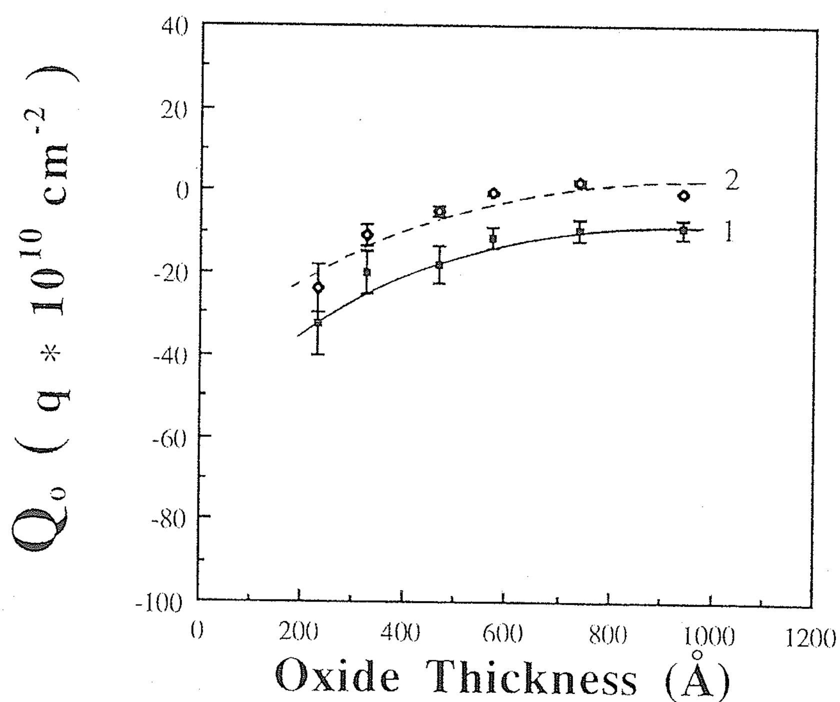

Fig. 4.13 Q_o as a function of oxide thickness for the anneal sample sets. Curve 1: after irradiation; curve 2: after final PMA treatment.

However, when the MOS devices are exposed to plasma, they are constantly biased by a plasma potential. The magnitude of the plasma potential is about 20 V under normal operating conditions. Thus, the floating potential V_f, relative to the plasma, is a negative potential as illustrated in Fig. 4.14. If we assume that the floating potential is constant throughout the radiation process; then the thinner the oxides, the higher the electric field exerted on the MOS devices. In other words, the thin oxides experience an electric field as high as 7-10 MV/cm during plasma radiation. This field can lead to electron injection from the Al gate electrodes into the SiO_2. Most of these electrons are subsequently trapped by the silicon dangling bonds created by bond rupture during ionizing radiation. These electron trapping activities contribute to the build-up of negative charges in our samples, especially conspicuous in thin oxides.

As the oxide thickness increases, the charges residing in the electrode and mask samples after irradiation become positive indicating the change of charge polarity. For the electrode sample set, the number of positive charges is generally lower than that of the pre-irradiation values (curve 1 in Fig. 4.3). This means a portion of the positive charges is neutralized by the radiation-induced negative charges. Therefore, the negative charge generation can be said to decrease with increasing oxide thickness. This trend is consistent even with the effect of electric field due to the floating potential during plasma radiation.

The amount of positive charges found in the mask sample set is higher than the pre-irradiation values. This implies that positive charges are generated on top of the positive charges originally residing in the samples. We believe that the positive charge generation is due to the hole trapping. Since the mask samples are masked by shadow masks during irradiation,

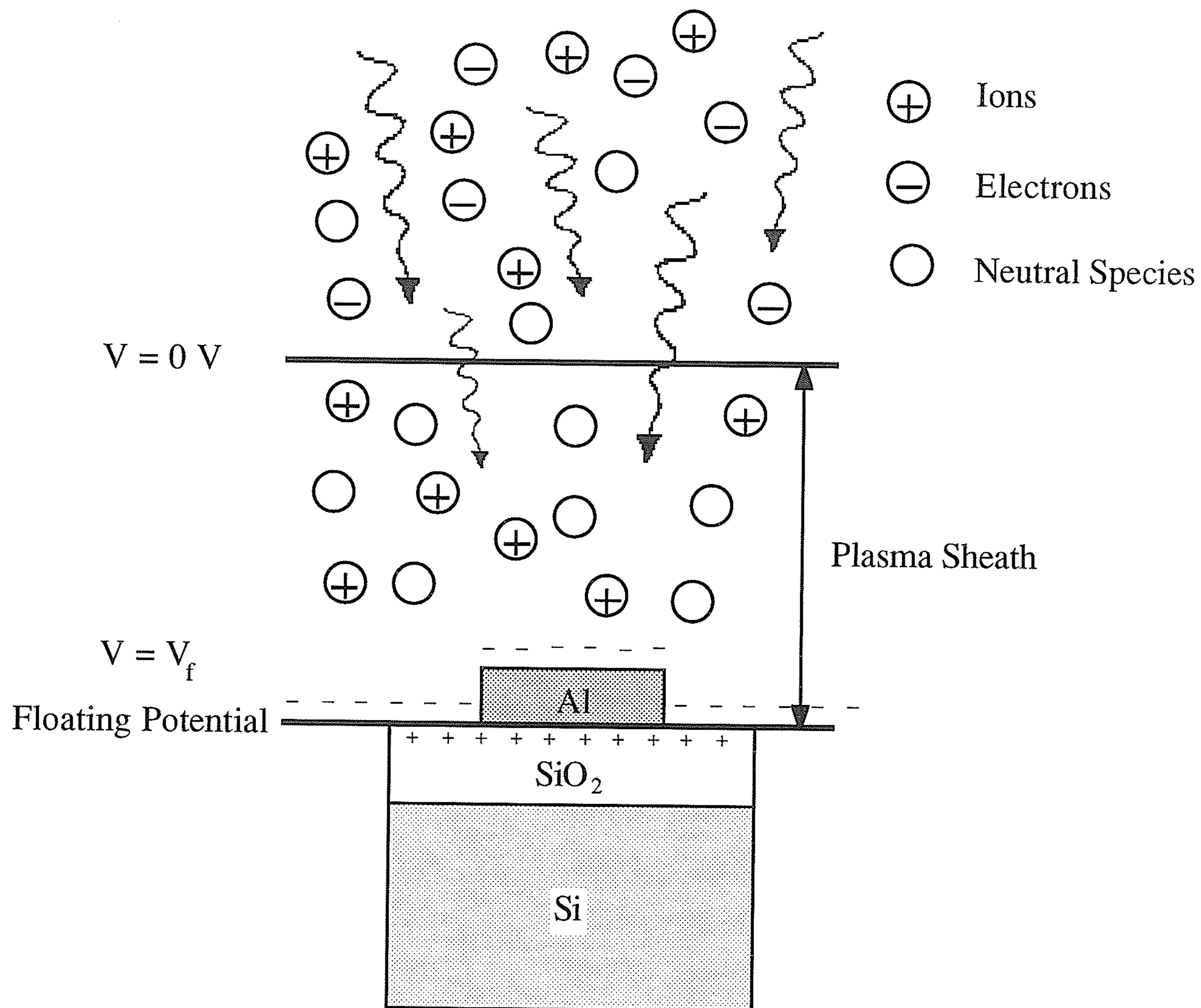

Fig. 4.14 Model of an MOS device during plasma radiation.

UV radiation is the only source from plasma that can penetrate the underlying oxides. Both the mask and the gate electrode areas can prevent other energetic particles such as ions or high energy electrons from reaching the SiO_2 film, thus the possibility of electron trapping by this means is greatly lowered.

The UV radiation absorbed by the SiO_2 film can produce electron-hole pairs in it and break the strained Si–O bonds. For thin oxides, the electric field due to the floating potential is higher so that more electrons would be injected from the contact. More electrons are therefore available to be trapped by the silicon dangling bonds, thus creating the negative charges. For thick oxides, the electrons have a better chance of averting entrapment, because the UV radiation is usually absorbed near the SiO_2 surface [18] so that the concentration of the radiation-induced electron-hole pairs is higher near the SiO_2 surface. A major portion of the mobile electrons can move out of the oxide bulk, avoiding to be captured by bulk traps. This leaves behind a majority of slow-moving holes and they are readily trapped by the bulk traps, thus creating the positive charges.

The bare sample set has accumulated the highest number of negative charges as shown in Fig. 4.12. The large number of negative charges is complemented by the slightly lower than expected interface traps generated in these samples. This means that more defects are located in the oxide bulk than at the interface. During plasma radiation, the entire oxide surface was exposed to the ambient environment. Without the gate electrodes or masks acting as shield, more energetic particles penetrate the oxide film, creating more electron-hole pairs and hence mobile electrons are available to be trapped by the oxide bulk traps. This results in an increase in negative charges.

In addition, the water moisture in the ambient always readily diffuse into the oxide at room temperature. The water moisture will react with ≡ Si–O–Si ≡ as follows:

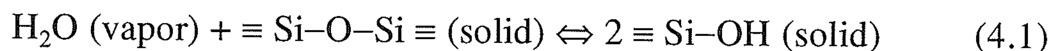

H_2O (vapor) + ≡ Si–O–Si ≡ (solid) ⇔ 2 ≡ Si–OH (solid) (4.1)

where the SiOH centers are the water-related traps. These SiOH centers can subsequently capture electrons and become negatively charged (SiO^-) [9]. At the same time, it will also release the atomic hydrogen as a by-product. This atomic hydrogen may diffuse toward the Si-SiO_2 interface and react with the silicon dangling bonds there. This action reduces the defects at the interface through the hydrogenation process. Therefore, the D_{it} value for the bare sample set is lower than expected, while the number of negative charges is increased.

In the anneal sample set, the concentration of negative charges is lower than that in the bare sample set. During the initial PMA treatment, negative charges have already been introduced to the oxide film. The subsequent irradiation of these samples only increases the number of these negative charges accumulated inside. The annealing of these samples prior to plasma radiation annihilates the potential traps such as the silicon dangling bonds and the oxygen dangling bonds. As a result, hydrogen-related chemical bonds such as SiH and SiOH are formed. Moreover, the strained Si–O bonds may be relaxed through the healing effect from the thermal annealing. Subsequently, the passivation of these potential traps tends to reduce the number of electrons to be captured after plasma radiation. As a result of this action, fewer negative charges are created in the anneal samples than those in the bare samples.

4.2.3 Annealing Effects

In Figs. 4.4-4.7, curve 2 shows that the D_{it} value after final PMA treatment increases with increasing oxide thickness. It can be seen that curve 2 shifts down from curve 1 sharply, indicating that most of the radiation-induced interface traps had been removed by the final PMA treatment. The D_{it} values obtained for the four sample sets after final PMA treatment are close to the reference values (curve 2 in Fig. 4.2) with the differences between the two less than ± 25 % for the four sample sets. This is a reasonable margin of error due to the limitations of our measurement instrumentation. It can be concluded that radiation-induced interface traps can be removed by a standard PMA treatment.

In Figs. 4.10-4.13, curve 2 shows that the Q_o value after final PMA treatment increases (in magnitude) with decreasing oxide thickness. For the four sample sets, the Q_o values after final PMA treatment are close to the reference values (curve 2) as shown in Fig. 4.3. The deviation between the two Q_o values is within ± 20 %. This is an acceptable margin of error. Again, the radiation-induced oxide charge can be removed by a standard PMA treatment.

Based on our findings, the radiation damage created by N_2O plasma can be annealed out by a final PMA treatment. It should be note that the anneal sample set shows that the application of an annealing treatment prior to plasma radiation results in a less damage at the interface. This step is a radiation-hardening effect. This implies that the pre-annealing makes the underlying oxide film more resistant to plasma radiation. The only drawback about this anneal sample set is that PMA treatment must be carried out at the outset. If the number of processing steps is a critical

issue, then the bare sample set may be the best alternative choice. It should also be noted that although the defects can be annealed out, it is not desirable to have such a large value of D_{it} resulting from plasma radiation, because the quality at the interface becomes harder to improve once the damage is done. For D_{it} values higher than 10^{13} cm^{-2} eV^{-1}, a high temperature annealing process is required to remove the defects accumulated at the Si-SiO_2 interface. However, the usage of a high temperature processing step creates other diffusion problems, which is why it is not preferrable to have a large concentration of interface traps at the Si-SiO_2 interface.

4.3 Device Temperature Dependence

The device temperature also plays an important role in defect generation during the plasma radiation process. Most studies done in this area have claimed that the increase in device temperature will accelerate the defect generation process [3,4]. However, the number of radiation-induced defects does not necessarily increase. For example, the number of interface traps may be created faster as device temperature increases during plasma radiation. This implies that the time required for a saturation value to be reached also depends upon the device temperature. Similarly, the trapping of carriers may also be accelerated as the device temperature is increased.

However, we need also to consider the annealing effects that an increase in device temperature may bring about. It has been reported [3, 4, 12, 19] that significant annealing occurs for device temperatures larger than 100 °C. If device temperature indeed has a pronounced annealing

effect on the MOS devices during irradiation, the radiation damage may be controlled by adjusting the device temperature.

4.3.1 Pre-Irradiation

Figures 4.15 (a) and (b) show the D_{it} values as functions of the device temperature for the anneal sample sets. Curves 1 and 2 show the D_{it} values before any treatment and after an initial PMA treatment, respectively. These values named as the pre-irradiation values, are used as references for comparison purposes. It can be seen that all the D_{it} values are constant indicating that all the MOS devices have similar D_{it} values before irradiation and after the initial PMA treatment. This ensures that subsequent changes in the D_{it} values are only due to the plasma radiation. The D_{it} value is about 3–4 x 10^{11} cm^{-2} eV^{-1} before any treatment and reduces to 5–6 x 10^{9} cm^{-2} eV^{-1} after initial PMA treatment for the thin oxide samples (228 Å). On the other hand, the D_{it} level stays between 1–2 x 10^{11} cm^{-2} eV^{-1} before any treatment and decreases to 1–2 x 10^{10} cm^{-2} eV^{-1} after initial PMA treatment for the thick oxide samples (941 Å).

Figures 4.16 (a) and (b) show the relationship between the Q_o value and the device temperature for the anneal sample sets. Similarly, all the Q_o values are constant before any treatment and after the initial PMA treatment indicating that the device quality is consistent. Under thermal annealing, negative charges are introduced to the oxides as curves 2 shift downwards from curve 1. This shows an accumulation of negative charges in the oxide bulk.

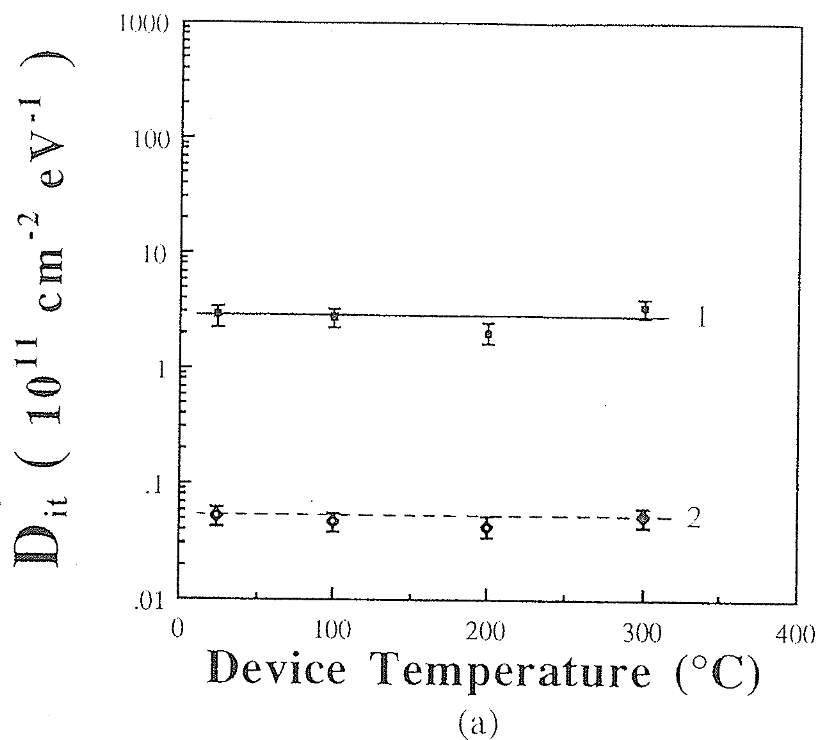

(a)

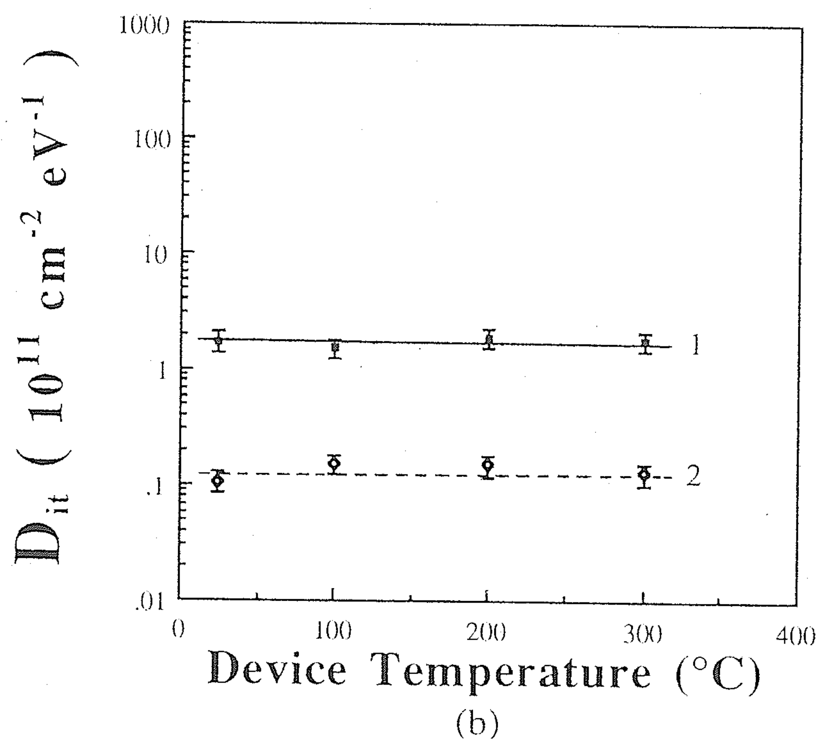

(b)

Fig. 4.15 Midgap D_{it} as a function of device temperature for the anneal sample sets with oxide thickness of (a) 228 Å; (b) 941 Å. Curve 1: before any treatment; curve 2: after initial treatment.

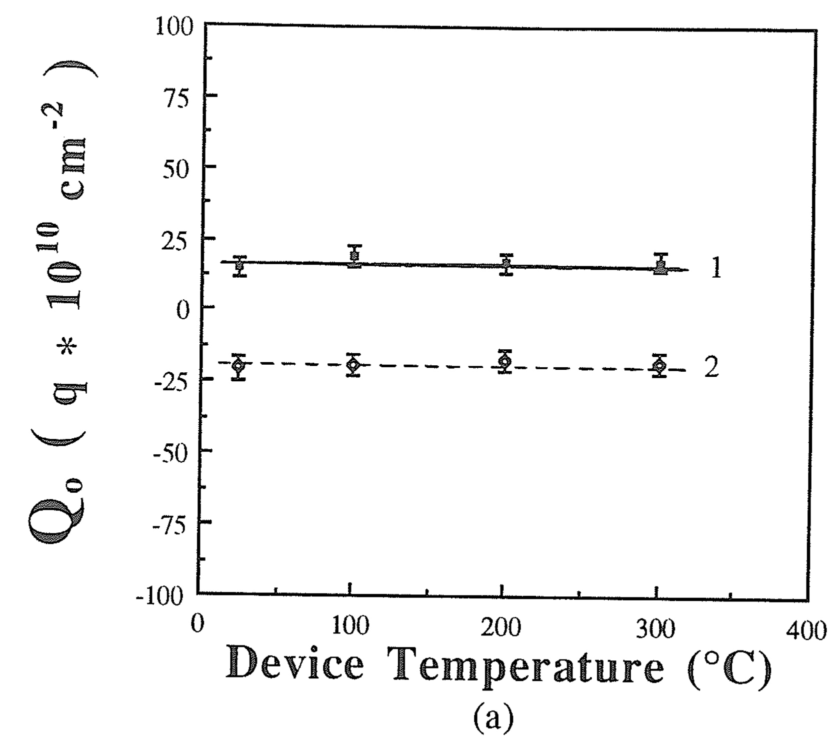

(a)

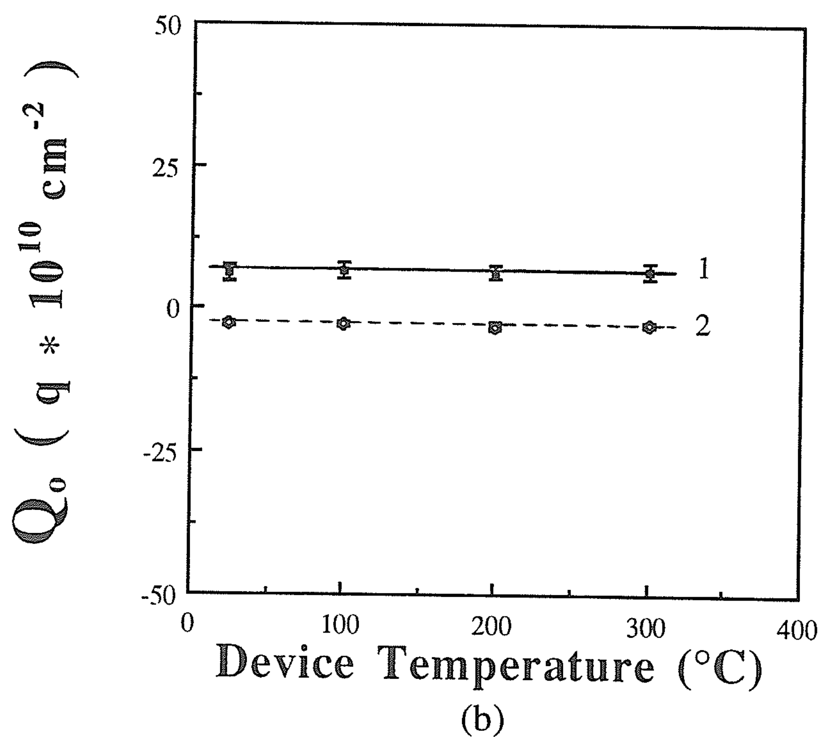

(b)

Fig. 4.16 Q_o as a function of device temperature for the anneal sample sets with oxide thickness of (a) 228 Å; (b) 941 Å. Curve 1: before any treatment; curve 2: after initial treatment.

4.3.2 The Plasma Radiation Effects

A. Interface Trap Density

The value of D_{it} always decreases with increasing device temperature up to 200 °C during plasma radiation, but for temperature higher than 200 °C this trend is reversed as shown in Figs. 4.17-4.20 for all four sample sets regardless of the oxide thickness. This implies that D_{it} reaches a minimum value at a device temperature of about 200 °C. We believe that the two distinct stages involve two different defect generation processes. The first stage concerns the defect generation and annihilation processes. These are two competing mechanisms occurring simultaneously during plasma radiation at an elevated device temperature. The defect generation process begins with the bombardment of various particles from the plasma. As the device temperature is held at 25 °C, these particles penetrate the oxides and break the strained Si–O bonds. The subsequent transport of these broken bond defects to the Si-SiO_2 interface leads to the formation of interface traps, thus increasing the value of D_{it}. As device temperature increases, a thermal annealing effect becomes important due to high device temperature. Curves 1 in Figs. 4.17-4.20 show a decreasing trend of D_{it} up to the device temperature of 200 °C. This means that the annihilation effect overrides the generation process. Hence, a net decrease of D_{it} is observed. This phenomenon can be explained on the basis of the recombination-enhanced defects reactions (REDR) theory [20].

According to the REDR theory, the recombination of an excess electron with a hole through a defect center releases a substantial amount of energy. This energy can cause excitations of the vibration state of the

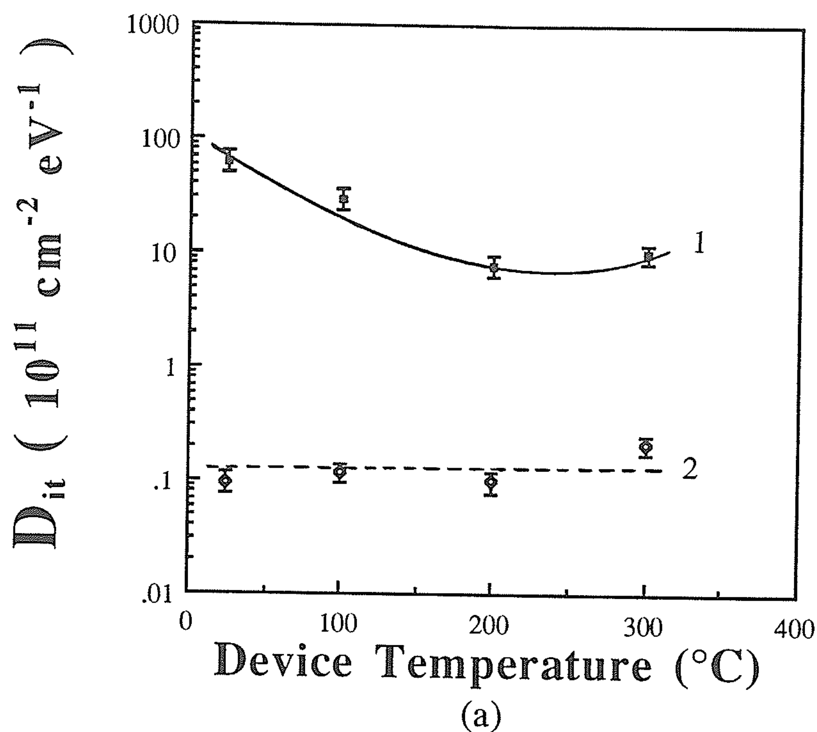

(a)

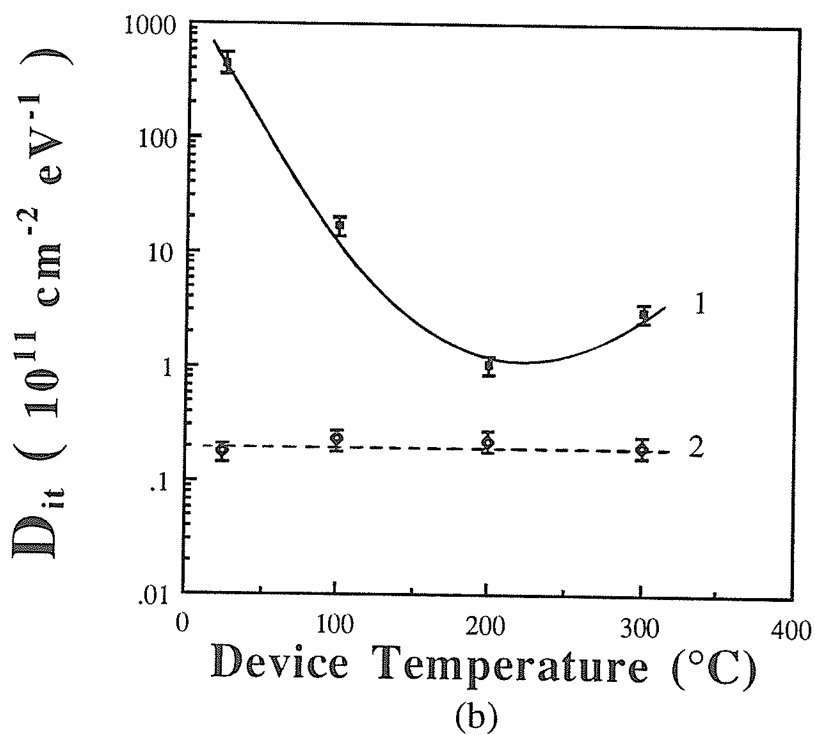

(b)

Fig. 4.17 Midgap D_{it} as a function of device temperature for the electrode sample sets with oxide thickness of (a) 228Å; (b) 941 Å. Curve 1: after irradiation; curve 2: after final PMA treatment.

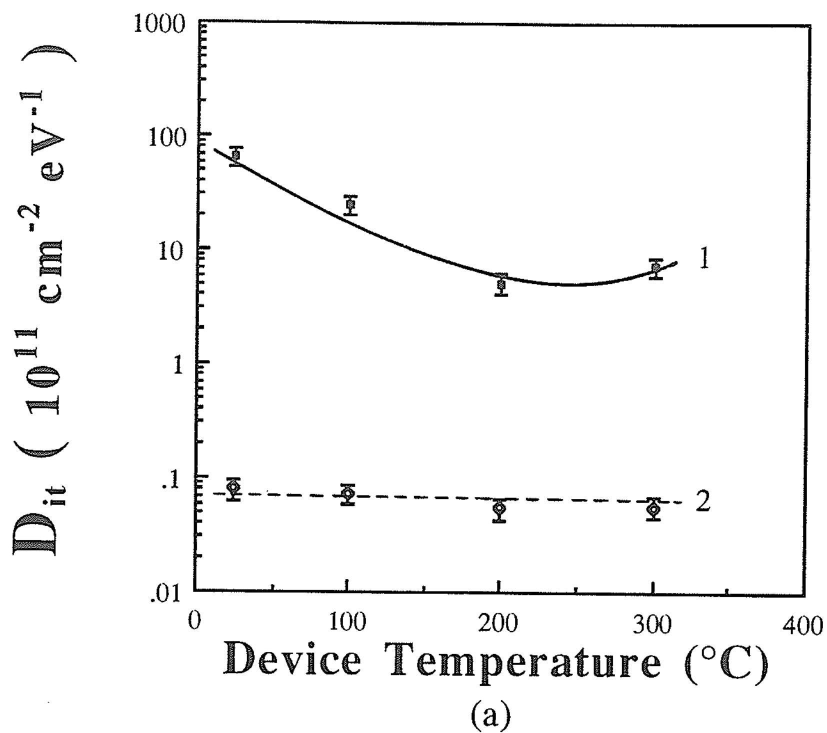

(a)

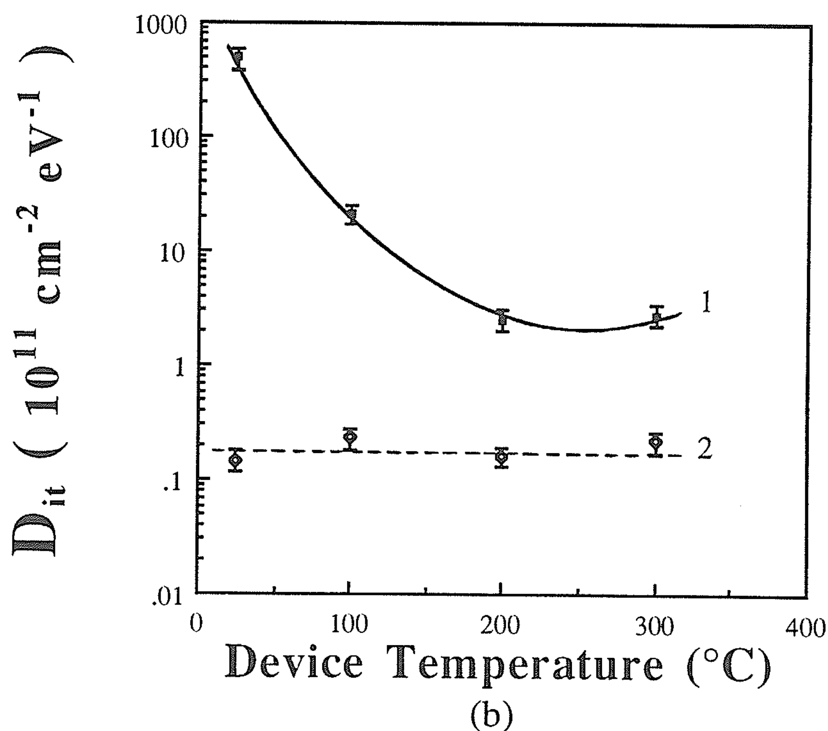

(b)

Fig. 4.18 Midgap D_{it} as a function of device temperature for the mask sample sets with oxide thickness of (a) 228Å; (b) 941 Å. Curve 1: after irradiation; curve 2: after final PMA treatment.

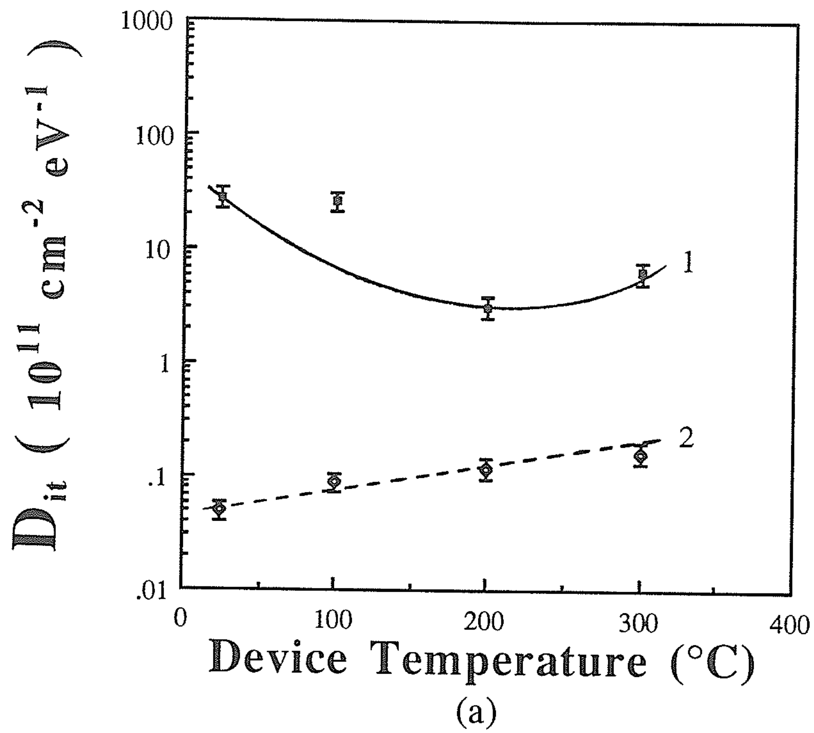

(a)

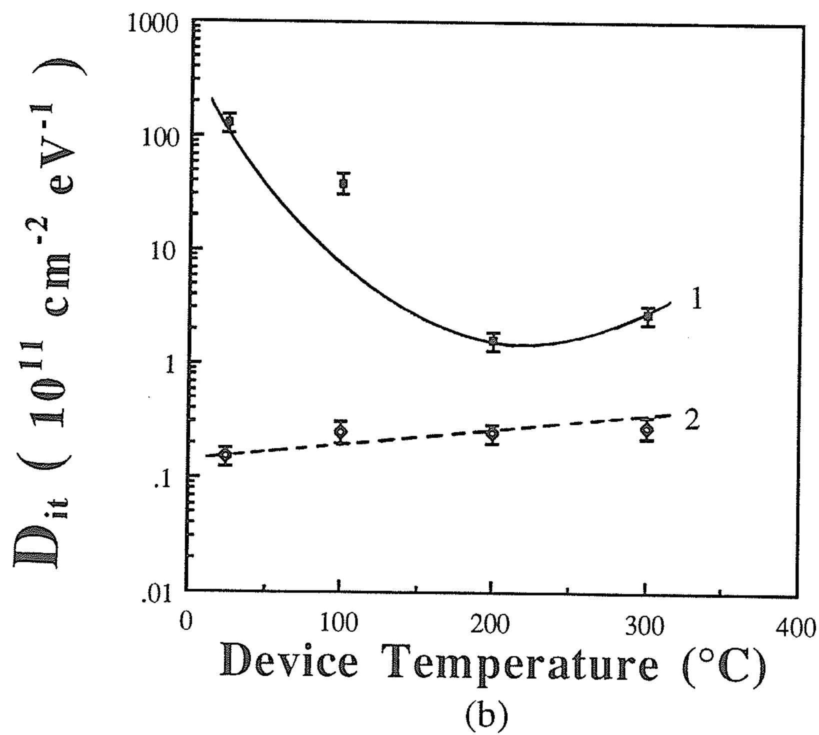

(b)

Fig. 4.19 Midgap D_{it} as a function of device temperature for the anneal sample sets with oxide thickness of (a) 228Å; (b) 941 Å. Curve 1: after irradiation; curve 2: after final PMA treatment.

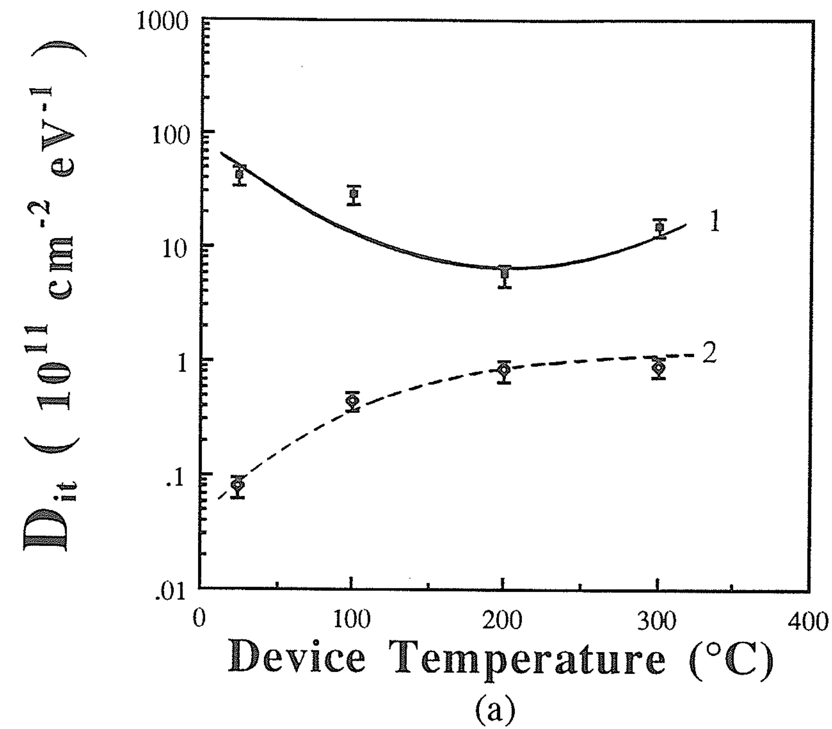

(a)

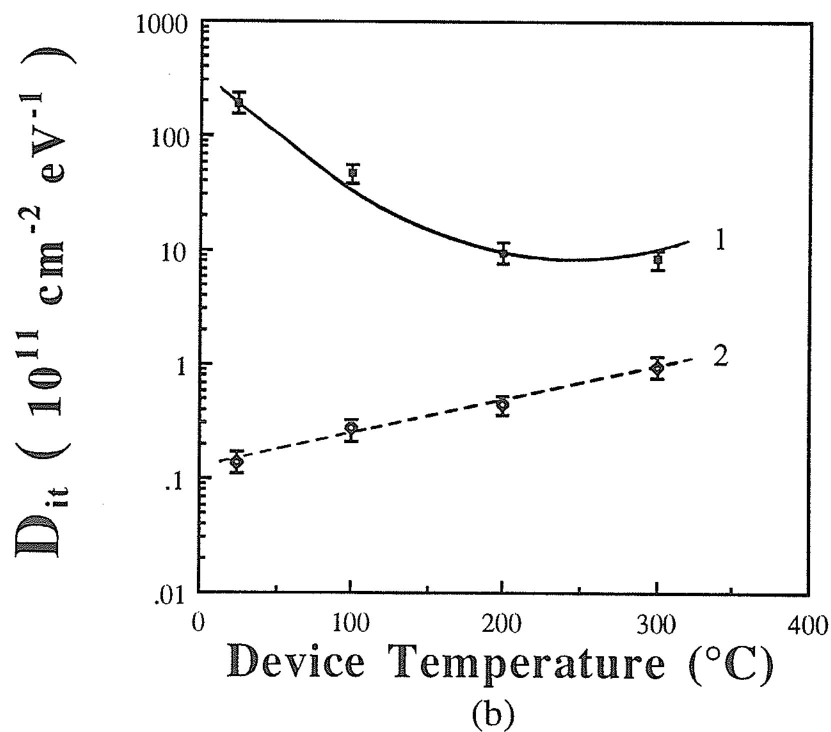

(b)

Fig. 4.20 Midgap D_{it} as a function of device temperature for the bare sample sets with oxide thickness of (a) 228Å; (b) 941 Å. Curve 1: after irradiation; curve 2: after final PMA treatment.

defect. Subsequent solid-state reactions involving the defects could be achieved upon this recombination process. For example, if proper external conditions exist, the diffusion, dissociation, and annihilation of the defects are more likely to happen when an additional thermal energy released from the recombination process is available. The external conditions can either be the variations of temperature, or doping concentration, or the application of an external bias. These factors can disturb the bulk equilibrium Fermi levels of the charge states, and hence they lead to the subsequent recombination reactions to re-establish the equilibrium conditions.

In the first stage, the defect annihilation effect overrides the generation process because the increase in device temperature enhances the thermal activities in the oxide bulk. This coupled with the thermal energy released from the recombination, makes annealing of defects possible. This is why D_{it} decreases with increasing device temperature up to the device temperature of 200 °C.

The second stage commences when the device temperature rises beyond 200 °C. Figures 4.17-4.20 show that the value of D_{it} starts to increase from 200 °C as the device temperature is further increased. This implies that the defect annihilation process comes to a saturation level. The increase in D_{it} is within the order of 10^{11} cm^{-2} eV^{-1} for all sample sets. We believe that the increase in D_{it} can be attributed to the negative bias-temperature aging effect. As discussed previously in Section 4.2.2.B, the MOS device experiences a negative bias during plasma radiation. This increase in D_{it} at temperatures higher than 200 °C indicates that the aging effect negates the recombination process by accelerating the carrier trapping mechanism. This action enhances the defect generation, thus

partially nullify the annealing effect. Therefore, this is why the trend in D_{it} is reversed at high device temperatures.

Nevertheless, the D_{it} values after plasma radiation remain higher than the pre-irradiation values (curves 1 in Fig. 4.15) within the range of device temperature under investigation. It should be noted that the increase of device temperature does not totally prevent the defect generation process, it just lowers the radiation damage. In the device temperature range of 200–300 °C, the D_{it} value is on the order of 10^{11} cm^{-2} eV^{-1}, which is significantly lower than the values at 25°C (10^{12}–10^{13} cm^{-2} eV^{-1}). This result is analogous to the temperature range being used in the SiO_2 film deposition process. Various studies [21-25] have shown that in the 250–300 °C device temperature range, the electrical characteristics of the PECVD SiO_2 films deposited at these temperatures approach to that of the thermal-quality SiO_2 films. Our results support this argument. We have found that irradiation at the device temperature range of 200–300 °C produces less interface traps. The D_{it} value of 10^{11} cm^{-2} eV^{-1} after plasma radiation is close to that of the standard high-quality thermal oxides. It is also a recognized industry standard level for D_{it}. The decrease of D_{it} to 10^{11} cm^{-2} eV^{-1} is largely due to the annealing effect enhanced by the additional thermal activities at elevated device temperatures.

For the four samples sets, we do not find a significant difference in the change of the D_{it} value with respect to the change of the device temperature, but the rate of decrease in D_{it} in the 25–200 °C temperature range is more drastic for the thick oxide samples. This is mainly due to the larger strain gradient in thick oxides. At elevated device temperatures, defect annihilation process becomes dominant because of the annealing effects. The mobile hydrogen species enhanced by the thermal activation

are able to passivate the broken bond defects to form SiH or SiOH bonds. This will reduce the potential trap sites to form interface trap charge at the Si-SiO_2 interface. In addition, large strain gradient is also responsible for the hydrogen transport by accelerating the hydrogenation process. This explains why D_{it} is decreased at a faster rate for thicker oxides.

On the other hand, the thin oxides have a lower D_{it} (10^{12} cm^{-2} eV^{-1}) than the thicker oxides after plasma radiation. This is due to the relatively smaller number of strained bonds, thus a smaller bond strain gradient in thin oxides. As a result, fewer defects are generated upon plasma radiation. As device temperature increases, the thin oxide samples experience a higher electric field stress. Defect annihilation is less efficient because the aging process is also taking place. This will suppress partially the annealing effects, thus inhibiting the reduction of D_{it}. Therefore, the decrease in D_{it} is not as fast as the case for the thick oxide samples in the device temperature range of 25–200 °C.

B. Oxide Charge Density

Figures 4.21-4.24 show the values of Q_o as functions of device temperature for the electrode, mask, anneal, and bare sample sets, respectively. There are two trends. The first trend is inferred from Figs.4.21-4.23 regarding the electrode, mask, and anneal samples. The number of positive charges accumulated in the three sample sets increases with increasing device temperature, regardless of the oxide thickness. At low temperatures, electron trapping process is dominant, especially for thin oxide samples. This is mainly due to the high electric field stress exerted on the thin oxide samples by the negative floating potential during plasma

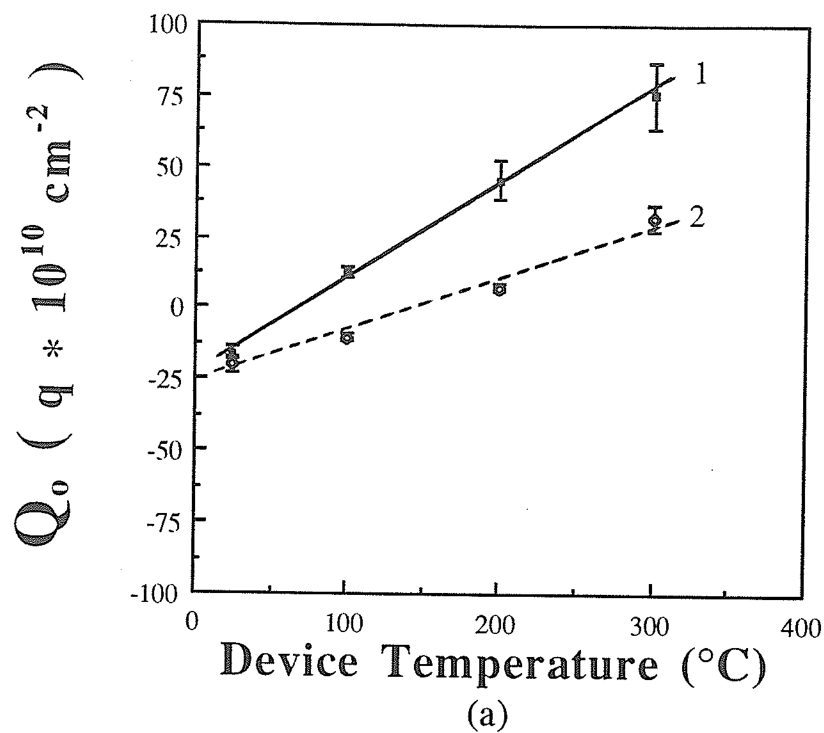

(a)

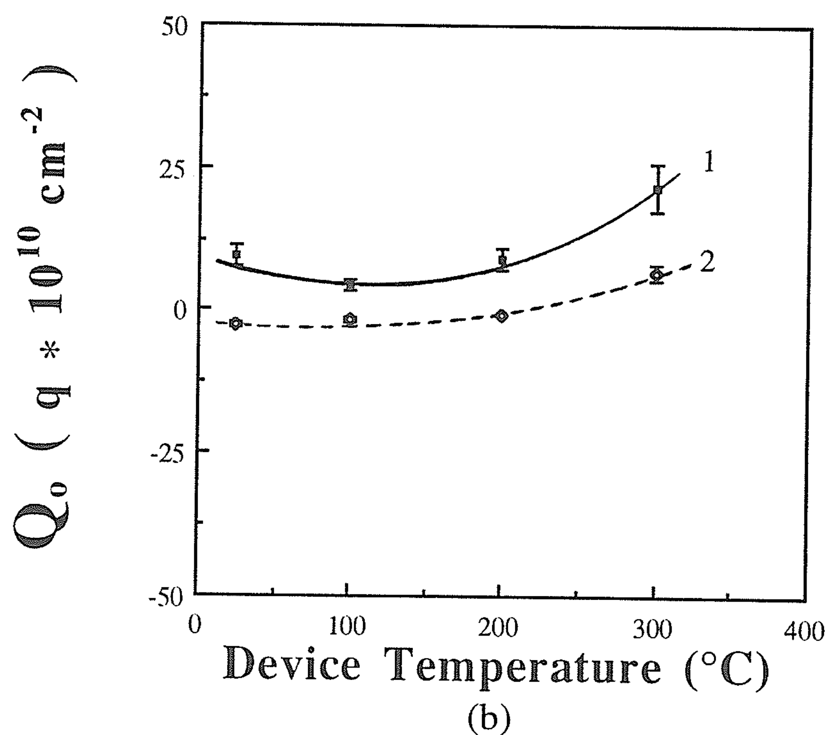

(b)

Fig. 4.21 Q_o as a function of device temperature for the electrode sample sets with oxide thickness of (a) 228Å; (b) 941 Å. Curve 1: after irradiation; curve 2: after final PMA treatment.

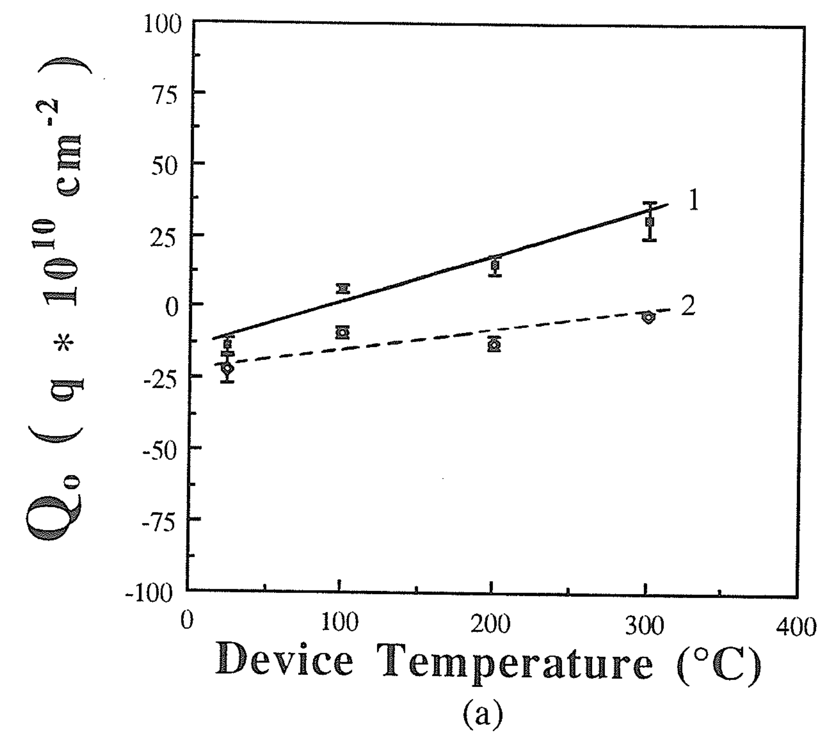

(a)

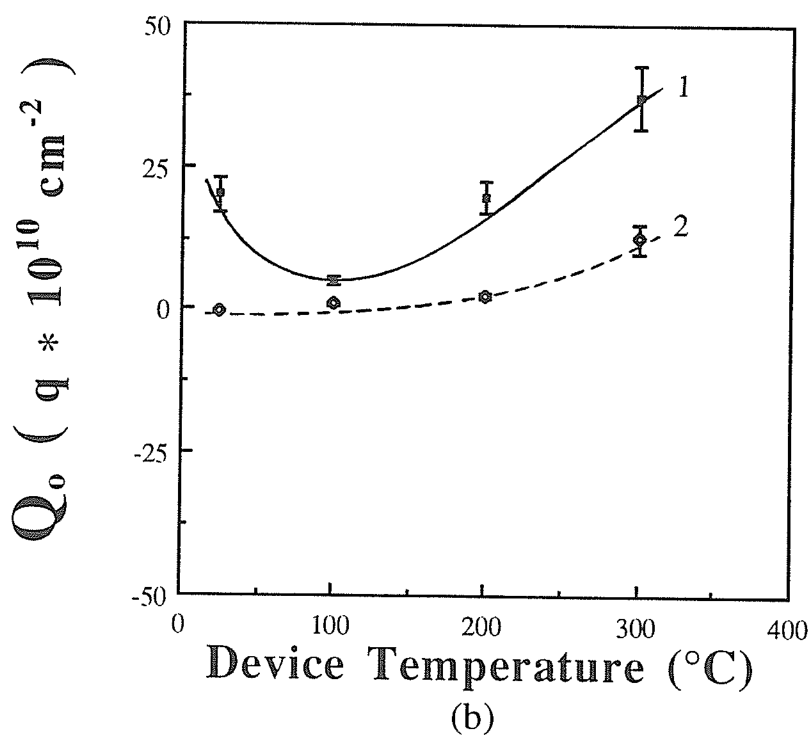

(b)

Fig. 4.22 Q_o as a function of device temperature for the mask sample sets with oxide thickness of (a) 228Å; (b) 941 Å. Curve 1: after irradiation; curve 2: after final PMA treatment.

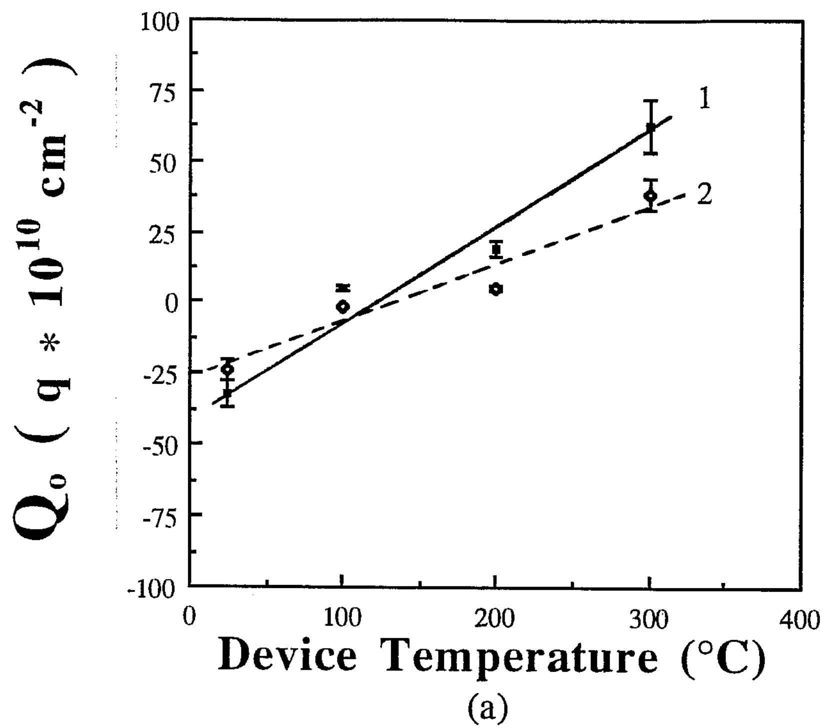

(a)

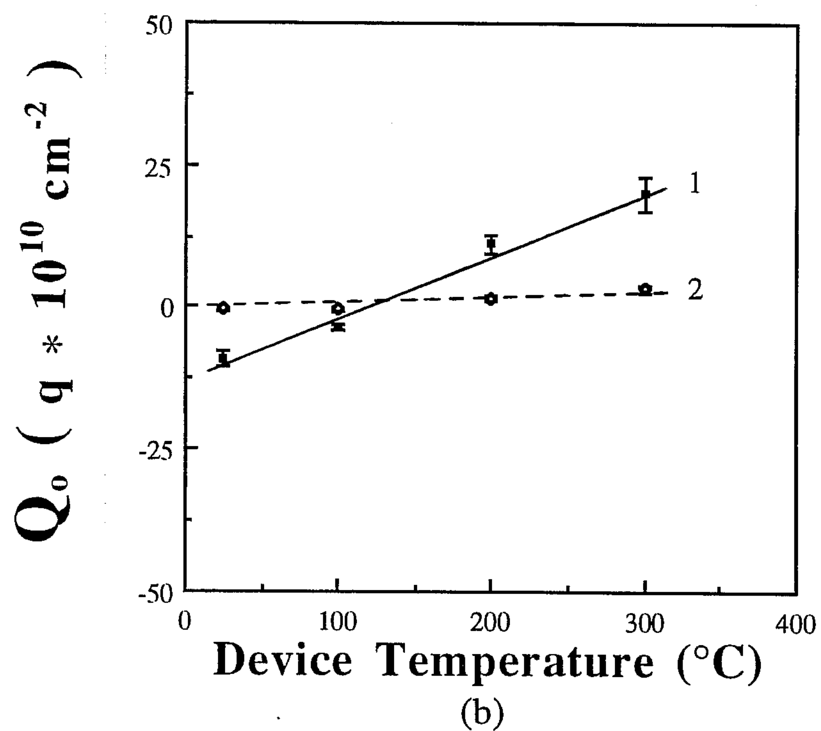

(b)

Fig. 4.23 Q_o as a function of device temperature for the anneal sample sets with oxide thickness of (a) 228Å; (b) 941 Å. Curve 1: after irradiation; curve 2: after final PMA treatment.

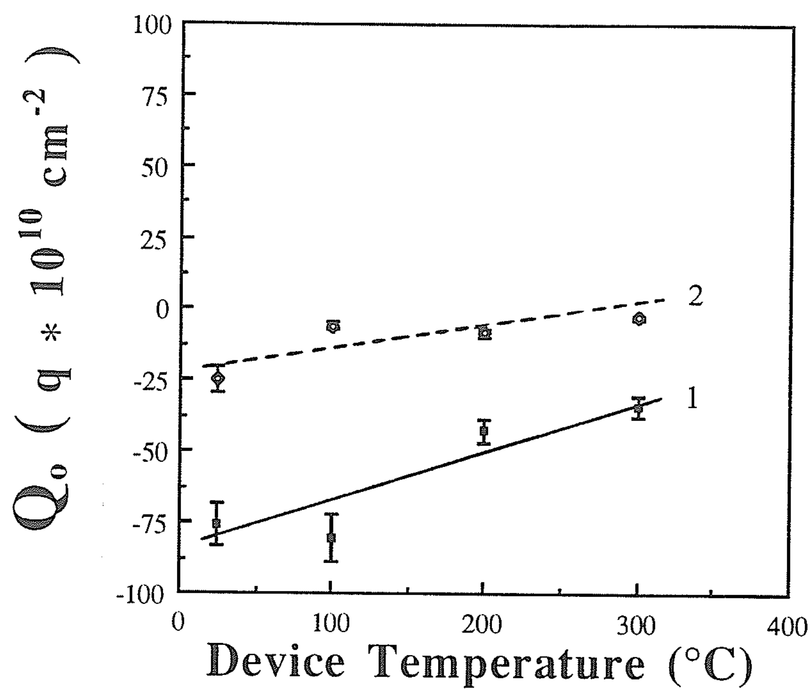

(a)

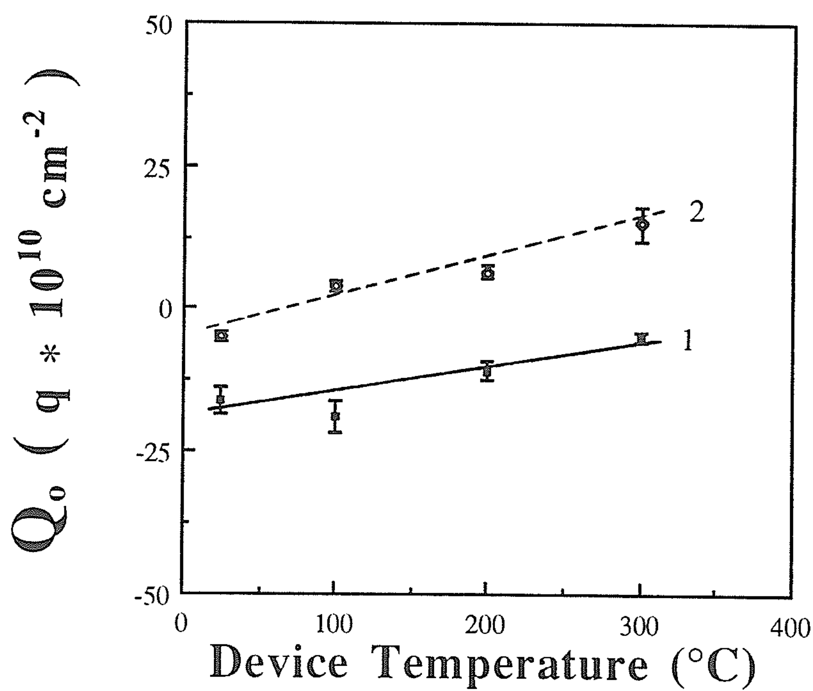

(b)

Fig. 4.24 Q_o as a function of device temperature for the bare sample sets with oxide thickness of (a) 228Å; (b) 941 Å. Curve 1: after irradiation; curve 2: after final PMA treatment.

radiation. As device temperature increases, defect annihilation becomes important because of the additional thermal energy released from the carrier recombination process. The negative charges are annealed out under this circumstance, leaving behind the positive charges in the oxide bulk. The number of positive charges in the oxide bulk increases with increasing device temperature from 100 to 300 °C, and is higher than the original Q_o values in these samples before any treatment (curves 1 in Fig. 4.16).

The formation of positive charges is largely due to the holes trapped in trap sites. When the ionizing radiation penetrates the underlying oxide films in these samples, electron-hole pairs are generated. The radiation-induced mobile electrons are usually swept out of the oxide films. With the additional thermal activation inside the oxide films at elevated temperatures, the electron driven-out process is enhanced. At the same time, the slow-moving holes are trapped by the bulk traps, resulting in the formation of positive charges in these samples. The number of these positive charges accumulated is generally higher in the thin oxide samples. This can be attributed to the higher concentration of radiation-induced holes and the injected holes at high electric fields, which are captured by the oxide bulk traps, thus leading to the increase in positive charges.

The second trend can be seen from Figs. 4.24 (a) and (b) for bare samples. The number of negative charges decreases with increasing device temperature. The bare sample receives more ionizing radiation, thus producing more electron-hole pairs. This makes more electrons to be captured by electron traps such as the silicon dangling bonds. Also, the possibility of hot electron bombardment and subsequent entrapment is increased because there is no Al gate electrode to stop the hot electrons to

impinge the oxide film. This leads to the high concentration of negative oxide charges in these samples initially.

Depending on the location of the transporting electrons, the number of electrons moving at higher device temperatures toward the nearest interface regions, that is, the Al-SiO_2 interface or the Si-SiO_2 interface increases. As more electrons move to the interface regions, less electrons are available to be trapped by the electron traps inside the oxide bulk. Therefore, the number of negative charges decreases as device temperature increases. Furthermore, the number of negative charges is higher in the thin oxide than the thick oxide, similar to the case for the electrode, mask and anneal samples, in which positive charge concentration is higher in thin oxide samples.

The thin oxide samples are more sensitive to oxide charging effects because charge concentration is higher in these samples after plasma radiation. The device structure, combined with the device temperature at the time of radiation can determine the type and the concentration of oxide charges to be generated in these MOS devices. With proper optimization of these two parameters, we may be able to control the oxide charging effect during radiation.

4.3.3 Annealing Effects

We have found two trends of D_{it} values after the final PMA treatment for the four sample sets. The first trend can be seen in Figs. 4.17 and 4.18 for the electrode and mask samples, where curves 2 show that the D_{it} values after final PMA treatment remain constant within the range of device temperature under investigation. These values are significantly

lower than the D_{it} values displayed by curves 1. This indicates that the PMA treatment has annealed out most of the radiation-induced interface traps at the Si-SiO_2 interface. When comparing these D_{it} values with the reference values shown in Fig. 4.15 for the two respective oxide thicknesses, we find close agreement between the two values. The deviations found from the comparisons are within the margin of errors, which are about ± 25%.

The second trend concerns the anneal and bare sample sets as shown in Figs. 4.19 and 4.20 in which the D_{it} value after the final PMA treatment increases with increasing device temperature. This increasing trend in D_{it} implies that the interface traps generated at the Si-SiO_2 interface during plasma radiation are more difficult to anneal out. We believe that it is largely due to the deep trapping of electrons at the Si-SiO_2 interface . For the bare samples, the penetration of hot electrons to the Si-SiO_2 interface or at the nearby region is very likely. Since the SiO_2 surface is entirely exposed to the ionizing radiation during the plasma radiation process, the energetic electrons that have escaped from the plasma sheath can impinge the Al gate electrodes to the oxide surface. Thus, this enables the hot electrons to scatter further deep into the oxide bulk near the Si-SiO_2 interface. Similarly, for the anneal samples, electrons are introduced into the oxide film during the initial PMA treatment where most of these electrons are in the oxide bulk.

As device temperature rises, the additional thermal energy provides the opportunity for the electrons in the oxide bulk or at the nearby Si-SiO_2 interface region for further transport. The enhanced scattering activities enable more electrons to be trapped at the Si-SiO_2 interface. These electrons trapped at the Si-SiO_2 interface are more difficult to be removed

by a standard PMA treatment. Hence, the D_{it} after final PMA treatment increases with increasing device temperature for both the bare and anneal sample sets. The degree of increase is more pronounced in the bare samples than the anneal samples, regardless of the oxide thickness. This reinforces the argument that hot electrons can penetrate directly to the Si-SiO_2 interface, forming the interface traps that are not removable by annealing at 400 °C.

The curves 2 in Figs. 4.21-4.24 show the Q_o values after final PMA treatment for the four sample sets. At the device temperature of 25 °C, we have mentioned in Section 4.2.3 that the PMA treatment can remove most of the radiation-induced oxide charge defects in the four sample sets. However, as device temperature increases to the range of 100–300 °C during plasma radiation, oxide charging has a more pronounced effect. When comparing these Q_o values for the four sample sets to the reference values shown in Figs. 4.16 (a) and (b), we can notice conspicuous deviations between the two values for the aforementioned device temperature range. This implies that the present PMA treatment cannot remove a major portion of the oxide charge defects. For the electrode, mask, and anneal samples, the positive charges accumulated after plasma radiation are partially removed. The same situation happens to the number of negative charges being removed in the bare samples.

We believe that the temperature aging process is partly responsible for the inability of annealing out the oxide charge defects in these samples. At the device temperature range of 100–300 °C, the aging process has enhanced the trapping activities inside the oxide bulk. This will likely cause the transporting carriers to be captured by deep traps due to the additional thermal activation in the oxide film. These carriers captured by deep traps

become the trapped oxide charges in the oxide and are difficult to anneal out. Hence, we can still see the accumulation of oxide charge defects inside the oxide films of the four samples after the standard PMA treatment.

4.4 Comparison Between Thermal and PECVD Oxides

The PECVD oxides have been the subjects of recent research on the issue of replacing thermal oxides as gate dielectrics [21-25]. Even though the as-deposited PECVD oxides have electronic properties approach to that of the high-quality thermal oxides, the viability of using PECVD oxides as gate oxides is still in question. One of the reasons that is deterring the progress of using PECVD oxides as gate oxides is the radiation damage issue. The PECVD oxides have been known to contain significant amount of radiation damage. The mechanisms for the creation of the damage during deposition have not been clearly established yet.

In an attempt to find out whether the processing plasmas are responsible for such damage, we had measured the defects generated during the plasma radiation of thermal and PECVD oxides. The two defect parameters, namely, the D_{it} and Q_o were determined after irradiation and subsequent annealing. They will be discussed below.

4.4.1 Plasma Radiation Effects

A. Interface Trap Density

Table 4.2 tabulates the D_{it} values for the various samples. Since the device temperature was held at 300 °C during plasma radiation, we expect that annealing effects must be involved. At this device temperature, the defect generation and annihilation occur simultaneously in thermal oxides during radiation. The electrode, mask, and anneal samples have D_{it} (after radiation) close to the reference values (before treatment) for the thermal oxide case, implying that the annealing effects have partially inhibited the generation of defects. The bare sample has a D_{it} of 8.3×10^{11} cm^{-2} eV^{-1} after radiation, which is higher than the other three samples with D_{it} of 2–3 x 10^{11} cm^{-2} eV^{-1}. This shows that the bare sample is more prone to radiation damage at the Si-SiO_2 interface and, that the bare sample without the protection from the Al gate electrodes is more likely to be bombarded by hot electrons from the plasma. These high-energy electrons escaped from the plasma sheath can penetrate deep into the Si-SiO_2 interface and create damage there. Such defects are more difficult to be removed because they are probably deep traps. Hence, the D_{it} value for the bare sample is comparatively high.

For the PECVD oxide samples, they have a high concentration of interface traps (8–10 x 10^{12} cm^{-2} eV^{-1}) before treatment. This indicates that they may have suffered severe radiation damage at the Si-SiO_2 interface during the deposition of SiO_2 films. Subsequent irradiation of these samples does not increase the D_{it} value. Conversely, the D_{it} value decreases significantly to 4–17 x 10^{11} cm^{-2} eV^{-1} after radiation. The decrease in D_{it}

Table 4.2 The D_{it} values of the MOS devices with electrode, mask, anneal, and bare structures after various processing steps.

		D_{it} (x 10^{11} cm^{-2} eV^{-1})		
Sample	Before Treatment	Initial PMA	After Radiation	Final PMA
1. Electrode				
Thermal Oxide	2.1	–	3.0	0.20
PECVD Oxide	83.0	–	4.2	3.5
PECVD Oxide*	86.5	–	81.3	4.0
2. Mask				
Thermal Oxide	–	–	2.8	0.19
PECVD Oxide	–	–	16.4	3.8
3. Anneal				
Thermal Oxide	1.8	0.15	2.7	0.26
PECVD Oxide	93.0	3.4	9.6	3.3
4. Bare				
Thermal Oxide	–	–	8.3	0.92
PECVD Oxide	–	–	5.2	4.3

*: This sample was irradiated at a device temperature of 25°C.

can be attributed to the annealing effects resulting from the irradiation at the device temperature of 300 °C. This implies that the PECVD oxide film contains high concentration of interface traps produced during the deposition process. The D_{it} value is about 8.13 x 10^{12} cm^{-2} eV^{-1} after radiation, which does not differ much from the pre-irradiation value. This indicates that the D_{it} at the Si-SiO_2 interface of the PECVD oxides does not change much after plasma radiation. At high device temperatures, defect annihilation process becomes important due to the annealing effects. It is therefore important to have the device temperature at a high temperature when exposing to plasma radiation.

The PECVD oxide film is deposited layer by layer onto the silicon substrate. During the deposition of the first few monolayers of SiO_2 film, the silicon substrate surface is also subjected to the bombardment of the energetic particles resulting from the chemical reactions at the surface. Thus, the Si-SiO_2 interface is already damaged and therefore the D_{it} value for the PECVD oxides is high. The subsequently deposited SiO_2 layers contain fewer strained bonds inside the SiO_2 network because the deposition process is at low temperatures. The Si-O bonding structures does not suffer the thermal stress as much as in the case of thermal oxides. The possibility of bond rupture during plasma radiation is greatly lowered, thus reducing the transport of broken bonds to the Si-SiO_2 interface. This is why the D_{it} at the Si-SiO_2 interface of the PECVD oxides does not change much after further plasma radiation.

The SiO_2 growth process by thermal oxidation depends on the diffusion of oxygen species into the silicon surface. The D_{it} value for thermal oxides is more dependent on the cleanliness of initial silicon surface and it is comparatively lower than the PECVD oxides. However,

thermal oxidation is a high temperature process, the thermal stress on neighboring Si-O bonds is high, and therefore, more strained bonds are created in thermal oxides. These strained bonds are more susceptible to breakage upon irradiation, this results in the radiation damage at the Si-SiO_2 interface in thermal oxides. It has been shown in Table 4.1 that the 941 Å thick thermal oxide sample irradiated at 25 °C have a D_{it} of the range 1–5 x 10^{13} cm^{-2} eV^{-1}. This demonstrates that thermal oxide is extremely sensitive to plasma radiation. At the device temperature of 300 °C, defect annihilation process is equally prominent. This is why the D_{it} value remains on the order of 10^{11} cm^{-2} eV^{-1} after radiation since most of the radiation-induced interface traps are annihilated concurrently.

B. Oxide Charge Density

Table 4.3, show that both types of oxides have similar positive Q_o values before treatment indicating that the Q_o values are independent of the fabrication process of the SiO_2 films. After plasma radiation, we observe two different trends. The first trend concerns with the electrode, mask, and anneal samples. The charges in these MOS devices are positive, and the number of these positive charges is higher than the pre-irradiation values, indicating an accumulation of positive charges. The second trend is that the oxide charge is negative and this is found only in the bare samples.

The electrode, mask, and anneal samples all have Al gate electrodes before radiation. During the plasma radiation, most of the energetic particles can only penetrate the neighboring SiO_2 regions that are not covered by electrodes but the UV light can penetrate the SiO_2 through the Al gate electrodes. For the mask samples, the UV light is the only radiation

Table 4.3 The Q_o values of the MOS devices with electrode, mask, anneal, and bare structures after various processing steps.

	Q_o (x 10^{10} q cm^{-2})			
Sample	Before Treatment	Initial PMA	After Radiation	Final PMA
1. Electrode				
Thermal Oxide	7.0	–	21.5	7.0
PECVD Oxide	5.7	–	23.9	18.3
PECVD Oxide*	6.5	–	10.7	2.2
2. Mask				
Thermal Oxide	–	–	37.6	14.5
PECVD Oxide	–	–	88.3	24.6
3. Anneal				
Thermal Oxide	6.8	-2.6	20.6	3.6
PECVD Oxide	6.0	9.0	15.5	9.8
4. Bare				
Thermal Oxide	–	–	-4.9	14.9
PECVD Oxide	–	–	-30.9	39.9

*: This sample was irradiated at a device temperature of 25°C.

source that passes through the electrodes. We therefore believe that the UV light is the main radiation source responsible for the generation of positive charges in these three sets of samples. The mask samples have the highest positive Q_o values regardless of the type of oxide films among the three sets of samples. The formation of positive charges is due to holes trapped in the bulk traps as has been discussed in Section 4.3.2.B.

On the other hand, the negative charges in bare samples are caused by electron trapped in traps. The number of negative charges is relatively higher in PECVD oxide. It is likely that the usage of silane (SiH_4) during the film deposition process involves the reaction between the hydrogen species and the Si-O bonds in the on-growing SiO_2 films. This leads to an increase in SiOH bonds formed in the SiO_2 films. However, these SiOH bonds are weakly bonded [26], and they can act as electron traps to capture electrons. The extra number of SiOH electron trap centers results in the higher number of negative charges in PECVD oxides after radiation.

The two aforementioned trends concerning the type of oxide charge generated after radiation can be seen in both the thermal and the PECVD oxides. This shows that the plasma radiation process has a more pronounced effect in the SiO_2 bulk than at the Si-SiO_2 interface. The D_{it} in PECVD oxides does not change as much as in the case of thermal oxides after radiation. On the other hand, the two trends of the oxide charging effects are equally observed in both types of oxides, though the degree of changes due to the oxide charging effects is different between the two oxides.

4.4.2 Annealing Effects

Table 4.2 shows that the D_{it} values after PMA treatment are reduced to the order of 10^{10} and 10^{11} cm^{-2} eV^{-1} for the thermal and the PECVD oxide samples, respectively. These values are reasonably close to the reference values (after initial PMA treatment) for the four sample sets except the thermally grown bare sample. The D_{it} values are generally within ± 25% of the reference values. We believe that the final PMA treatment is able to remove most of the interface traps at the Si-SiO_2 interface for the samples mentioned above. The D_{it} for the thermally grown bare sample remains relatively high (9.2×10^{10} cm^{-2} eV^{-1}) after final PMA treatment as compared to the values for the other samples. It is likely due to the entrapment of hot electrons at the Si-SiO_2 interface as we have mentioned in Section 4.3.3. The removal of such defects usually requires high temperature anneal (> 600 °C) so that bond rearrangement is possible to unite adjacent dangling bonds at the interface. The present PMA treatment at 400 °C does not have enough thermal energy to annihilate most of the aforementioned defects, which is why the D_{it} for the thermally grown bare sample remains at a relatively high concentration.

There are two trends from Table 4.3 regarding the values of Q_o after the final PMA treatment. These two trends are analogous to the two obtained after radiation. The first trend shows that a portion of positive charges is annealed out for the electrode, mask, and anneal samples after the final PMA treatment. There is a reduction of positive charges in these three sets of samples compared to the values after radiation. However, the radiation-induced positive charges are not totally removed when compared to the values after the initial PMA treatment. There is still a significant

amount of positive charges remained behind regardless of the type of oxide films, thus implying that the positive oxide charges are captured by deep traps. These positive charges are not removed at the present annealing temperature, indicating a high temperature anneal is required.

The second trend concerns with the bare samples where negative charges are annealed, leaving behind an excessive amount of positive charges. This shows that the carrier charging process during plasma radiation has trapped a significant amount of electrons. These mobile electrons are swept out of oxide bulk during subsequent annealing. This oxide charging effect will pose a potential device stability problem if the carrier charging process is not properly controlled after plasma radiation.

The fluctuations of the amount of oxide charge in SiO_2 films is more severe for the PECVD oxides, especially from the plasma radiation process to the subsequent annealing process for the mask and bare samples. This agrees with the argument mentioned earlier that the plasma radiation process has a pronounced effect in the SiO_2 bulk. Table 4.3 has shown that the changes in Q_o between the two processes are very significant for the two aforementioned samples.

Based on the results we have shown, the plasma radiation process not only creates defects at the Si-SiO_2 interface, but also in the SiO_2 bulk. This demonstrates that processing plasmas are partly responsible for the radiation damage in PECVD oxides during the SiO_2 film deposition process. In addition, oxide charging effects are observed to be a major problem in both the thermal and the PECVD oxides during plasma radiation at high temperatures. Oxide charging can lead to carrier injection and trapping , thus endangering device stability during operation at elevated temperature environment.

References for Chapter 4:

[1] T. P. Ma, "Oxide Thickness Dependence of Electron-Induced Surface States in MOS Structures," *Appl. Phys. Lett.* **27**(11), 615 (1975).

[2] C. R. Viswanathan and J. Maserjian, "Model for Thickness Dependence of Radiation Charging in MOS Structures," *IEEE Trans. Nucl. Sci.* **NS-23**(6), 1540 (1976).

[3] P. S. Winokur, Radiation-Induced Interface Traps in *Ionizing Radiation Effects in MOS Devices and Circuits*, T. P. Ma and P. V. Dressendorfer, Eds., John Wiley & Sons, New York, 1989, Ch. 4.

[4] F. B. McLean, H. E. Boesch, Jr., and T. R. Oldham, Electron-Hole Generation, Transport, and Trapping in SiO_2 in *Ionizing Radiation Effects in MOS Devices and Circuits*, T. P. Ma and P. V. Dressendorfer, Eds., John Wiley & Sons, New York, 1989, Ch. 3.

[5] A. B. Joshi and D. L. Kwong, "Dependence of Radiation Induced Damage on Gate Oxide Thickness in MOS capacitors with Ultrathin Gate Oxides," *Electron. Lett.* **28**(8), 744 (1992).

[6] J. Kassabov, E. Atanassova, J. Vassileva, and D. Dimitrov, "Influence of U. V. Radiation and Source-To-Bulk Bias on the Processes in the Si-SiO_2 Inversion Channel," *Solid-State Electron.* **35**, 1621 (1992).

[7] K. K. Hung and Y. C. Cheng, "Process Dependence of the Si-SiO_2 Interface Trap Density for Thin Oxides," *J. Electronchem. Soc.* **134**, 2814 (1987).

[8] H. Fuknda, M. Yasuda, T. Iwabuchi, S. Kaneko, T. Ueno, and Iwao Ohdomari, "Process Dependence of the SiO_2/Si(100) Interface Trap Density of Ultrathin SiO_2 Films," *J. Appl. Phys.* **72**, 1906 (1992).

[9] E. H. Nicollian and J. R. Brews, *MOS (Metal Oxide Semiconductor) Physics and Technology,* John Wiley & Sons, New York, (1982).

[10] B. E. Deal and A. S. Grove, "General Relationship for the Thermal Oxidation of Silicon," *J. Appl. Phys.* **36**, 3770 (1965).

[11] E. H. Snow, A. S. Grove, "Effects of Ionizing Radiation on Oxidized Silicon Surfaces and Planar Devices," *Proc. IEEE* **55**(7), 1168 (1967).

[12] A. G. Sabnis, "Characterization of Annealing of Co^{60} Gamma-Ray Damage at the Si-SiO_2 Interface," *IEEE Trans. Nucl. Sci.* **NS-30**(6), 4094 (1983).

[13] F. J. Grunthaner, P. J. Grunthaner, and J. Maserjian, "Radiation-Induced Defects in SiO_2 as Determined with XPS," *IEEE Trans. Nucl. Sci.* **NS-29**(6), 1462 (1982).

[14] F. J. Grunthaner, B. F. Lewis, N. Zamini, and J. Maserjian, "XPS Studies of Structure-Induced Radiation Effects at the Si/SiO_2 Interface," *IEEE Trans. Nucl. Sci.* **NS-27**(6), 1640 (1980).

[15] S. K. Lai, "Interface Traps Generation in Silicon Dioxide when Electrons are Captured by Trapped Holes," *J. Appl. Phys.* **54**, 2540 (1983).

[16] C. T. Sah, "Models and Experiments on Degradation of Oxidized Silicon," *Solid-State Electron.* **33**, 147 (1990).

[17] T. P. Ma, Process-Induced Radiation Effects in *Ionizing Radiation Effects in MOS Devices and Circuits*, T. P. Ma and P. V. Dressendorfer, Eds., John Wiley & Sons, New York, 1989, Ch. 7.

[18] K. Yokogawa, Y. Yajima, T. Mizutani, S. Nishimatsu, and K. Suzuki, "Positive Charges and E' Centers Formed by Vacuum Ultraviolet Radiation in SiO_2 Grown on Si," *J. J. Appl. Phys.* **29**, 2265 (1990).

[19] P. S. Winokur, H. E. Boesch, Jr., J. M. McGarrity, and F. B. McLean, "Field - and Time - Dependent Radiation Effects at the SiO_2/Si Interface of Hardened MOS Capacitors," *IEEE Trans. Nucl. Sci.* **NS-24**(6), 2113 (1977).

[20] L. C. Kimerling, "Recombination-Enhanced Defect Reactions," *Solid-State Electron.* **21**, 1391 (1978).

[21] J. Batey and E. Tierney, "Low Temperature Deposition of High-Quality Silicon Dioxide by Plasma-Enhanced Chemical Vapor Deposition," *J. Appl. Phys.* **60**, 3136 (1986).

[22] T. T. Chau, S. R. Mejia, and K. C. Kao, "Electronic Properties of Thin SiO_2 Films Deposited at Low Temperatures by New ECR Microwave PECVD Process," *Electron. Lett.* **25**, 1088 (1989).

[23] T. V. Herak and D. J. Thomson, "Effects of Substrate Temperature on the Electrical and Physical Properties of Silicon Dioxide Films Deposited from Electron Cyclotron Resonant Microwave Plasmas," *J. Appl. Phys.* **67**, 6347 (1990).

[24] T. T. Chau, S. R. Mejia, and K. C. Kao, "The Effects of Deposition Temperature on Properties of SiO_2 Films Fabricated by a New Electron Cyclotron Resonance Microwave Plasma-Enhanced Chemical-Vapor Deposition Process," *Can. J. Phys.* **69**, 165 (1991).

[25] T. T. Chau, S. R. Mejia, and K. C. Kao, "High-Quality 100 Å SiO_2 Films Fabricated by a New ECR Microwave PECVD Process," *J. Electrochem. Soc.* **138**, 325 (1991).

[26] C. T. Sah, "Origin of Interface States and Oxide Charges Generated by Ionizing Radiation," *IEEE Trans. Nucl. Sci.* **NS-23**(6), 1563 (1976).

Chapter 5

Conclusions

The radiation damage in MOS devices due to N_2O plasma radiation has been studied. Two defect parameters, namely, the interface trap density D_{it} and the oxide charge density Q_o are used to evaluate the damage for the MOS devices with various SiO_2 thicknesses and device temperatures during irradiation. Based on this study, the following conclusions are drawn:

The radiation damage in MOS devices is dependent upon the SiO_2 thickness of the devices. In general, the D_{it} increases with increasing SiO_2 thickness after plasma radiation. The increase in D_{it} follows a power law t_{ox}^{n} with n ranging 0.3–0.6 for our samples. Both positive and negative charges can be found after radiation, depending on the device structure during radiation. The number of positive oxide charges increases with increasing SiO_2 thickness for device structure covered with aluminum (Al) gate electrodes (Al-SiO_2-Si structure). On the other hand, the number of negative oxide charges decreases with increasing SiO_2 thickness for bare device structure (Si-SiO_2 structure).

The increase in device temperature during plasma radiation yields two trends for the temperature dependence of D_{it}. One trend is that D_{it} decreases with increasing temperature for the temperature up to 200 °C, while the other trend is that D_{it} increases with increasing temperature for temperatures higher than 200 °C. The change in Q_o with respect to the increase of device temperature during plasma radiation also depends on the

device structure. The number of positive oxide charges in MOS devices of Al-SiO_2-Si structure increases with increasing temperature, while the number of negative oxide charges in MOS devices of Si-SiO_2 structure decreases with increasing device temperature.

The Si-SiO_2 interface of MOS devices fabricated by PECVD oxides is more immune to plasma radiation than the devices with thermal oxides. However, the oxide charging effect is more pronounced for devices with PECVD oxide than those with thermal oxide.

Most of the radiation-induced damage can be annealed out by a standard PMA treatment. The annealing efficiency is lower at higher device temperature during radiation indicating that some radiation damage still remains inside the MOS devices even after the PMA treatment.

The above experimental facts suggest that

(a) The radiation damage depends on the radiation dose applied to the device.

(b) The MOS devices experience a floating potential during plasma radiation, thus leading to electron injection from contacts.

(c) The amount of UV radiation absorbed by the underlying oxide films of MOS devices can determine the type of oxide charge being trapped in the oxides.

(d) The increase in device temperature during plasma radiation will enhance the thermal annealing effect. A further increase in device temperature beyond 300 °C will cause the temperature aging effect overriding the annealing effect.

(e) The amount of radiation damage can be reduced during the plasma etching process if it is conducted in the temperature range of 200–300 °C, where the least D_{it} is generated.

(f) Plasma radiation creates traps both in the oxide bulk and at the Si-SiO_2 interface. These traps may trap carriers and also the trapped carriers may be released from the traps depending on the temperature. This may result in a serious instability problem in MOS devices.

(g) The MOS devices with PECVD oxides have some radiation damage due to plasma involved in the PECVD processing.

Appendix A

Capacitance-Voltage Method

(I) Calculation of Interface Trap Density

The primary method for determining interface trap density (D_{it}) in MOS devices is the high-low frequency capacitance method [1]. This method is based on the fact that the interface trap charge can exchange charges with silicon; therefore we can apply a gate voltage bias V_g on the MOS device to measure the D_{it} with respect to the corresponding change in the capacitance values. The usual "stretch out" observed from the C-V curve is an indication of the variation in the D_{it} level at the Si-SiO_2 interface.

Typically, the gate voltage bias used in the measurements is implemented by a ramped voltage technique to apply the voltage sweep on the MOS device. The C-V curves are usually produced via the voltage sweep of the MOS device from either the accumulation mode to the inversion mode or vice versa. The resulting high-low frequency C-V curves enable us to compute the values for the interface trap capacitance C_{it} without additional computation. This is because this technique eliminates the need for a theoretical computation of the silicon surface capacitance C_s for the MOS device. Since the total capacitance at high frequencies (~1–10 MHz) C_{HF} is given by

$$C_{HF} = \frac{C_s\, C_{ox}}{C_s + C_{ox}} \qquad (1)$$

which is equivalent to the series combination of the oxide capacitance C_{ox} and the C_s of the MOS device. However, at high frequencies, the interface traps cannot respond rapidly enough to the ac gate voltage so that the contribution from the interface trap capacitance is negligible. The total capacitance at low frequencies (~1–10 Hz) C_{LF} is expressed as

$$\frac{1}{C_{LF}} = \frac{1}{C_{ox}} + \frac{1}{C_s + C_{it}} \qquad (2)$$

where the ac response of the interface traps can be accounted for at these frequencies, because the response from the interface traps is immediate, which contributes to a significant amount of C_{it}. Since both Eqs. (1) and (2) contain the C_s term, the combination of high-low frequency measurements omits the evaluation of C_s. By rearranging Eqs. (1) and (2), we can obtain the following expressions for the interface trap capacitance

$$C_{it} = \left[\frac{1}{C_{LF}} - \frac{1}{C_{ox}}\right]^{-1} - \left[\frac{1}{C_{HF}} - \frac{1}{C_{ox}}\right]^{-1} \qquad (3)$$

However, C_{it} is

$$C_{it}(\Psi_s) \equiv -\frac{dQ_{it}}{d\Psi_s} \approx q\, D_{it}(\phi_s) \qquad (4)$$

where Ψ_s = band bending, Q_{it} = interface trap charge per unit area, and ϕ_s = surface potential measured from intrinsic level at the silicon surface. Substituting Eq. (3) in Eq. (4) and solving for D_{it} yields

$$D_{it} = \frac{1}{q}\left[\left(\frac{1}{C_{LF}} - \frac{1}{C_{ox}}\right)^{-1} - \left(\frac{1}{C_{HF}} - \frac{1}{C_{ox}}\right)^{-1}\right] \quad (5)$$

where C_{HF} and C_{LF} denote the capacitance values at high frequency (HF) and low frequency (LF), respectively.

Extraction of the D_{it} value is often quoted at the midgap of the silicon bandgap because it is a better representation of the overall value across the silicon bandgap. This is due to the D_{it} near the band edges becomes less precise in describing the number of the interface traps at these regions. As a result, the D_{it} values are usually obtained from the separation between the HF and the LF C-V curves in the depletion region. In order to extract this midgap value, the D_{it} is converted from a function of gate bias to a function of energy level (E_c – E) in the silicon bandgap through the following relations [1]

$$\Psi_s(V_g) = \int_{V_{fb}}^{V_g}\left(1 - \frac{C_{LF}(V_g)}{C_{ox}}\right) dV_g \quad (6)$$

$$\frac{E_c - E}{q} = \frac{E_g}{2q} + \Psi_s - \phi_B \quad (7)$$

where V_{fb} = flatband voltage, E_c = conduction band edge energy, E = energy level in the gap, E_g = bandgap energy, and ϕ_B = potential difference between the thermal equilibrium Fermi level and the intrinsic Fermi level in the silicon bulk. Using the above relations, we can compute the D_{it} value at midgap, which is 0.55 eV below E_c with E_g = 1.1 eV for Si at room temperature.

All the capacitance values quoted above are per unit area. They are also normalized to the oxide capacitance values so that the C-V measurements will not be affected by device geometry like gate area and oxide thickness. Usage of capacitance values in the calculation of oxide charge density is also treated the same way. The LF C-V curve after normalization will be referred to as the quasi-static (QS) C-V curve.

(II) Calculation of Oxide Charge Density

The determination of oxide charge density (Q_o) is mainly based on the HF capacitance method [1, 2]. We can usually infer this density from the "flatband voltage shift" in the HF C-V curve of the MOS device. However, in doing so, we must first locate the flatband capacitance C_{fb} and the corresponding flatband voltage V_{fb} on the C-V curves. Since Nicollian and Brews [1] have described a widely used flatband capacitance method to determine the V_{fb}, we adopt their method because of its simplicity. It is based on the following relations

$$C_{fb} = \frac{C_{fbs}\, C_{ox}}{C_{fbs} + C_{ox}} \tag{8}$$

with

$$C_{fbs} = \sqrt{\frac{q^2 N_D\, \varepsilon_s}{k\, T}} \tag{9}$$

where C_{fbs} = silicon flatband capacitance, C_{ox} = oxide capacitance, N_D = donor concentration, and ε_s = permittivity of the silicon. Knowing the values of C_{fb}, we can identify the corresponding V_{fb} values from the HF C-V curves.

With the flatband voltage values determined; we can evaluate the oxide charge density by using an appropriate equation. In doing so, we can relate these values with the work function difference between the gate metal and the silicon W_{ms}. In an ideal case, the flatband voltage is equal to W_{ms} for charge free condition at flatband. However, there is a certain amount of intrinsic oxide charge residing in the oxide film causing the apparent deviation between V_{fb} and W_{ms}, which we denote as $V_{fb} - W_{ms}$. This deviation is equivalent to a parallel shift of the HF C-V curve compared to the one in an ideal charge free situation. Subsequent injection or trapping of carriers can also lead to a corresponding flatband shift of the HF C-V curve. The direction of the shift is dependent on the polarity of the charge carriers. Thus, the Q_o can be related to the flatband voltage shift through [1]

$$V_{fb} - W_{ms} = -\frac{Q_o}{C_{ox}} = -\frac{d_{ox} Q_o}{\varepsilon_{ox}} \qquad (10)$$

where d_{ox} = oxide thickness, and ε_{ox} = permittivity of the oxide in which the relation $C_{ox} = \varepsilon_{ox}/d_{ox}$ is used in the expression.

References for Appendix A:

[1] E. H. Nicollian and J. R. Brews, *MOS (Metal Oxide Semiconductor) Physics and Technology*, John Wiley & Sons, New York, (1982).

[2] S. M. Sze, *Physics of Semiconductor Devices*, John Wiley & Sons, New York, (1981).